

ISSN 1881-7815    Online ISSN 1881-7823

# **BST**

## **BioScience Trends**

**Volume 13, Number 3**  
**June, 2019**



[www.biosciencetrends.com](http://www.biosciencetrends.com)



# BST

## BioScience Trends



ISSN: 1881-7815

Online ISSN: 1881-7823

CODEN: BTIRCZ

Issues/Year: 6

Language: English

Publisher: IACMHR Co., Ltd.

**BioScience Trends** is one of a series of peer-reviewed journals of the International Research and Cooperation Association for Bio & Socio-Sciences Advancement (IRCA-BSSA) Group and is published bimonthly by the International Advancement Center for Medicine & Health Research Co., Ltd. (IACMHR Co., Ltd.) and supported by the IRCA-BSSA and Shandong University China-Japan Cooperation Center for Drug Discovery & Screening (SDU-DDSC).

**BioScience Trends** devotes to publishing the latest and most exciting advances in scientific research. Articles cover fields of life science such as biochemistry, molecular biology, clinical research, public health, medical care system, and social science in order to encourage cooperation and exchange among scientists and clinical researchers.

**BioScience Trends** publishes Original Articles, Brief Reports, Reviews, Policy Forum articles, Case Reports, News, and Letters on all aspects of the field of life science. All contributions should seek to promote international collaboration.

## Editorial Board

### Editor-in-Chief:

Norihiro KOKUDO  
*National Center for Global Health and Medicine, Tokyo, Japan*

### Co-Editors-in-Chief:

Xue-Tao CAO  
*Nankai University, Tianjin, China*  
Rajendra PRASAD  
*University of Delhi, Delhi, India*  
Arthur D. RIGGS  
*Beckman Research Institute of the City of Hope, Duarte, CA, USA*

### Chief Director & Executive Editor:

Wei TANG  
*National Center for Global Health and Medicine, Tokyo, Japan*

### Senior Editors:

Xunjia CHENG  
*Fudan University, Shanghai, China*  
Yoko FUJITA-YAMAGUCHI  
*Beckman Research Institute of the City of Hope, Duarte, CA, USA*  
Na HE  
*Fudan University, Shanghai, China*  
Kiyoshi KITAMURA  
*The University of Tokyo, Tokyo, Japan*  
Misao MATSUSHITA  
*Tokai University, Hiratsuka, Japan*  
Munehiro NAKATA  
*Tokai University, Hiratsuka, Japan*  
Takashi SEKINE

*Toho University, Tokyo, Japan*  
Fanghua QI  
*Shandong Provincial Hospital, Ji'nan, China*  
Ri SHO  
*Yamagata University, Yamagata, Japan*  
Yasuhiko SUGAWARA  
*Kumamoto University, Kumamoto, Japan*  
Ling WANG  
*Fudan University, Shanghai, China*

### Managing Editor:

Jianjun GAO  
*Qingdao University, Qingdao, China*

### Web Editor:

Yu CHEN  
*The University of Tokyo, Tokyo, Japan*

### Proofreaders:

Curtis BENTLEY  
*Roswell, GA, USA*  
Thomas R. LEBON  
*Los Angeles, CA, USA*

### Editorial Office

Pearl City Koishikawa 603,  
2-4-5 Kasuga, Bunkyo-ku, Tokyo 112-0003, Japan  
Tel: +81-3-5840-8764 Fax: +81-3-5840-8765  
E-mail: office@biosciencetrends.com

# BioScience Trends

## Editorial and Head Office

Pearl City Koishikawa 603, 2-4-5 Kasuga, Bunkyo-ku,  
Tokyo 112-0003, Japan

Tel: +81-3-5840-8764, Fax: +81-3-5840-8765  
E-mail: office@biosciencetrends.com  
URL: www.biosciencetrends.com

## Editorial Board Members

Girdhar G. AGARWAL <i>(Lucknow, India)</i>	Takahiro HIGASHI <i>(Tokyo, Japan)</i>	Masatoshi MAKUUCHI <i>(Tokyo, Japan)</i>	Shin'ichi TAKEDA <i>(Tokyo, Japan)</i>
Hirotugu AIGA <i>(Geneva, Switzerland)</i>	De-Fei HONG <i>(Hangzhou, China)</i>	Francesco MAROTTA <i>(Milano, Italy)</i>	Sumihito TAMURA <i>(Tokyo, Japan)</i>
Hidechika AKASHI <i>(Tokyo, Japan)</i>	De-Xing HOU <i>(Kagoshima, Japan)</i>	Yutaka MATSUYAMA <i>(Tokyo, Japan)</i>	Puay Hoon TAN <i>(Singapore, Singapore)</i>
Moazzam ALI <i>(Geneva, Switzerland)</i>	Sheng-Tao HOU <i>(Ottawa, Canada)</i>	Qingyue MENG <i>(Beijing, China)</i>	Koji TANAKA <i>(Tsu, Japan)</i>
Ping AO <i>(Shanghai, China)</i>	Yong HUANG <i>(Ji'ning, China)</i>	Mark MEUTH <i>(Sheffi eld, UK)</i>	John TERMINI <i>(Duarte, CA, USA)</i>
Hisao ASAMURA <i>(Tokyo, Japan)</i>	Hirofumi INAGAKI <i>(Tokyo, Japan)</i>	Satoko NAGATA <i>(Tokyo, Japan)</i>	Usa C. THISYAKORN <i>(Bangkok, Thailand)</i>
Michael E. BARISH <i>(Duarte, CA, USA)</i>	Masamine JIMBA <i>(Tokyo, Japan)</i>	Miho OBA <i>(Odawara, Japan)</i>	Toshifumi TSUKAHARA <i>(Nomi, Japan)</i>
Boon-Huat BAY <i>(Singapore, Singapore)</i>	Chunlin JIN <i>(Shanghai, China)</i>	Xianjun QU <i>(Beijing, China)</i>	Kohjiro UEKI <i>(Tokyo, Japan)</i>
Yasumasa BESSHO <i>(Nara, Japan)</i>	Kimitaka KAGA <i>(Tokyo, Japan)</i>	John J. ROSSI <i>(Duarte, CA, USA)</i>	Masahiro UMEZAKI <i>(Tokyo, Japan)</i>
Generoso BEVILACQUA <i>(Pisa, Italy)</i>	Ichiro KAI <i>(Tokyo, Japan)</i>	Carlos SAINZ-FERNANDEZ <i>(Santander, Spain)</i>	Junming WANG <i>(Jackson, MS, USA)</i>
Shiuan CHEN <i>(Duarte, CA, USA)</i>	Kazuhiro KAKIMOTO <i>(Osaka, Japan)</i>	Yoshihiro SAKAMOTO <i>(Tokyo, Japan)</i>	Xiang-Dong Wang <i>(Boston, MA, USA)</i>
Yuan CHEN <i>(Duarte, CA, USA)</i>	Kiyoko KAMIBEPPU <i>(Tokyo, Japan)</i>	Erin SATO <i>(Shizuoka, Japan)</i>	Hisashi WATANABE <i>(Tokyo, Japan)</i>
Naoshi DOHMAE <i>(Wako, Japan)</i>	Haidong KAN <i>(Shanghai, China)</i>	Takehito SATO <i>(Isehara, Japan)</i>	Jufeng XIA <i>(Tokyo, Japan)</i>
Zhen FAN <i>(Houston, TX, USA)</i>	Bok-Luel LEE <i>(Busan, Korea)</i>	Akihito SHIMAZU <i>(Tokyo, Japan)</i>	Lingzhong XU <i>(Ji'nan, China)</i>
Ding-Zhi FANG <i>(Chengdu, China)</i>	Mingjie LI <i>(St. Louis, MO, USA)</i>	Zhifeng SHAO <i>(Shanghai, China)</i>	Masatake YAMAUCHI <i>(Chiba, Japan)</i>
Xiaobin FENG <i>(Beijing, China)</i>	Shixue LI <i>(Ji'nan, China)</i>	Judith SINGER-SAM <i>(Duarte, CA, USA)</i>	Aitian YIN <i>(Ji'nan, China)</i>
Yoshiharu FUKUDA <i>(Ube, Japan)</i>	Ren-Jang LIN <i>(Duarte, CA, USA)</i>	Raj K. SINGH <i>(Dehradun, India)</i>	George W-C. YIP <i>(Singapore, Singapore)</i>
Rajiv GARG <i>(Lucknow, India)</i>	Lianxin LIU <i>(Hefei, China)</i>	Peipei SONG <i>(Tokyo, Japan)</i>	Xue-Jie YU <i>(Galveston, TX, USA)</i>
Ravindra K. GARG <i>(Lucknow, India)</i>	Xinqi LIU <i>(Tianjin, China)</i>	Junko SUGAMA <i>(Kanazawa, Japan)</i>	Benny C-Y ZEE <i>(Hong Kong, China)</i>
Makoto GOTO <i>(Tokyo, Japan)</i>	Daru LU <i>(Shanghai, China)</i>	Hiroshi TACHIBANA <i>(Isehara, Japan)</i>	Yong ZENG <i>(Chengdu, China)</i>
Demin HAN <i>(Beijing, China)</i>	Hongzhou LU <i>(Shanghai, China)</i>	Tomoko TAKAMURA <i>(Tokyo, Japan)</i>	Xiaomei ZHU <i>(Seattle, WA, USA)</i>
David M. HELFMAN <i>(Daejeon, Korea)</i>	Duan MA <i>(Shanghai, China)</i>	Tadatoshi TAKAYAMA <i>(Tokyo, Japan)</i>	<i>(as of February 28, 2019)</i>

---

**Original Article**

---

- 216 - 224 **MLS128 antibody-induced suppression of colon cancer cell growth is mediated by a desmocollin and a 110 kDa glycoprotein.**  
*Sarah C. Shuck, Teresa Hong, Markus Kalkum, Ryo Igarashi, Kota Kajiya, John Termini, Kazuo Yamamoto, Yoko Fujita-Yamaguchi*
- 225 - 233 **Conserved amino acids around the DIII-DI linker region of the Newcastle disease virus fusion protein are critical for protein folding and fusion activity.**  
*Miaomiao Chi, Wenyan Xie, Ying Liu, Chi Zhang, Yaqing Liu, Hongling Wen, Li Zhao, Yanyan Song, Na Liu, Lianli Chi, Zhiyu Wang*
- 234 - 244 **Knockdown expression of *MECR*, a novel gene of mitochondrial FAS II inhibits growth and colony-formation, promotes apoptosis of hepatocellular carcinoma cells.**  
*Yulong Cai, Yixin Lin, Xianze Xiong, Jiong Lu, Rongxing Zhou, Yanwen Jin, Zhen You, Hui Ye, Fuyu Li, Nansheng Cheng*
- 245 - 252 **Higher  $\beta$ -human chorionic gonadotropin and estrogen levels during the first 6 weeks of pregnancy are associated with threatened abortion.**  
*Ling Xu, Qun Wei, Qiong Wu, Yanbo Zhong, Yangfang Li, Jun Xu, Yunheng Zhu*
- 253 - 260 **Protection of paeonol against epirubicin-induced hepatotoxicity: A metabolomic study.**  
*Xu Jing, Chao Sun, Huigang Chen, Jing Sun, Ying Zhang, Jing Wu*

---

**Brief Report**

---

- 261 - 266 **Analysis of mutations in the *FOXJ1* and *KCNJ10* genes in infants with a single-allele *SLC26A4* mutation.**  
*Xuelei Zhao, Xiaohua Cheng, Lihui Huang, Xianlei Wang, Cheng Wen, Xueyao Wang, Liping Zhao*
- 267 - 272 **Design and synthesis of novel histone deacetylase 6 inhibitors with benzyl-triazole as the core skeleton.**  
*Zishuo Mou, Jianjun Gao, He Miao, Li Zhang, Li Su, Baolei Wang, Yepeng Luan*

---

**Communication**

---

- 273 - 275 **The Epidemic of major sexually transmitted diseases in Shanghai, China, 2009-2018**  
*Qi Tang, Xuting Zhang, Hongzhou Lu*
- 276 - 278 **Super-aged society: Constructing an integrated information platform of self-recording lifelogs and medical records to support health care in Japan.**  
*Kenji Karako, Yu Chen, Peipei Song, Wei Tang*

## CONTENTS

(Continued)

---

- 279 - 281      **The community-based integrated care system in Japan: Health care and nursing care challenges posed by super-aged society.**  
*Peipri Song, Wei Tang*

### Letter

---

- 282 - 283      **Overshadowed prospect of programmed cell death protein-1 (PD-1) inhibitor as monotherapy for patients with advanced hepatocellular carcinoma.**  
*Xu Yao, Lei Wang, Jianjun Gao*

- 284 - 285      **New thoughts in exploring the pathogenesis, diagnosis, and treatment of threatened abortion.**  
*Jing Zhou, Zengshu Huang, Xinyao Pan, Wing Ting Leung, Chuyu Li, Lijia Chen, Yanzhi Zhang, Lan Wang, Yizhen Sima, Na Zhang, Xuemin Qiu, Lisha Li, Ling Wang*

### Guide for Authors

---

### Copyright

---

# MLS128 antibody-induced suppression of colon cancer cell growth is mediated by a desmocolin and a 110 kDa glycoprotein

Sarah C. Shuck<sup>1</sup>, Teresa Hong<sup>2</sup>, Markus Kalkum<sup>2</sup>, Ryo Igarashi<sup>1</sup>, Kota Kajiya<sup>1</sup>, John Termini<sup>1</sup>, Kazuo Yamamoto<sup>3</sup>, Yoko Fujita-Yamaguchi<sup>4,\*</sup>

<sup>1</sup>Department of Molecular Medicine, Beckman Research Institute, City of Hope, Duarte, CA, USA;

<sup>2</sup>Department of Molecular Imaging and Therapy, Beckman Research Institute, City of Hope, Duarte, CA, USA;

<sup>3</sup>Department of Integrated Biosciences, Graduate School of Frontier Sciences, The University of Tokyo, Kashiwa, Japan;

<sup>4</sup>Department of Diabetes Complications & Metabolism, Beckman Research Institute, City of Hope, Duarte, CA, USA.

## Summary

Protein glycosylation is a diverse form of post-translational modification. Two to three consecutive O-linked N-acetylgalactosamines (Tn-antigens) are recognized by antibodies such as MLS128. MLS128 mAb inhibited cell growth and bound to a 110 kDa glycoprotein (GP) in LS180 and HT29 colon cancer cells. However, purification and identification of the 110 kDa GP was unsuccessful due to its low abundance. The present study used a highly sophisticated and sensitive mass spectrometry method to identify proteins immunoprecipitated with MLS128 and separated by two-dimensional gel electrophoresis. Three desmosome components were identified. Of these, desmocolin and desmoglein shared many similar characteristics, including molecular mass, pI, and potential Tn-antigen sites. Western blotting analyses of LS180 cell lysates revealed a common 110 kDa band recognized by MLS128 and anti-desmocolin, but not by anti-desmoglein. Immunofluorescence microscopy of LS180 cells revealed that desmocolin is membrane-bound, while desmoglein is primarily localized in the cytosol. Confocal microscopy demonstrated colocalization of the desmocolin-specific antibody with the MLS128 antibody on the cell membrane, suggesting that desmocolin may contain Tn-antigens recognized by MLS128. Treatment of LS180 cells with siRNA to knock down desmocolin expression or a desmocolin-specific antibody decreased cell viability, suggesting a critical role for this protein in cell growth and survival. N-glycosidase F digestion of the 110 kDa GP and desmocolin suggested that although both proteins contain N-glycosylation sites, they are not identical. These findings suggest that desmocolin colocalizes with the 110 kDa GP and that growth inhibition induced by the MLS128 antibody may be mediated through a mechanism that involves desmocolin.

**Keywords:** Desmocolin, colon cancer, MLS128, receptor, growth inhibitory mAb, anti-Tn antigen, desmosome

## 1. Introduction

Mouse immunization with cancer cells, glycoproteins, and mucins has been performed to produce cancer-

specific monoclonal antibodies (mAbs); many of which have been isolated and characterized as carbohydrate-specific. Two antibodies identified in this way, MLS128 and 83D4, were found to recognize Tn-antigens, which are two or three consecutively arranged N-acetylgalactosamines (GalNAc) conjugated to serine and/or threonine residues (1-4). The Tn-antigen is one of the most common aberrations associated with cancer progression and metastasis, and thus is an excellent target for development of cancer diagnostics and therapeutics (5-9). MLS128 (IgG3) was derived from a mouse immunized with mucins secreted by LS180 human colon

Released online in J-STAGE as advance publication June 5, 2019.

\*Address correspondence to:

Dr. Yoko Fujita-Yamaguchi, Diabetes & Metabolism Research Institute, Beckman Research Institute, City of Hope, Duarte, CA 91010, USA.

E-mail: yyamaguchi@coh.org

carcinoma cells (10) whereas 83D4 mAb (IgM) was derived from a mouse immunized with human breast cancer tissue-paraffin sections (11).

Previous studies in our laboratory revealed that MLS128 binds a membrane glycoprotein (GP) with a molecular weight of 110 kDa. This 110 kDa GP contains N-glycans in addition to O-glycans consisting of 2 or 3 consecutive Tn-antigens which are recognized by MLS128 (12). Tn-antigens are found in over 67% of colon cancer cell lines tested, but not in MCF-7 breast cancer cell lines (12,13). MLS128 antibody treatment inhibited growth of LS180 and HT29 colon cancer cells (13,14). Efforts to purify and identify the 110 kDa GP bound by MLS128 have been very difficult, mainly due to its low abundance.

In this study, our goal was to identify the 110 kDa GP. To do this, we immunoprecipitated membrane proteins with MLS128, separated them by 2-D gel electrophoresis, digested them with trypsin/Lys-C, and analyzed them by liquid chromatography multistage mass spectrometry (LC-MS/MS). Proteomics analysis identified several putative candidates for the 110 kDa GP, which we further examined in various cell lines using Western blotting, immunofluorescence microscopy, antibody treatments, and siRNA knockdowns.

## 2. Materials and Methods

### 2.1. Materials

Production and characterization of the MLS128 antibody was previously described (1,11). Desmocollin (ab150382) and desmoglein (ab124798) antibodies, horseradish peroxidase (HRP)-conjugated goat anti-mouse IgG3, anti-rabbit IgG (H+L), and Fluoroshield DAPI mounting media were obtained from Abcam (Cambridge, MA). Goat anti-rabbit Alexa Fluor<sup>®</sup> 488, goat anti-mouse Alexa Fluor<sup>®</sup> 647, Mem-PER Membrane protein isolation kit, and protease inhibitor (87886) were from Thermo Fisher Scientific (Waltham, MA). Cell culture media (Dulbecco's Modified Eagles Medium (DMEM) and McCoy's 5A) were purchased from Gibco (Grand Island, NY). N-glycosidase F was purchased from Roche Applied Science (Indianapolis, IN).

### 2.2. Cell lines and culture

Cell lines used in this study, human colon adenocarcinoma LS180 cells, human breast carcinoma MCF-7 cells, and human normal mammary epithelial MCF-10A cells, were obtained from American Tissue Type Culture Collection. LS180 colon cancer cells were cultured in DMEM containing 10% fetal bovine serum (FBS), 4.5 mg/mL D-glucose, and 110 µg/mL pyruvic acid as described (12). MCF-7 breast cancer and MCF-10A cells were cultured in DMEM containing 10% FBS.

### 2.3. Preparation of whole cell lysates and membrane and cytosolic fractions

LS180 cells were cultured in 75 cm flasks as previously described (12). Whole cell extracts were prepared by scraping followed by centrifugation at  $200 \times g$  for 5 min and solubilized on ice for 15 min in solubilization buffer (50 mM Tris-HCl buffer, pH 7.4, containing 1% NP40, 2 mM EDTA, 100 mM NaCl, 10 mM sodium orthovanadate, 1 mM PMSF, and protease inhibitors). Supernatants were obtained from solubilized cells by centrifugation at  $17,000 \times g$  for 10 min. Protein concentrations were measured using Bradford reagent (Bio-Rad, Hercules, CA). Membrane and cytosolic fractions were prepared using the Mem-PER membrane protein isolation kit (Thermo Fisher Scientific) according to manufacturer's instructions.

### 2.4. Western blot analyses

Solubilized proteins (10 µg) from LS180 cells were separated by sodium dodecyl sulfate-polyacrylamide gel electrophoresis (SDS-PAGE) and transferred onto poly vinylidene difluoride (PVDF) membranes. The membrane was blocked with 3% BSA in 50 mM Tris-HCl buffer, pH 7.4, containing 0.15 M NaCl and 0.1% Tween 20 (TBST) for 1 h at room temperature. Western blotting was carried out with primary antibodies as indicated, and then detected with HRP-conjugated secondary antibodies and color development using Ez West blue (ATTO Co., Tokyo, Japan).

### 2.5. Treatment of LS180 cell membrane and cytosolic fractions with N-glycosidase F and Western blotting

Cytosolic and membrane protein fractions were isolated as described above. Fractions (200 µg) were incubated at 90°C for 3 min in 40 µL of PBS containing 0.5% SDS and 1% β-mercaptoethanol. After cooling to room temperature, 0, 1, or 3 U of N-glycosidase F and 10 µL of 5% NP-40 were added. After overnight incubation at 37°C, the reaction was stopped by addition of SDS-PAGE sample buffer (62.5 mM Tris-HCl, pH 8). Cytosolic and membrane fractions (10 µg) were loaded onto a 4-12% gradient Bis-Tris gel (NuPAGE, Thermo Fisher Scientific) and electrophoresed at 170 V for 1 h. Gels were transferred onto PVDF membranes at 50 V for 2 h followed by blocking with 2% blotting-grade blocker (Bio-Rad) in PBS with 0.05% Tween-20. Membranes were immunoblotted with MLS128 or anti-desmocollin (1:1,000) in blocking buffer for 1 h and then washed 3 times with PBS containing 0.05% Tween (wash buffer). Secondary antibodies, goat anti-mouse anti for MLS128 or goat anti-rabbit for anti-desmocollin were added and incubated for 1 h. Membranes were then washed 3 times with the wash buffer and visualized using Clarity Western ECL

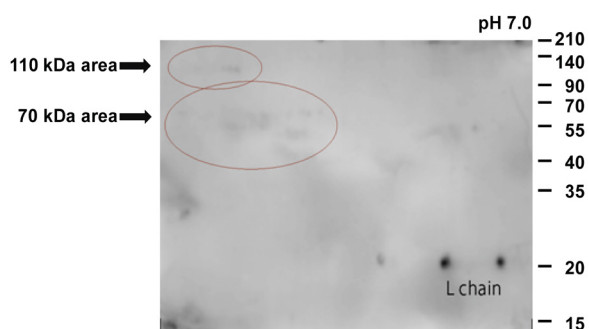


**Figure 1. Western blotting with MLS128 of two-dimensional (2-D) electrophoresis of MLS128-IP sample.** MLS128 antibody was used to IP proteins from  $1.4 \times 10^7$  LS180 cells. Resulting IP samples were subjected to 2-D gel electrophoresis as previously described (13). 1st dimension was conducted at pH 4-7 linear gradient on the 11 cm strip which was placed on 10% SDS-PAGE gel then electrophoresed under reducing conditions. Shown is the Western blotting of the resulting 2D-gel in which very faint positive staining with MLS128 can be seen. Since IgG light chain (L chain) contains O-glycans, and since the MLS128 was used for IP, those are clearly detected.

Substrate (Bio-Rad) with imaging on a ChemiDoc Imaging Station (Bio-Rad).

#### 2.6. 2-D gel electrophoresis and LC-MS/MS analyses

To identify peptides derived from 110 kDa proteins, in-gel digestion and mass spectrometric analyses were performed as previously described (15,16). Immunoprecipitation (IP) of 110 kDa GP was carried out and resulting IP samples were subjected to 2-D gel electrophoresis as previously described (14). The 2-D gels were stained with SimplyBlue SafeStain solution (Life Technologies, Carlsbad, CA) to visualize proteins. Two areas designated in Figure 1 (110 and 70 kDa) were excised and destained in ammonium bicarbonate (100 mM)/acetonitrile (45%) followed by in-gel digestion, which included reduction with Tris(carboxyethyl) phosphine (10 mM), alkylation with iodoacetamide (50 mM) and digestion with Trypsin/Lys-C Mix, Mass Spec Grade (300 ng per band, Promega, Fitchburg, WI), in 100 mM ammonium bicarbonate, pH 7.9. Extracted peptides were acidified with formic acid (1%) and injected into the LC-MS system.

Mass spectrometric analyses of the digested peptides were conducted on an Orbitrap Fusion Tribrid mass spectrometer (Thermo Fisher Scientific) equipped with an Easynano UHPLC, using a  $75 \mu\text{m} \times 250 \text{ mm}$  Pepmap RSLC reverse phase column with a PepMap 1000 trapping column (Thermo Fisher Scientific). Ten  $\mu\text{L}$  of digested peptide samples were loaded at  $4 \mu\text{L}$  per min. LC was performed with a gradient mobile phase system containing mobile phase A (0.1% formic acid) and mobile phase B (100% acetonitrile/0.1% formic acid). A 40 min gradient was conducted from 3% to 80% B, followed by 45-60 minutes at 90% B. Flow rate was 300 nL/min. Full mass scans (200-4,000 Da)

were collected by the orbitrap mass analyzer, operated at 120K resolution. MS/MS spectra were generated in data-dependent mode using collision-induced dissociation (CID) and the linear trap mass analyzer. The resulting data sets were analyzed with PEAKS Studio (Bioinformatics Solutions Inc., Waterloo, ON, Canada) and Proteome Discoverer (Thermo Fisher Scientific) and matched against a non-redundant human protein database (Swiss Prot and NR). Database searches were carried out by considering three missed enzymatic cleavages, a precursor ion mass tolerance of 5 ppm, and 0.02 Da mass tolerance for fragment ions. Search parameters also included cysteine carbamidomethylation and methionine oxidation as expected amino acid modifications.

#### 2.7. Confocal microscopy for detection of desmocollin and MLS128

Cells were plated at a density of 30,000 cells/well on collagen-coated coverslips in a 24-well plate. Following overnight adherence, media were removed, cells were washed with PBS, and then fixed with 4% paraformaldehyde with 0.2% glutaraldehyde for 30 min at room temperature. Paraformaldehyde was then inactivated by the addition of 25 mM glycine for 10 min at room temperature. Cells were then washed for 5 min three times with PBS containing 0.01% Tween-20 and then blocked for 15 min with 5% BSA in PBS. Blocking buffer was then removed and primary antibodies (anti-desmocollin and MLS128) added at a final dilution of 1:50 with incubation at room temperature for 1 h. It should be noted that while MLS128 recognizes two to three consecutive O-linked GalNAc, the desmocollin antibody (Abcam ab 150382) recognizes an epitope within amino acids 850-950 on the C-terminus of desmocollin. Following incubation, cells were washed for 5 min 3 times with PBS and then secondary antibodies were added at a dilution of 1:100 and incubated overnight at  $4^\circ\text{C}$ . Cells were then washed and coverslips mounted onto Rite-On Frosted Slides (Thermo Fisher Scientific) using Fluoroshield DAPI mounting media (Abcam). Immunofluorescence was detected using a Zeiss LSM 880 confocal microscope with an LCI Plan-Neofluar  $63\times/1.3 \text{ NA}$  Multi-Imm Corr objective (Zeiss). Laser scanning modes used include diode 405 nm, argon Laser 458, 488, and 514 nm, and helium/neon Lasers at 594 and 633 nm. Optical slices were obtained using  $0.7 \mu\text{m}$  intervals. Images were processed using Zen Blue software (Zeiss version 2.3). Colocalization between MLS128 and desmocollin antibodies was determined using Zen Blue. The Pearson correlation coefficient was determined for MLS128 and desmocollin antibodies within each cell. There was a minimum of 100 cells analyzed in three independent experiments. Data is presented as the average Pearson correlation coefficient and standard deviation for all experiments.

### 2.8. siRNA knockdown of desmocollin

LS180 cells were plated at a density of 50,000 cells/well in 24-well plates and allowed to adhere overnight. Desmocollin-targeting siRNAs SASI\_Hs01\_00172856 (siRNA 1, approximate start site nucleotide 388) and SASI\_Hs02\_00338620 (siRNA 2, approximate start site nucleotide 732), as well as non-coding siRNAs were obtained from Sigma-Aldrich (St. Louis, MI). siRNAs were transfected using RNAi max transfection reagent (Thermo Fisher Scientific) according to manufacturer's instructions and incubated for 48 h. Following incubation, RNA was isolated using Trizol (Zymo Research, Irvine, CA) and concentrations determined using NanoDrop™ with absorbance readings at 260 nm (Thermo Fisher Scientific).

The extent of desmocollin knockdown was determined by synthesizing cDNA from isolated RNA (500 ng), dNTPs (40 mM), RNase inhibitor (1U, Promega), random primers (3 µg, Invitrogen, Waltham, MA), reverse transcriptase (200U, BioChain, Newark, CA), and reaction buffer (5× reaction buffer is composed of 250 mM Tris-HCl, pH 8.3, 375 mM KCl, 15 mM MgCl<sub>2</sub>, and 50 mM DTT, BioChain). The cDNA synthesis reaction was performed at 25°C for 10 min, 45°C for 30 min, and 85°C for 5 min. qRT-PCR was performed with primers specific for desmocollin. The forward primer was 5'-TTTGAGTGAGGAGTGTGGCA-3' and the reverse primer sequence was 5'-AAGTTACCGAAGTGTGTGTGT-3'. Tubulin forward (5'-TTCAATCTCCCTCCAAGCTC-3') and reverse (5'-GGGAAGGATTCCAAGTGTGTGT-3') primers were used for normalization. Reactions included cDNA, primers, and Applied Biosystems™ Power SYBR Green PCR Master Mix (Thermo Fisher Scientific) and were performed with initial denaturation at 95°C for 10 min followed by 44 cycles of denaturation (95°C for 15s) and annealing and extension (at 60°C for 30s). Relative gene expression was calculated using cycle threshold values for each gene.

### 2.9. Effects of antibody and siRNA treatment on cell viability

LS180 cells were plated onto 96-well plates at a density

of 104 cells/well in DMEM supplemented with 1% FBS and 4.5 g/L D-glucose. After adhering overnight, cells were treated with increasing amounts of anti-desmocollin, anti-desmoglein, MLS128, or anti-IgG antibodies for 48 h. Following treatment, wells were washed with PBS and then incubated with crystal violet solution (0.5% crystal violet in 25% MeOH) for 10 min at room temperature. Wells were then washed twice with PBS and crystal violet solution, then cells were solubilized by the addition of 1% SDS. Absorbance was measured at 570 nm on a BioTek Synergy 4 spectrophotometer using Gen5 2.09 software (BioTek, Winooski, VT). Cell viability was normalized to IgG control antibody.

To determine viability following siRNA treatment, cells were plated as described above and then treated with increasing concentrations of control, SASI\_Hs01\_00172856 (siRNA1), or SASI\_Hs02\_00338620 (siRNA2) for 48 hr. Viability was then determined using crystal violet analysis as described above.

## 3. Results

### 3.1. 2-D gel electrophoresis and identification of candidate proteins by LC-MS/MS

MLS128-IP samples were prepared from  $1.4 \times 10^7$  LS180 cells and proteins separated using 2-D gel electrophoresis. The gel was transferred and probed with MLS128 antibody. Seven 2-D gels were prepared for further analysis. A typical result of 2-D gel analysis is shown in Figure 1. The areas marked on the Western blot were cut out from seven slightly-stained 2-D gels for proteomic analyses. Fifty µL of peptide digests from A (110 kDa area) and B (70 kDa area) of Gel #1 and #2 were prepared. For the 1st experiment, 10 µL of each sample and for the 2nd and 3rd experiment, twice-concentrated samples were analyzed by LC-MS/MS. The results are summarized in Table 1 and identified protein amino acid sequences are presented in Table 2.

Identified 110 kDa GP candidates include "desmocollin 1", consisting of 894 amino acids with molecular weight (MW) of 99.8 kDa and isoelectric point (pI) of 5.25, "desmoglein 1" consisting of 1049 amino acids, MW of 113.7 kDa, and pI of 4.90, and "junction plakoglobin" containing 745 amino acids,

**Table 1. List of candidates for 110kDa GP detected by an Orbitrap Fusion hybrid mass spectrometer**

Items	Candidate proteins	110 kD area (probability*)	70 kD area
Experiment 1	Desmoglein-1 preproprotein	2 (80-94%)	2 (over 95%)
Experiment 2	Desmoglein-1 preproprotein	2 (over 95%)	7 (over 95%)
	Desmocollin-1	2 (80-94%)	2 (over 95%)
Experiment 3	Junction plakoglobin	1 (over 95%)	2 (over 95%)
	Junction plakoglobin	1 (80-94%)	3 (over 95%)
	Desmoglein-1 preproprotein	4 (over 95%)	2 (over 95%)
	Desmocollin-1		3 (over 95%)

\*protein probability values as calculated by Scaffold proteome software at 1% protein FDR.

**Table 2. Examples of peptide sequences derived from the candidate proteins**

Protein	Peptide	Amino acids
Desmocollin	IEDDNDNAPYFEHR	232-245
Desmocollin	VTATDLDEPDTLHTR	264-278
Desmocollin	VQDQDLNTPHSK	377-389
Desmoglein	IHSDCAANQQVTYR	73-86
Desmoglein	ISGVGIDQPPYGIFVINQK	87-105
Desmoglein	IIRQEPSDSPMFIINR	198-213
Desmoglein	TMNNFLDREQYGQYALAVR	220-238
Desmoglein	TYVVTGNMGSNDK	391-303
Desmoglein	DGGADGMSAECECNK	243-258
Desmoglein	YVMGNNPADLLAVDSR	423-438
Desmoglein	ESSNVVVTER	916-925
Junction plakoglobin	SAIVHLINYQDDAELATR	125-142
Junction plakoglobin	LLNDEDPVVVTK	150-161
Junction plakoglobin	TMQNTSDLDTAR	192-293
Junction plakoglobin	ISEDKNPDYR	652-661

MW of 81.74 kDa, and pI of 5.75. In addition to similar MW and pI expected for the 110 kDa GP, all three candidates contain potential O-glycosylation sites for MLS128 recognition. In addition, two candidates, desmocollin and desmoglein, contain potential N-glycosylation sites which are known to be present in the 110 kDa GP [(12), Figure 6 in this article]. Desmocollin contains 12 potential MLS128 binding sites along with two N-glycosylation sites. Desmoglein contains 22 potential MLS128 binding sites and 3 N-glycosylation sites. Junction plakoglobin has 13 potential MLS128 binding sites but no N-glycosylation sites. Thus, we focused on desmocollin and desmoglein for the following studies.

### 3.2. MLS128 and desmocollin antibodies bind a 110 kDa protein

Western blotting analyses of LS180 cell lysates showed both MLS128 and desmocollin antibodies recognized a 110 kDa band (Figure 2A and 2B), whereas the desmoglein antibody did not (Figure 2C). These results suggested that desmocollin was the best candidate for the 110 kDa GP.

### 3.3. MLS128 colocalizes with desmocollin in LS180 cells

To determine if MLS128 and desmocollin antibodies colocalize, immunofluorescence microscopy was performed using LS180 colon cancer cells as well as breast cancer (MCF7) and normal mammary epithelial (MCF10A) cell lines. In LS180 cells, desmocollin was localized to the membrane and showed significant colocalization with the MLS128 antibody (Figure 3A upper panel and 3B). Desmoglein, however, showed more diffuse staining throughout the cytoplasm and had lower correlation for colocalization (Figure 3A lower panel and B). The breast cancer cell line MCF7 showed significantly lower levels of staining with anti-

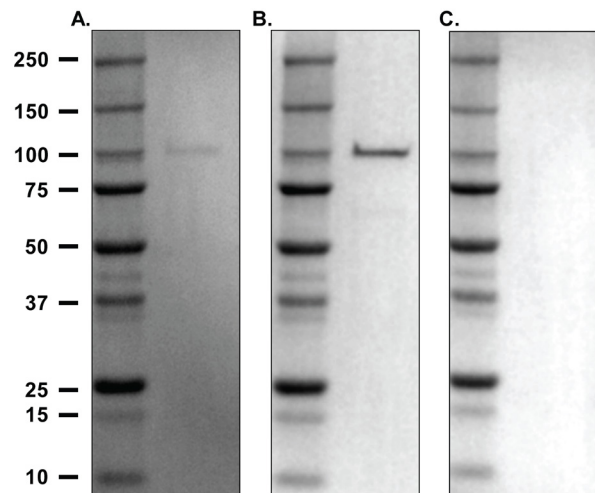


**Figure 2. MLS128 and desmocollin antibodies recognized a 110 kDa protein.** LS180 cell lysates were prepared and analyzed by Western blotting with MLS128 antibody (A) anti-desmocollin (B), and anti-desmoglein (C).

desmocollin and anti-desmoglein compared to LS180 cells (Figure 3C). Interestingly, the normal breast epithelial line MCF10A showed no staining by anti-desmocollin, anti-desmoglein, or MLS128 antibodies (Figure 3D). Since desmosomes, together with adherens junctions, represent the major adhesive cell-junctions of epithelial cells, it was expected that human normal mammary epithelial MCF10A cells should be expressing desmosomal proteins. Why we did not detect desmosomal proteins may in fact be due to the cells being sparsely grown instead of tightly associated. It is notable that MCF7 but not MCF10A cells express MLS128 receptors, which is consistent to previous observations by Western blotting (13). Above-mentioned experiments showing colocalization of MLS128 and anti-desmocollin suggested that desmocollin may be the 110 kDa protein recognized by the MLS128 antibody or may be associated with this protein.

### 3.4. Effect of desmocollin antibody or siRNA treatment on LS180 cell viability

Previously, we reported LS180 cell growth is inhibited by MLS128 (13), therefore, we investigated if treatment with desmocollin or desmoglein antibodies also decreases LS180 cell growth. LS180 cells were treated with increasing concentrations of anti-desmocollin, anti-desmoglein, or MLS128 antibody for 48 hr. Crystal violet staining was used to determine cell viability. While all antibodies were cytotoxic, the desmocollin antibody was the most cytotoxic, displaying a 20-times lower IC<sub>50</sub> compared to MLS128 and desmoglein antibodies (Figure 4).

To further investigate the role of desmocollin in LS180 cell viability, we transfected cells with two siRNAs targeting desmocollin (see Methods for sequence). Transfection was performed for 48 h and

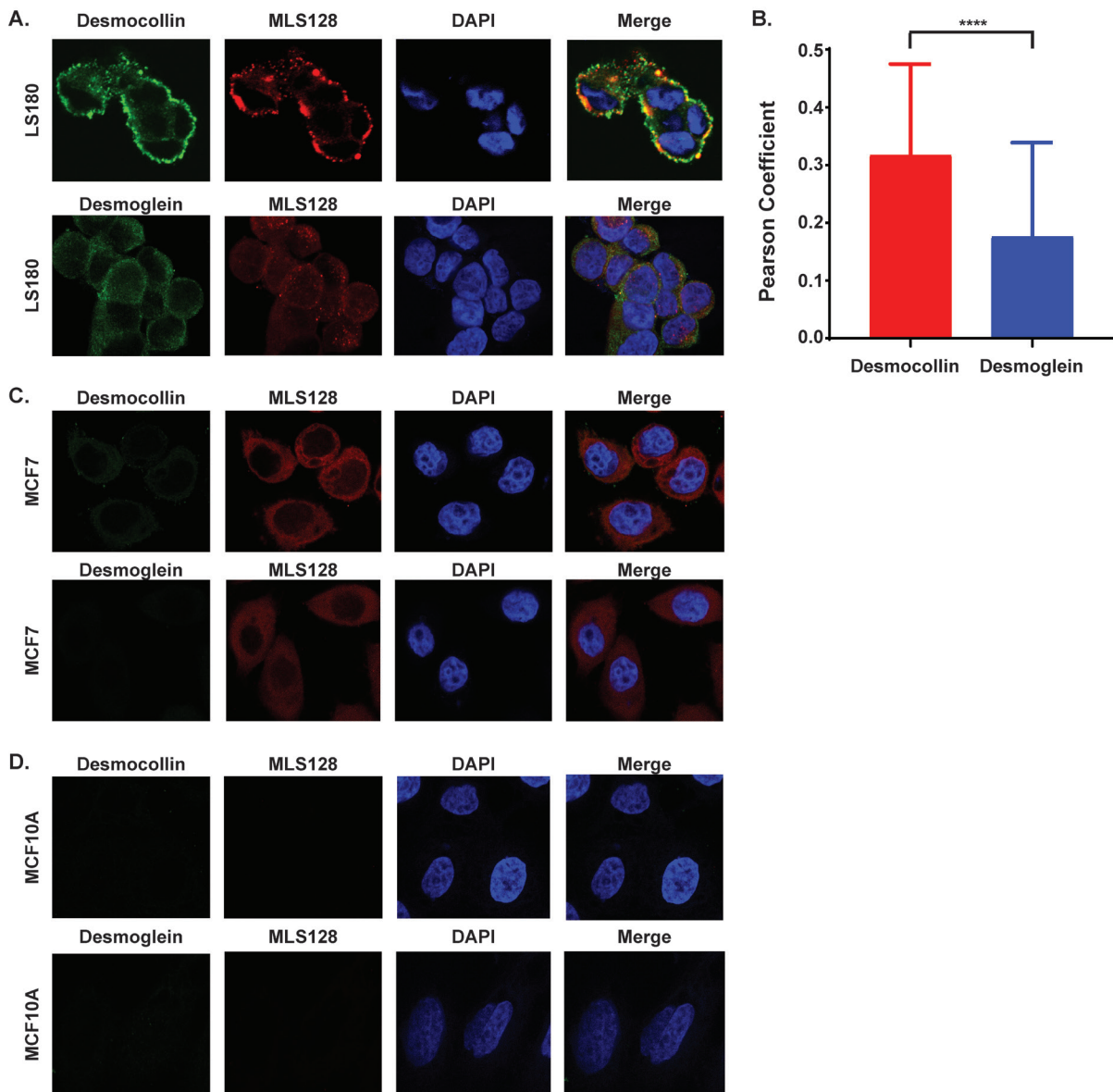


**Figure 3. Immunofluorescence staining of LS180, MCF-7, and MCF-10A cells suggests colocalization of anti-desmocollin and MLS128 antibodies.** Cells were stained with anti-desmocollin or anti-desmoglein (green) along with MLS128 (red) antibodies (A, C, D). (A) shows the immunostaining of LS180 cells; (B) Colocalization was determined using Zen Blue software with calculation of Pearson correlation coefficients. Average coefficients and standard deviations were calculated from a minimum of 100 cells in three independent experiments (C) and (D) represent the immunostaining of MCF-7 and MCF-10A, respectively.

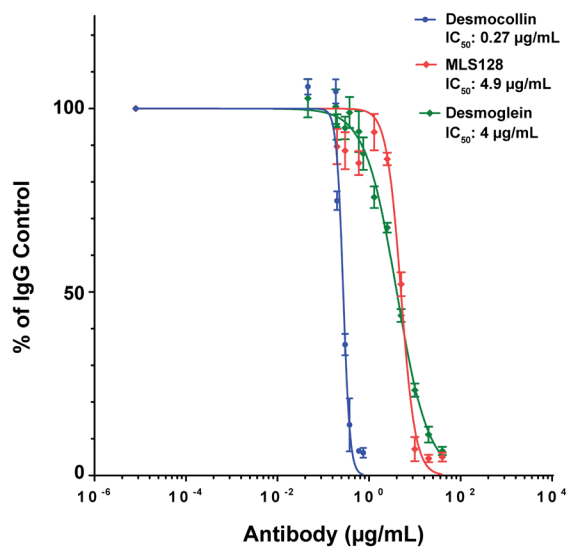


**Figure 4. Treatment of anti-desmocollin, anti-desmoglein, and MLS128 antibodies on LS180 cell decreased viability.** LS180 cells were treated with increasing amounts of each antibody and viability measured using crystal violet. Viability was normalized to treatment with an IgG control antibody.

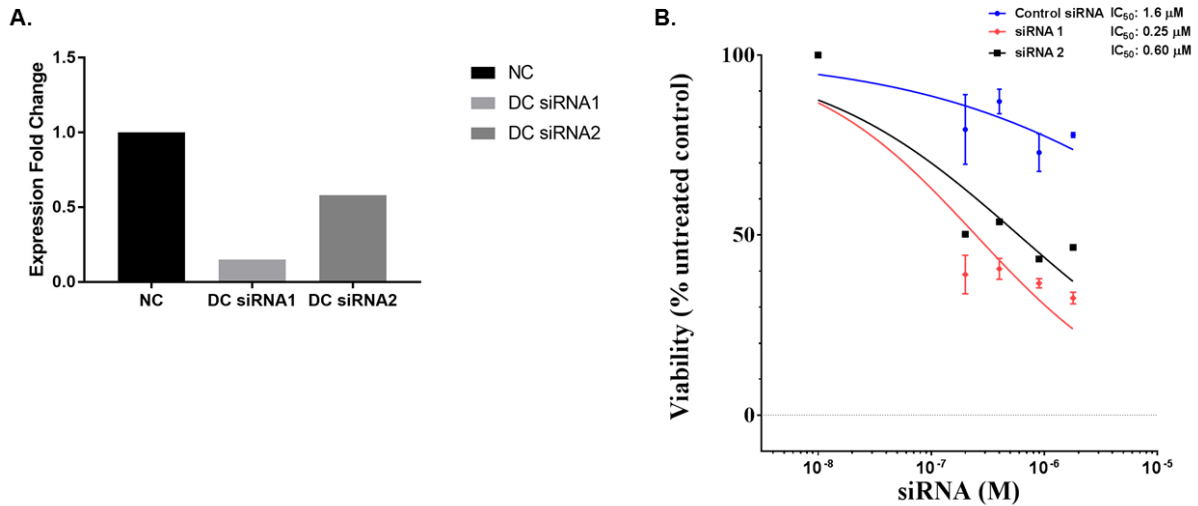


**Figure 5. Desmocollin siRNA decreased LS180 cell viability.** (A), LS180 cells were treated with control scramble or two different desmocollin siRNAs for 48 hr. A. siRNA1 and siRNA2 decreased desmocollin expression by ~90% and ~50%, respectively. (B), LS180 cells were treated with increasing amounts of control or desmocollin siRNAs for 48 hr. Viability was determined using crystal violet and was normalized to untreated control.

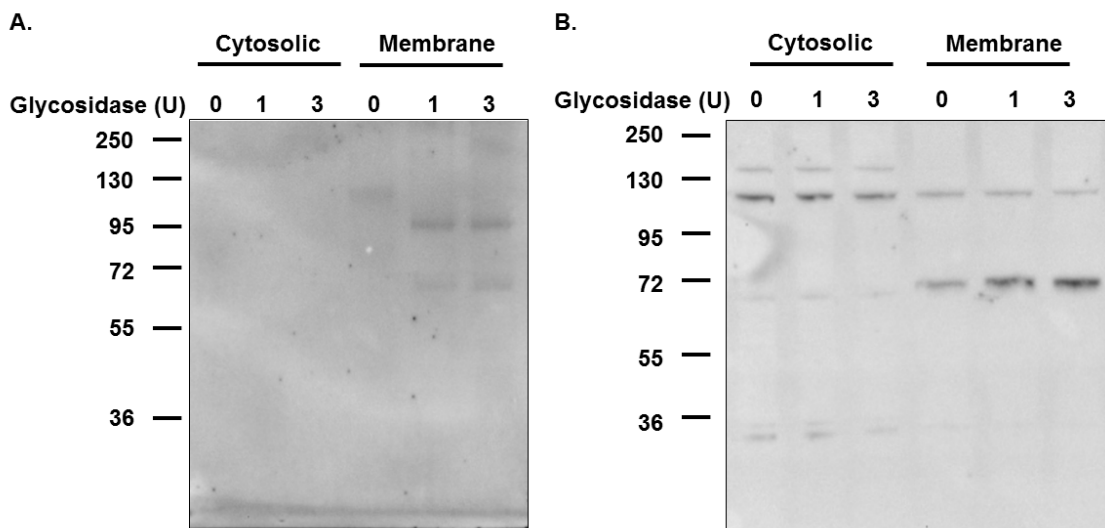


**Figure 6. N-glycosidase F digestion and Western blotting analyses of cytosolic and membrane fractions of LS180 colon cancer cells suggest the presence of N-glycosylation in both the 110 kDa GP and desmocollin.** Both fractions were treated with N-glycosidase F (0, 1, or 3 unit) and then analyzed by Western blotting with MLS 128 (A) or anti-desmocollin (B).

then qPCR was used to quantify mRNA transcript levels. siRNA1 targeting desmocollin decreased mRNA levels by ~90% while siRNA2 only decreased levels by ~50% (Figure 5A). We next analyzed how the treatment with siRNAs affected cell viability. We found that cells transfected for 48 h with siRNA targeting desmocollin were less viable than those treated with scrambled siRNA. In accordance with the PCR data, siRNA1 had an IC<sub>50</sub> value three times lower than siRNA2 (Figure 5B).

### 3.5. The 110 kDa GP and desmocollin contain N-glycosylation modifications

LS180 membrane and cytosolic fractions were digested

with N-Glycosidase F followed by Western blotting with MLS128 or anti-desmocollin. A 110 kDa protein was recognized in the membrane fraction by both the MLS128 and desmocollin antibodies. Following glycosidase treatment, bands recognized by MLS128 decreased in size to ~95 and 70 kDa (Figure 6A); while the desmocollin antibody recognized two bands at 110 and 70 kDa (Figure 6B). Following N-glycosidase treatment, the 110 kDa band intensity decreased slightly while the 70 kDa band intensity increased (Figure 6B). This result suggested that the 110 kDa band recognized by both desmocollin and MLS128 antibodies may both have N-glycosylation sites, but whether the 110 kDa recognized by anti-desmocollin represents the same GP bound by MLS128 requires further study.

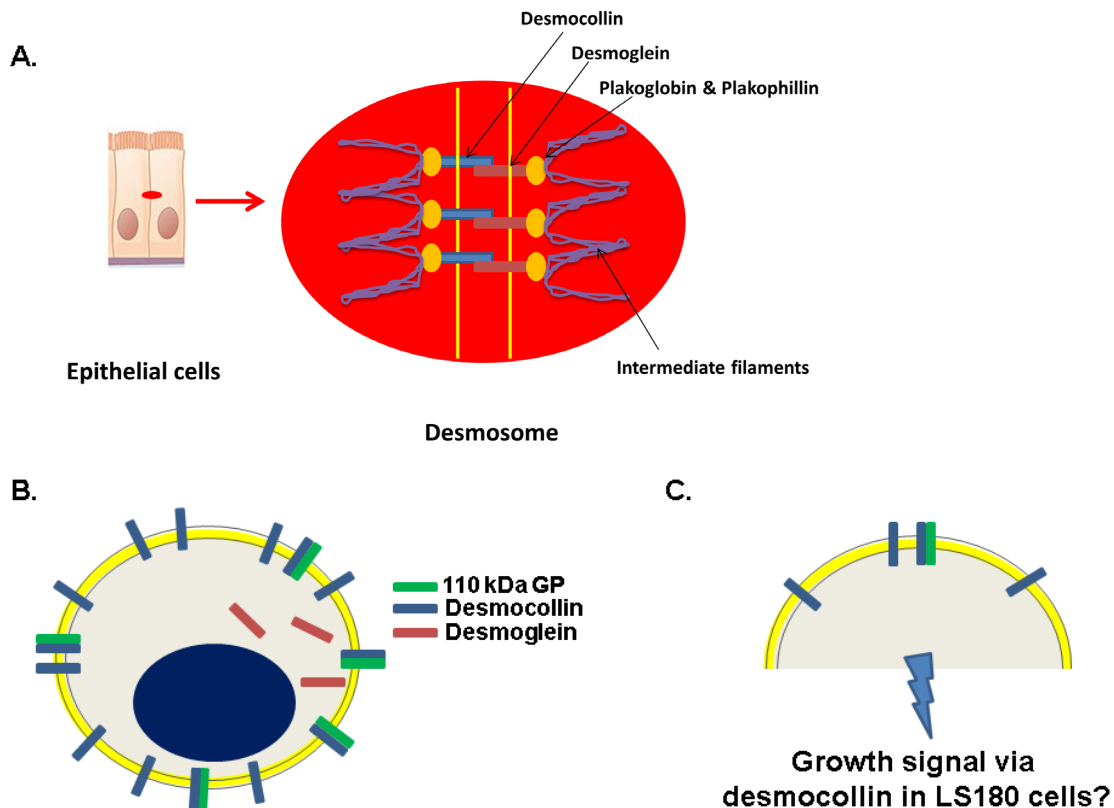


**Figure 7. Potential roles of desmocollin and 110 kDa GP in LS180 colon cancer cell growth.** (A), a desmosome structure in non-cancerous epithelial cells is illustrated. (B), desmocollin (light blue), 110 kDa GP (green), and desmoglein (pale red) in LS180 cells are highlighted to reflect the results of this study. (C) illustrates our hypothesis that LS180 cell growth is mediated by desmocollin and 110 kDa GP. Other illustrations include desmosome (red), plakoglobin (orange), intermediate filaments (purple), nuclei (blue) and cell membranes (yellow).

#### 4. Discussion

Western blotting of LS180 and HT29 colon cancer cells with MLS128 antibody clearly showed the detection of a 110 kDa protein (12,14). Purification of the 110 kDa GP from these cells, however, has been unsuccessful although our laboratory has extensive experience in affinity chromatography (17).

This study thus used a very sophisticated and sensitive mass spectrometry method that can detect extremely low peptide levels. Three desmosome proteins as illustrated in Figure 7A were identified using this method, and among these, desmocollin had characteristics similar to the 110 kDa GP. It has a molecular weight of ~110 kDa, contains putative Tn-antigen sites that can be recognized by MLS128, and contains N-glycosylation sites. Desmoglein was another candidate protein that also shared these characteristics, but the desmoglein antibody did not recognize a 110 kDa band in Western blot analysis (Figure 2C). Immunofluorescence microscopy of LS180 cells revealed that desmocollin was membrane-bound while desmoglein was localized to the cytosol (Figure 3A). This indicated random dispersion of desmosome components on the cell membrane and in the cytosol in LS180 colon cancer cells, whereas in normal cells

desmocollin and desmoglein hold epithelial cells in tight association (Figure 7B). Many of the membrane-bound desmocollin proteins were colocalized with the MLS128 binding molecules as clearly seen in the merged panel of Figure 3A. Statistical analysis of Pearson correlation coefficients revealed significant colocalization between desmocollin and MLS128 antibodies (Figure 3B).

We demonstrated that blocking desmocollin function by antibody or siRNA decreased cell viability, suggesting a critical role for desmocollin in LS180 cell growth and survival. Colocalization of MLS128 and desmocollin antibodies suggested either that some but not all desmocollin molecules contained Tn-antigens recognized by MLS128, or that the 110 kDa GP was associated with desmocollin. These results provide new insight into how MLS128 antibody inhibits colon cancer cell growth.

We previously reported that MLS128 binding to its receptor on LS180 cells caused downregulation of the IGF-I receptor, involved in cell growth and survival, and that both 110 kDa GP and IGF-I receptor were colocalized in microdomains (14). The previous study thus suggested that MLS128 treatment resulted in modulation of the signaling molecules localized in the microdomains. New findings from this study suggest that growth inhibition by MLS128 antibody treatment

is likely to be mediated by desmocollin (Figure 7C). It is plausible to state that although desmocollin functions in keeping epithelial cells adhered, in colon cancer cells it plays another important role in promoting cell growth and survival. Consistent with our hypothesis, previous studies by other groups supported that loss of desmosome adhesion is a prerequisite for the epithelial-mesenchymal transition, implicating epithelial cell invasion and metastasis (18), and that modulation in expression levels of the three desmocollin subtypes could play an important role in colorectal cancer (19).

In summary, our goal to identify the 110 kDa GP has not been completed. It is possible that we may have missed 110 kDa GP-derived peptides for the following reason. Since heavy O- and N-glycosylations are anticipated, the enzyme-specific cleavage sites of 110 kDa GP may not be accessible to digestion by Trypsin/Lys-C, resulting in no elution of its peptides from the 2-D gels. Alternatively, glycosylated peptides may not produce sufficient sequence information in the CID MS/MS experiments conducted. This study, however, provides an attractive working hypothesis that growth inhibition induced by MLS128 antibody is mediated via the 110 kDa GP/desmocollin dimer or association of the two molecules in microdomains.

### Acknowledgements

We thank Fmie Oura and Dr. Tetsu Akiyama for their contributions to preparing MLS128 IP samples. This work was supported by grants (17570120 and 22570125) from Japan Society for the Promotion of Science. We also thank Dr. Brian Armstrong, Loren Quintanar, and Michael Nelson for their assistance using the Light Microscopy Core facility at the Beckman Research Institute. The Mass Spectrometry & Proteomics Core facility of City of Hope was supported in parts by the National Cancer Institute of the National Institutes of Health under award number P30CA033572.

### References

- Nakada H, Inoue M, Numata Y, Tanaka N, Funakoshi I, Fukui S, Mellors A, Yamashina I. Epitopic structure of Tn glycoprotein A for an anti-Tn antibody (MLS 128). *Proc Natl Acad Sci U S A*. 1993; 90:2495-2499.
- Nakada H, Numata Y, Inoue M, Tanaka N, Kitagawa H, Funakoshi I, Fukui S, Yamashina I. Elucidation of an essential structure recognized by an anti-GalNAc alpha-Ser(Thr) monoclonal antibody (MLS 128). *J Biol Chem*. 1991; 266:12402-12405.
- Osinaga E, Bay S, Tello D, Babino A, Pritsch O, Assemat K, Cantacuzene D, Nakada H, Alzari P. Analysis of the fine specificity of Tn-binding proteins using synthetic glycopeptide epitopes and a biosensor based on surface plasmon resonance spectroscopy. *FEBS Lett*. 2000; 469:24-28.
- Matsumoto-Takasaki A, Hanashima S, Aoki A, Yuasa N, Ogawa H, Sato R, Kawakami H, Mizuno M, Nakada H, Yamaguchi Y, Fujita-Yamaguchi Y. Surface plasmon resonance and NMR analyses of anti Tn-antigen MLS128 monoclonal antibody binding to two or three consecutive Tn-antigen clusters. *J Biochem*. 2012; 151:273-282.
- Springer GF. Immunoreactive T and Tn epitopes in cancer diagnosis, prognosis, and immunotherapy. *J Mol Med (Berl)*. 1997; 75:594-602.
- Yu LG. The oncofetal Thomsen-Friedenreich carbohydrate antigen in cancer progression. *Glycoconj J*. 2007; 24:411-420.
- Avichezer D, Springer GF, Schechter B, Arnon R. Immunoreactivities of polyclonal and monoclonal anti-T and anti-Tn antibodies with human carcinoma cells, grown in vitro and in a xenograft model. *Int J Cancer*. 1997; 72:119-127.
- Wang BL, Springer GF, Carlstedt SC. Quantitative computerized image analysis of Tn and T (Thomsen-Friedenreich) epitopes in prognostication of human breast carcinoma. *J Histochem Cytochem*. 1997; 45:1393-1400.
- Fujita-Yamaguchi Y. Renewed interest in basic and applied research involving monoclonal antibodies against an oncofetal Tn-antigen. *J Biochem*. 2013; 154:103-105.
- Numata Y, Nakada H, Fukui S, Kitagawa H, Ozaki K, Inoue M, Kawasaki T, Funakoshi I, Yamashina I. A monoclonal antibody directed to Tn antigen. *Biochem Biophys Res Commun*. 1990; 170:981-985.
- Babino A, Pritsch O, Opezzo P, Du Pasquier R, Roseto A, Osinaga E, Alzari PM. Molecular cloning of a monoclonal anti-tumor antibody specific for the Tn antigen and expression of an active single-chain Fv fragment. *Hybridoma*. 1997; 16:317-324.
- Oura F, Yajima Y, Nakada M, Taniue K, Akiyama T, Nakada H, Yamamoto K, Fujita-Yamaguchi Y. Susceptibility to proteases of anti-Tn-antigen MLS128 binding glycoproteins expressed in human colon cancer cells. *Biosci Trends*. 2015; 9:49-55.
- Morita N, Yajima Y, Asanuma H, Nakada H, Fujita-Yamaguchi Y. Inhibition of cancer cell growth by anti-Tn monoclonal antibody MLS128. *Biosci Trends*. 2009; 3:32-37.
- Zamri N, Masuda N, Oura F, Kabayama K, Yajima Y, Nakada H, Yamamoto K, Fujita-Yamaguchi Y. Characterization of anti-Tn-antigen MLS128 binding proteins involved in inhibiting the growth of human colorectal cancer cells. *Biosci Trends*. 2013; 7:221-229.
- Murai K, Sun G, Ye P, *et al*. The TLX-miR-219 cascade regulates neural stem cell proliferation in neurodevelopment and schizophrenia iPSC model. *Nat Commun*. 2016; 7:10965.
- Tew BY, Hong TB, Otto-Duessel M, Elix C, Castro E, He M, Wu X, Pal SK, Kalkum M, Jones JO. Vitamin K epoxide reductase regulation of androgen receptor activity. *Oncotarget*. 2017; 8:13818-13831.
- Fujita-Yamaguchi Y. Affinity chromatography of native and recombinant proteins from receptors for insulin and IGF-I to recombinant single chain antibodies. *Front Endocrinol (Lausanne)*. 2015; 6:166.
- Chidgey M, Dawson C. Desmosomes: A role in cancer? *Br J Cancer*. 2007; 96:1783-1787.
- Khan K, Hardy R, Haq A, Ogunbiyi O, Morton D, Chidgey M. Desmocollin switching in colorectal cancer. *Br J Cancer*. 2006; 95:1367-1370.

(Received March 20, 2019; Revised May 22, 2019; Accepted May 28, 2019)

# Conserved amino acids around the DIII-DI linker region of the Newcastle disease virus fusion protein are critical for protein folding and fusion activity

Miaomiao Chi<sup>1</sup>, Wenyan Xie<sup>2</sup>, Ying Liu<sup>1</sup>, Chi Zhang<sup>1</sup>, Yaqing Liu<sup>1</sup>, Hongling Wen<sup>1</sup>, Li Zhao<sup>1</sup>, Yanyan Song<sup>1</sup>, Na Liu<sup>1</sup>, Lianli Chi<sup>3</sup>, Zhiyu Wang<sup>1,4,\*</sup>

<sup>1</sup> Department of Virology, School of Public Health, Shandong University, Ji'nan, Shandong, China;

<sup>2</sup> Department of Laboratory Medicine, Shandong Provincial Qianfoshan Hospital, Shandong University, Ji'nan, Shandong, China;

<sup>3</sup> State Key Laboratory of Microbial Technology, National Glycoengineering Research Center, Shandong University, Ji'nan, Shandong, China;

<sup>4</sup> The Key Laboratory for Experimental Teratology of the Ministry of Education, Shandong University, Ji'nan, Shandong, China.

## Summary

Newcastle disease virus (NDV), an avian paramyxovirus, causes Newcastle disease (ND) which is a highly contagious and fatal viral disease affecting poultry and most species of birds. The fusion (F) protein of NDV mediates membrane fusion, which is essential to the processes of viral entry, replication, and dissemination. Although several domains of NDV F are known to have important effects on regulating the membrane fusion activity, the role of the region around domain III (DIII) and domain I (DI) still remains ill-defined. Site-directed mutagenesis was utilized to change the conserved amino acids at 269, 274, 277, 286, 287, 290, 295, and 297 to alanine in order to investigate the effects of these conserved amino acids around the DIII and DI linker region of the NDV F protein on fusion activity. It was found that five of these substitutions almost abolished fusion activity except for mutants I269A, Q286A, and N297A, which showed 57.1%, 161.1%, and 97.7% of the wt F level, respectively. Four (I274A, D277A, V287A, and P290A) of these five mutants likely result in interfering with folding or transporting of the molecule since these proteins were minimally expressed at the cell surface, formed aggregates, or not proteolytically cleaved. However, mutant L295A almost abolished fusion activity even with a similar level of cell surface expression. These data indicated that conserved amino acids around the DIII-DI linker region are critical for the folding of the F protein and have an important influence on fusion activity.

**Keywords:** NDV, F protein, Membrane fusion, Protein folding and transport

## 1. Introduction

Newcastle disease virus (NDV) causes fatal infections in chicken (1), resulting in huge economic losses to the poultry industry. Current vaccination strategies are not fully efficacious and the development of new concepts for vaccine generation are needed since multiple outbreaks still occur worldwide (2) and NDV strains

have been isolated from vaccinated chicken flocks (1). To develop new vaccines or therapeutic drugs, it is necessary to further clarify the fusion process caused by NDV.

Two viral surface glycoproteins, the hemagglutinin-neuraminidase (HN) protein and the fusion (F) protein, work together to accomplish the process of viral entry of NDV (3,4). HN glycoprotein is responsible for NDV's recognizing and binding to its target cells (5), whereas the F protein is the ultimate performer of membrane fusion, involved in the merger of the host-cell plasma membranes (6,7).

The NDV F protein, which belongs to type I integral membrane proteins (8), is initially synthesized as an inactive precursor, designated F<sub>0</sub>, which is then

Released online in J-STAGE as advance publication May 28, 2019.

\*Address correspondence to:

Dr. Zhiyu Wang, Department of Virology, School of Public Health, Shandong University, Ji'nan 250012, Shandong, China.  
E-mail: zhiyu.wang@sdu.edu.cn



*al.* (14) can induce fusion without the HN protein. In addition, mutant L268A, which can attenuate F protein fusion, is also located around this region. Yin *et al.* (13) suggested an important site 304 in the NDV F protein around this region, corresponding to site 290 in parainfluenza virus 5 (PIV5) F, which is the determinant of the HN independent fusion induced by PIV5 F. Also, the amino acids of this segment are considered to be a key region that constitutes the radial channels (15) of the head of the F protein, which play an important role in the docking of FP.

Conserved sites were found around this junction region (peptide 268-304) by sequence alignment of the F protein from NDV, hPIV3, and PIV5 (Figure 1B), and we speculated that these amino acids were conserved due to important roles in the folding or fusion function of the F protein. To address this, mutational analysis of conserved amino acids between L268 and E304 was performed.

The alanine residue was introduced into sites I269, I274, D277, Q286, V287, P290, L295, and N297 with site-directed mutagenesis. The effects on the fusion activity, cell surface expression, and cleavage activity of each mutated F protein were examined. As a result, most of the mutants had a decreased fusogenic activity except for mutants Q286A and N297A. This decreased fusogenic activity may likely result from interfering with folding or transport of the molecule since most mutated proteins were minimally expressed at the cell surface. The results indicated that conserved amino acids around the DIII and DI junction are critical to the F protein's proper folding, transport, and membrane fusion activity.

## 2. Materials and Methods

### 2.1. Homology modeling

The structure of the NDV F protein in the pre-fusion conformation was generated based on the pre-fusion PIV5 F protein (16) (PDB ID 2B9B) on the SWISS-MODEL protein-modeling server (17). 2B9B was chosen as a template to generate the trimerical structure of NDV F because of its better coverage with NCBI Blast.

### 2.2. Cell lines and viruses

BHK-21 cells, obtained from the American Type Culture Collection, were maintained in Dulbecco's modified Eagle's medium (DMEM) (Biological Industries (BI), Beit-Haemek, Israel) supplemented with 1% (v/v) glutamine, 10% (v/v) fetal calf serum (FCS) (BI), and 1% (v/v) penicillin-streptomycin (BI). The wild type (wt) vaccinia virus was used as a control to quantify cell fusion, while the recombinant vaccinia virus was used to provide the T7 RNA polymerase for the vaccinia-T7 RNA polymerase (vTF7-3) expression system.

### 2.3. Site-directed mutagenesis

Complementary oligonucleotide primers (Sangon Biotech Co. Ltd., Shanghai, China) with the appropriate sequence of the NDV F gene were designed to mutate these identified conserved amino acids. Overlapping PCR was used to produce each pair of the recombinant plasmids. Two products with a short homologous sequence were co-transformed into *Escherichia coli* DH5 $\alpha$  cells, where they recombined to form a complete plasmid. All mutants were sequenced to verify that the mutations were successful.

### 2.4. Syncytium formation assay

BHK-21 cells were placed into 24-well plates 12 h before transfection. At 80% confluence, the cells were co-transfected with wt F or F mutant genes along with the NDV HN gene or the empty vector after incubation with the recombinant vaccinia virus 1h earlier at 37°C. At 24 h post transfection, monolayers were stained with Giemsa solution for syncytia observation under an inverted microscope (Olympus, Tokyo, Japan). Syncytia are cells with three or more nuclei.

### 2.5. Content mixing assay

To quantify the fusion activities mediated by different F mutants, a modified reporter gene assay was performed as previously described (18,19). Briefly, monolayers of BHK-21 cells infected with the recombinant vaccinia virus 1 h earlier at 37°C were co-transfected with the desired F and NDV HN genes. Monolayers of BHK-21 target cells infected with the wild-type vaccinia virus at a MOI of 10 1 h earlier at 37°C were transfected with 1  $\mu$ g of plasmid pG1NT7  $\beta$ -gal which encodes  $\beta$ -galactosidase. Following a 16 h incubation at 37°C, equal numbers ( $1 \times 10^5$ ) of the effector and target cells were combined in duplicate wells of a 96-well microtiter plate. After 7 h incubation at 37°C, the cells were assayed for  $\beta$ -galactosidase activity according to the procedures of the  $\beta$ -galactosidase assay kit (Beyotime Biotechnology, Shanghai, China). The level of fusion was quantified by subtracting background fusion of BHK-21 cells transfected with comparable amounts of the vector or only wt F.

### 2.6. Dye transfer assay of lipid mixing

The abilities of NDV F mutants and wt F to mediate lipid mixing were assessed by the transfer of octadecyl rhodamine b chloride (R18) (Invitrogen, California, USA) (20) from chicken red blood cells (RBCs) to BHK-21 cells co-transfected with NDV F and HN genes, using a modification of a protocol described by Bagai *et al.* (21). At 24 h post transfection, cell monolayers co-expressing the wt or mutated F and their

HN protein were washed and incubated with 50 mU/mL of neuraminidase (Sigma Chemical Co., St. Louis, Mo., USA) at 37°C for 1 h. Then the R18-labeled RBCs were added and incubated at 4°C for 30 min. Unbound RBCs were washed, and then the plate was incubated at 37°C for 1 h to initiate fusion. A fluorescent microscope (Olympus) was used to photograph the events of lipid mixing.

### 2.7. Indirect immunofluorescence assay (IIFA)

BHK-21 cells were seeded into 24-well plates and transfected with wt F and F mutant genes. The monolayers were fixed with 4% paraformaldehyde after 24 h transfection, then incubated with anti-NDV antiserum (Abcam, Cambridge, UK) and a goat anti-chicken Alexa Fluor 488-conjugated immunoglobulin Y (H + L) (Abcam) was used as the secondary antibody. Photographs of the cells were taken under a fluorescent microscope (Olympus) after the secondary antibody was washed twice with cold PBS.

### 2.8. Flow cytometry analysis

Fluorescence-activated cell sorter (FACS) analysis was used to assay the cell surface expression of the wt F and each mutated F proteins as previously described (22). At 24 h post transfection, the monolayers were removed from plates by treatment with 5 mM EDTA in PBS, pelleted by centrifugation, washed twice, and blocked with PBSA (PBS with 3% bovine serum albumin) for 30 min on ice. The primary antibody and the secondary antibody were the same those as used in the IIFA assay. Then, the cells were fixed with 4% paraformaldehyde and re-suspended in 0.4 mL of PBSA for analysis with the CytoFLEX S Flow Cytometer (Beckman Coulter, Inc., California, USA). Cells transfected with only the vector were used as negative controls.

### 2.9. Western blot (WB)

To examine the cleavage activity of wt F and F mutants, BHK-21 cells were transfected with wt F and F mutant plasmids using a standard transfection protocol. At 24 h post transfection, cell monolayers were removed from the 12-well plate by treatment with 50 mM EDTA in PBS, pelleted, and then lysed. Polypeptides were analyzed under a nonreducing condition using 10% SDS-PAGE without boiling. Anti-NDV antiserum recognizing the NDV F protein (Abcam) and an IRDye® 800CW donkey anti-chicken IgG (H + L) (LI-COR, Lincoln, Nebraska, USA) as the second antibody were used, and then the protein bands were scanned and visualized using Odyssey (LI-COR). To test for expression of D277A-His, an anti-His antibody (Proteintech, Wuhan, Hubei, China) and an IRDye® 800CW goat anti-mouse IgG (H + L) (LI-COR) were used.

### 2.10. Statistical analysis

All results were from at least three separate experiments and indicated as the mean  $\pm$  SD. Statistical analysis was calculated by SPSS 17.0 using the Student's *t* test with a significance level of  $p < 0.05$  (\*),  $p < 0.01$ (\*\*) and  $p < 0.001$  (\*\*\*), respectively.

## 3. Results

### 3.1. Identification and mutagenesis of conserved amino acid residues around the DIII-DI linker region of the NDV F protein

In order to identify the conserved amino acid residues around the DIII-DI linker region of the F protein, sequences from NDV, hPIV3, and PIV5 F proteins were aligned and analyzed. Eight conserved amino acid residues were found and site-directed mutagenesis was utilized to mutate to alanine at these sites (I269, I274, D277, Q286, V287, P290, L295, and N297) in order to determine the function for these conserved sites around the DIII-DI linker in the NDV F protein (Figure 1B).

The NDV F protein in the pre-fusion conformation was generated based on the pre-fusion PIV5 F protein (16) (PDB ID 2B9B) on the SWISS-MODEL protein-modeling server. These conserved sites were exhibited on the NDV F homology modeling structure (Figures 1C and 1D). Most of these sites were located within the F protein, while sites L295 and N297 were situated on the surface of this protein (Figure 1D).

### 3.2. Fusion activity assessment for wt F and its mutants

In order to explore the effects of these single amino acid substitutions of the conserved amino acids around the DIII-DI linker region of the NDV F protein on their fusogenic activity, three different types of membrane fusion assays were done.

The syncytium formation was initially observed to evaluate an overall level of cell-cell fusion. NDV wt or mutated F proteins were co-expressed in BHK-21 cells with their homologous HN protein. At 24 h post transfection, an inverted microscope was used to observe multinucleated giant cells and representative photomicrographs of syncytia are shown in Figure 2A. The cells expressing only the NDV wt F protein were used as negative controls. It was found that fewer syncytia were formed by mutant I269A compared with those produced by wt F and HN proteins. However, mutants I274A, P290A, and L295A had very limited ability to form syncytia and no syncytia were observed for mutants D277A and V287A. Only mutant Q286A produced significantly larger syncytia than wt F, while N297A did not affect the formation of syncytia. These results suggested that most of these mutants impaired the formation of syncytia except for mutants Q286A

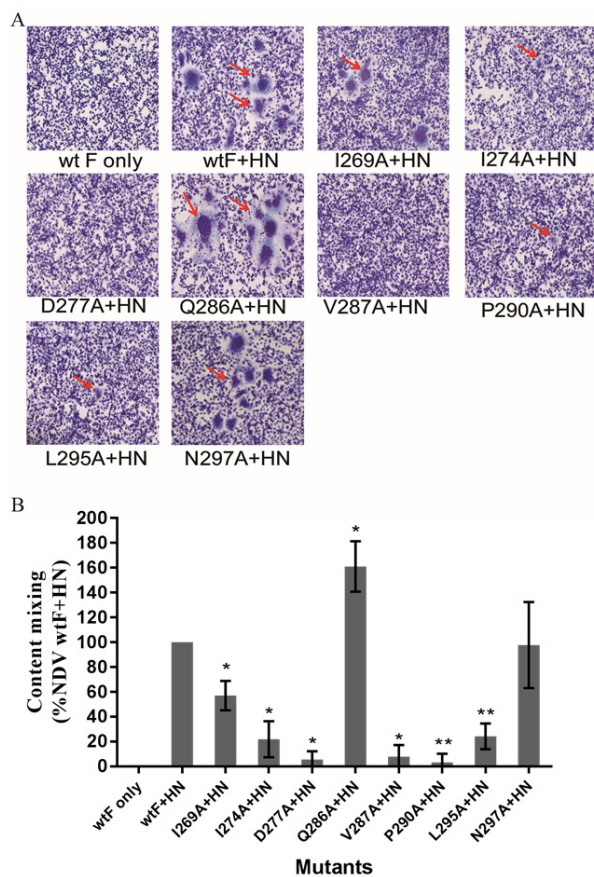


**Figure 2. Syncytium formation and content mixing of NDV wt and mutated F proteins. (A)** Syncytium formation in monolayers co-expressing wt or F mutant proteins and NDV HN. At 24 h post-transfection, BHK-21 monolayers transfected with only wt F, wt F and HN, or F mutants and HN were fixed with methanol and stained with Giemsa solution. Images were immediately acquired with a 10× objective under an inverted microscope. **(B)** Content mixing of wt F and F mutant proteins co-expressed with NDV HN. Values are expressed as percentages of content mixing detected in cells transfected with wt F and HN. The data represent the means of three independent experiments plus standard deviations. *P* values were calculated using the Student's *t* test to determine statistical significance of differences between each mutated F and wt F. (\*,  $p < 0.05$ ; \*\*,  $p < 0.01$ ; otherwise,  $p > 0.05$ )

and N297A.

To quantify the fusogenicity of these F mutations, a modification of the reporter gene assay was carried out to measure content mixing. Two populations of cells are indispensable for this assay: BHK-21 effector cells and BHK-21 target cells. Values were expressed as percentages of content mixing detected in cells transfected with wt F and HN proteins. The data are summarized in Figure 2B and Table 1. The F protein carrying the individual I269A mutation resulted in weakened content mixing, retaining only 57.1% of the wt F level, when co-expressed with the NDV HN protein. Mutants I274A and L295A reduced the levels of content mixing to extremely lower levels, 21.9% and 24.2% of that of wt F proteins. Additionally, a background level of fusion activity, 5.6%, 7.8%, and 3.0% of wt F, respectively, was detected for mutants

**Table 1. Functional profile of mutants around the DIII-I linker of NDV F (%wt F)**

Name	Cell fusion (% of wt)	Cell surface expression (CSE)
wt F	100	100
I269A	57.1 ± 11.8	30.1 ± 3.8
I274A	21.9 ± 14.5	#
D277A	5.6 ± 6.7	#
Q286A	161.1 ± 20.3	94 ± 26.2
V287A	7.8 ± 9.4	#
P290A	3.0 ± 6.9	31.5 ± 19
L295A	24.2 ± 10.3	100 ± 21.6
N297A	97.7 ± 34.6	86.8 ± 23.9

The average of cell surface expression and cell fusion were determined with FACS and Report Gene Method, respectively. The data are averages of three independent experiments. Values are expressed as percentages of wt F. # means no detectable data.

D277A, V287A, and P290A. Mutant Q286A produced fusion activity over 1.5 fold of the level of the wt F, whereas mutant N297A showed a similar amount of fusion, approximately 97.7% of the wt F ( $p > 0.05$ ). Therefore, most of the mutated F proteins led to reduction in content mixing except for Q286A and N297A, reflecting the results observed in the syncytial assay in Figure 2A.

Through the process of membrane fusion, activation of F and insertion of the FP into the target membrane initially led to the merger of the lipid bilayers before fusion pore formation and content mixing (23). To address whether or not the mutated F proteins impaired their ability to mediate lipid mixing, a dye transfer assay with R18-labeled RBCs was carried out to assess the extent of the lipophilic probe R18 transfer from RBC membranes to transfected BHK-21 cell membranes. Two negative controls were set for this experiment: cells expressing only NDV HN and only the F protein. As expected, cells expressing the HN protein bound RBCs, but there was no transfer of fluorescence from the RBCs to the BHK-21 cells. In contrast, cells expressing both HN and wt F proteins became more fluorescent as a result of the dye transfer (Figure 3). The results of lipid mixing almost mirrored the Giemsa staining results of wt or mutated F and the HN protein. Five of these mutants (I274A, D277A, V287A, P290A, and L295A) produced only a very small number of fusion events, almost similar to the negative control level. In addition, mutant I269A showed less and weak fluorescence. However, mutant Q286A showed a stronger fluorescence than wt F, while mutant N297A produced a similar level in lipid mixing. Therefore, these alanine substitutions also resulted in defects in mediating lipid mixing except for Q286A and N297A.

### 3.3. Cell surface expression of wt F and its mutants

Indirect immunofluorescence detection of the F protein on the surfaces of intact cells transfected with mutant F

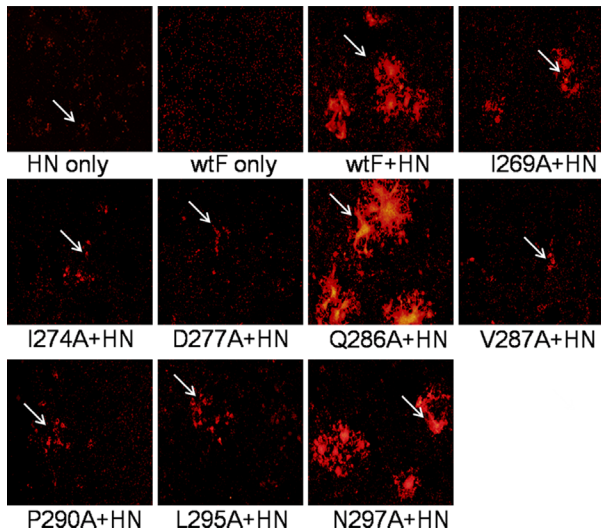


**Figure 3. Promotion of lipid mixing for NDV wt and mutant F proteins.** The extent of lipid mixing is shown by the spread of the dye transferred from R18-labeled red blood cells (RBCs) into the cell membranes of transfected BHK-21 cells. Labeled RBCs were added to each monolayer, and then the cells were incubated on ice for 30 min. After 30 min, the cells were washed and fusion between the transfected cells and RBCs was initiated by transferring the cells to 37°C for 1 h. Images were immediately acquired under a fluorescent microscope

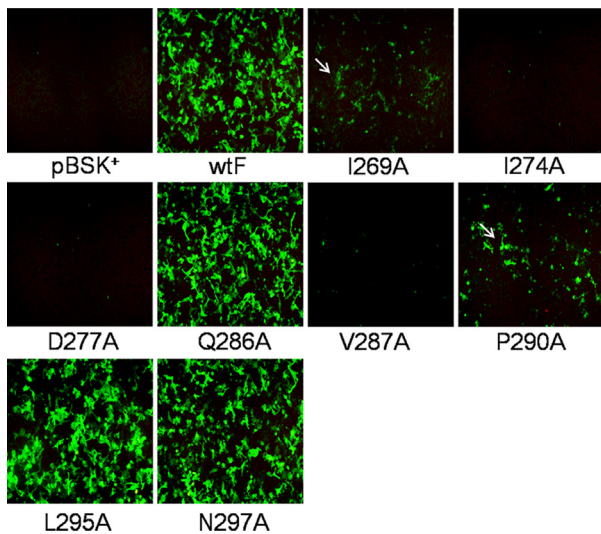


**Figure 4. Expression of wt F and F mutant proteins detected with indirect immunofluorescent assay (IIFA).** Intact confluent monolayers of BHK-21 cells transfected with wild-type or mutant F protein cDNAs were incubated with anti-NDV antiserum and then with fluorescent-labeled goat anti-chicken antibody. All fields shown were obtained using a 20× objective. White arrows indicate scattered fluorescent points.

protein genes was used to determine whether or not the mutant proteins were expressed at the cell surface. As shown in Figure 4, three of these F mutants (Q286A, L295A, and N297A) were detected at the surface, with a fluorescent signal similar to that of the wild-type protein. Mutant I269A and P290A were also detected at the surface, although the signal was much less intense than that of wt F. However, mutants I274A, D277A,

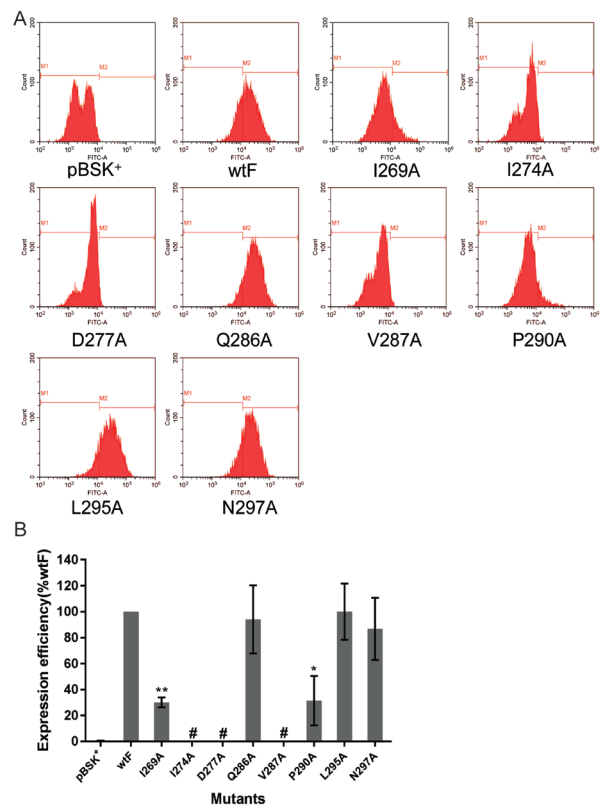


**Figure 5. Quantitative expression of wt F and F mutant proteins detected with FACS analysis.** Surface expression levels of wt F and F mutants were determined with FACS analysis at 24 h post-transfection using anti-NDV antiserum and then with fluorescent-labeled goat anti-chicken antibody, the same as used in the IIFA assay. (A) Representative fluorescent histograms for each mutant are shown. The x axis is the fluorescent intensity values shown in log scale and the y axis is cell counts. (B) Quantitation of the cell surface expression level detected by FACS analysis. Data were normalized to the value obtained with wt F. The means and standard errors are from triplicate experiments, # means no detectable data. (\*,  $p < 0.05$ ; \*\*,  $p < 0.01$ ; otherwise,  $p > 0.05$ ).

and V287A were not detected at the cell surface.

Surface expressions of these mutants were quantitated with FACS analysis and compared with that of wt F. Mutants I274A, D277A, and V287A could not be detected with FACS, while mutants Q286A, L295A, and N297A were very well expressed, 94%, 100%, and 86.8% of that of wt F, respectively ( $p > 0.05$ ). However, mutants I269A and P290A showed a reduced expression level, only about one-thirds of that of wt F (Figure 5 and Table 1).

### 3.4. Cleavage activity of NDV wt F and mutants

The cleavage abilities of the NDV wt F and mutants expressed in BHK-21 cells were detected with total cell lysates. The results from Western blot assay showed that mutants I274A, D277A, and V287A were non-cleaved and expressed less than the wt F protein (Figure 6). Mutants I269A, Q286A, P290A, L295A, and N297A showed similar cleavage efficiency. However, a high expression level in total cell lysate for P290A

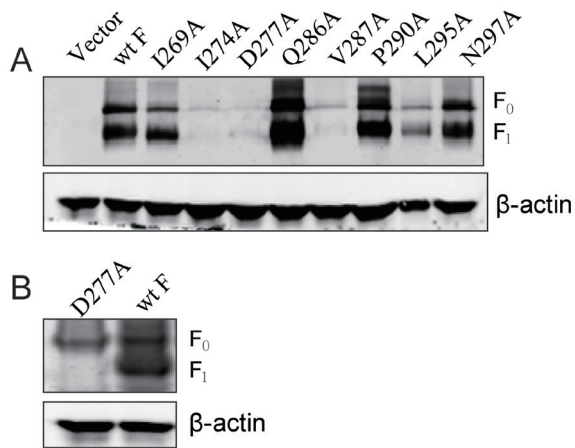


**Figure 6. Expression and cleavage of NDV wt F and F mutants transfected without HN.** At 24 h post-transfection, the wt F and F mutants transfected BHK-21 cells were harvested and lysed. (A) Expression and cleavage of NDV F proteins from total cell lysates were detected using Western blot without boiling or reducing. (B) To detect total expression of D277A, a 6× His was introduced at C-terminal. The total cell lysates were detected with His tag antibody under a boiling and reducing condition. The positions of precursor ( $F_0$ ) and cleaved subunit ( $F_1$ ) of the F protein are shown.

was detected, which was contrary to its reduced cell surface expression levels detected with FACS. It is worth noting that an extra slower-migrating band than  $F_0$  was detected for mutants Q286A and P290A, which may have been protein aggregates due to high level expression of whole protein molecules.

#### 4. Discussion

F protein-mediated membrane fusion is an important process for NDV to complete cell invasion and dissemination. The exact steps of the F protein from a pre-fusion conformation to a post-fusion conformation during the fusion process are not fully understood, but biochemical and physiological evidences along with X-crystal structures outline how the F protein mediates viral and cell membrane fusion (10,11,13,15,24-27). The key conformational changes in the F-protein refolding pathway have been highlighted, including the insertion of FP (25) and the forming of 6HB (10). Through this process, DI-DIII domains rearranged their orientation or structure to help achieve fusion. DI and DII as rigid modules are repositioned during the conformational transition, while a refolding process occurs in DIII (15,16). In this condition, potential hinge points, especially the linker between domains I and III, could be important for potential structural and functional changes (13).

In the present study, eight conserved sites near the junction of domains DIII and DI were found and the impacts of these sites on protein expression and membrane fusion were assessed after site-directed mutagenesis. The results showed that the fusion activities of the majority of mutant proteins were

reduced, among which three mutants (I274A, D277A, and V287A) completely lost fusion ability. However, Q286A exhibited an increased ability to mediate cell fusion and N297A performed a similar level of fusion compared with wt F.

The lost fusion ability was found to be closely related to undetected cell surface protein expression. Three mutants (I274A, D277A, and V287A), for example, were poorly expressed at the cell surface and as a result no fusion activities were detected. Only a weak  $F_0$  band was detected by anti-NDV antiserum. This reduction in expression may be attributed to the abnormal structure since the anti-NDV antiserum only recognizes natural NDV F trimers. To further detect expression of D277A (an example of the mutants undetectable with NDV antiserum), a 6× His tag was introduced at the C-terminal and a reducing WB was carried out. The results showed that D277A displayed a single  $F_0$  band without  $F_1$  compared with wt F. Thus, this lost fusion capability of these three mutants (I274A, D277A, and V287A) may directly correlate with the non-cleavage of the F protein. Interestingly, these three mutants were present within the structure of NDV F (Figure 1D), suggesting important roles of these inside amino acids in protein folding. As expected, mutant I269A and P290A, which are located inside the F protein, also showed a reduced surface expression level, with only about 30% of that of wt F. However, these kinds of reduced surface expression were different from those of I274A, D277A, and V287A, which may result from defects in transport to the cell surface (Figures 4 and 6). Mutant P290A showed an impaired expression on the cell surface but a higher level in total protein expression than wt F (Figure 6A). This indicated that the P290A protein may accumulate within the cell cytoplasm and cannot be properly transported to the cell membrane (9). However, another inside site, mutant Q286A produced an F protein, which exhibited a hyperfusogenic phenotype in our study. A similar inside site, like L289A (Figure 1D, colored as black), was reported to increase the fusion activity or even induce HN independent fusion (14). However, Q286A did not induce the same HN-independent fusion as L289A in our study, while it expressed in BHK-21 cells alone (Data not shown). Whether or not the Q286A mutant could induce fusion without HN needs to be further tested in more cell lines, since the HN-independent fusion of L289A is cell-specific (28). Two mutants, T458D and G459D, in the linker between domain I and HRB of NDV F are proved to increase fusion activity and induce HN independent fusion regardless of cell types (22). Our results along with these results suggested important roles of the connecting region between different domains in regulating the fusion activity of the NDV F protein.

A special site was mutant L295A, which almost lost fusion activity with a similar level of cell surface

expression. Shown as the generated pre-fusion form of the NDV F protein (Figure 1D), this amino acid was located on the surface of the protein molecule. Thus, a possible explanation is that this mutant may have an influence on the interaction between HN and F (24). In addition, mutant N297A was another site located on the surface of the protein structure (Figure 1D) without affecting expression. However, N297A had a similar level of fusion to wt F. The different levels of fusion activity for these two surface amino acids indicated that a hydrophobic amino acid is more likely to participate in the interaction between HN and F (24). Thus, site L295 could be a potential drug target to block the interplay between HN and F by a mimic peptide (29) with the sequence surrounding this site.

In the NDV F protein, the above conserved sites are located within or near the radial channels (14,15). The radial channels are considered to be the "dock" of the FP (13,15), which plays an important role in the correct insertion of the FP into the host cell membrane. Thus, these sites may be important in maintaining the correct structure of radial channels and mutations of these sites could influence the intrinsic radial channels, resulting in defects in the protein structure. A more detailed description of the refolding process of PIV5 F found that two peptides, 239-272 and 273-308, showed significant changes in oxidation states during the release of FP (25). These two peptides correspond to peptides 250-283 and 284-319, respectively, of the NDV F, which is the area surrounding the DIII-DI (peptide 268-304) junction. Thus, conservative amino acid mutant introduction may destroy the relative activities of these two fragments, affecting the fusion process F proteins. Given that the DIII-DI connection region appears to be a conserved structure in paramyxovirus F proteins, this region presents an alternative way to investigate structure-based rational vaccine or drug designs (30,31).

In conclusion, this study identified eight conserved amino acids at the junction of domains DIII and DI, seven of which play important roles in the folding, transport and regulation of the F protein's fusion activity. However, different sites play different roles. For example, sites I274, D277, and V287 are important for F's folding and cleavage activation. And two other sites, I269 and P290, are essential for protein transport. In addition, site L295 may participate in the interaction between HN and F. A deeper understanding of the roles of this junction region in the structure and function of the F protein could lay the foundation for developing new structure-based antiviral vaccines or drugs.

### Acknowledgements

We gratefully thank Dr. Ronald M. Iorio for providing the recombinant plasmid vectors and Dr. Bernard Moss for the recombinant vaccinia virus, vTF7-3. This work was supported by grants from National Natural Science

Foundation of China (No.81672011; No.81271806) and the Fundamental Research Funds of Shandong University (2015JC044). Thanks to Dr. Edward C. Mignot, Shandong University, for linguistic advice.

### References

- Zhu J, Hu S, Xu H, Liu J, Zhao Z, Wang X, Liu X. Characterization of virulent Newcastle disease viruses from vaccinated chicken flocks in Eastern China. *BMC Vet Res.* 2016; 12:113.
- Dimitrov KM, Afonso CL, Yu Q, Miller PJ. Newcastle disease vaccines-A solved problem or a continuous challenge? *Vet Microbiol.* 2017; 206:126-136.
- Paterson RG, Johnson ML, Lamb RA. Paramyxovirus fusion (F) protein and hemagglutinin-neuraminidase (HN) protein interactions: Intracellular retention of F and HN does not affect transport of the homotypic HN or F protein. *Virology.* 1997; 237:1-9.
- Tong S, Compans RW. Alternative mechanisms of interaction between homotypic and heterotypic parainfluenza virus HN and F proteins. *J Gen Virol.* 1999; 80:107-115.
- Iorio RM, Syddall RJ, Sheehan JP, Bratt MA, Glickman RL, Riel AM. Neutralization map of the hemagglutinin-neuraminidase glycoprotein of Newcastle disease virus: Domains recognized by monoclonal antibodies that prevent receptor recognition. *J Virol.* 1991; 65:4999-5006.
- Dutch RE, Jardetzky TS, Lamb RA. Virus Membrane Fusion Proteins: Biological Machines that Undergo a Metamorphosis. *Biosci Rep.* 2000; 20:597-612.
- Weissenhorn W, Hinz A, Gaudin Y. Virus membrane fusion. *FEBS Lett.* 2007; 581:2150-2155.
- White JM, Delos SE, Brecher M, Schornberg K. Structures and mechanisms of viral membrane fusion proteins: Multiple variations on a common theme. *Crit Rev Biochem Mol Biol.* 2008; 43:189-219.
- Gardner AE, Martin KL, Dutch RE. A conserved region between the heptad repeats of paramyxovirus fusion proteins is critical for proper F protein folding. *Biochemistry.* 2007; 46:5094-5105.
- Yu M, Wang E, Liu Y, Cao D, Jin N, Zhang CW, Bartlam M, Rao Z, Tien P, Gao GF. Six-helix bundle assembly and characterization of heptad repeat regions from the F protein of Newcastle disease virus. *J Gen Virol.* 2002; 83:623-629.
- Baker KA, Dutch RE, Lamb RA, Jardetzky TS. Structural basis for paramyxovirus-mediated membrane fusion. *Mol Cell.* 1999; 3:309-319.
- Epand RM. Fusion peptides and the mechanism of viral fusion. *Biochim Biophys Acta.* 2003; 1614:116-121.
- Yin HS, Paterson RG, Wen X, Lamb RA, Jardetzky TS. Structure of the uncleaved ectodomain of the paramyxovirus (hPIV3) fusion protein. *Proc Natl Acad Sci U S A.* 2005; 102:9288-9293.
- Sergel TA, McGinnes LW, Morrison TG. A single amino acid change in the Newcastle disease virus fusion protein alters the requirement for HN protein in fusion. *J Virol.* 2000; 74:5101-5107.
- Chen L, Gorman JJ, McKimm-Breschkin J, Lawrence LJ, Tulloch PA, Smith BJ, Colman PM, Lawrence MC. The structure of the fusion glycoprotein of Newcastle disease virus suggests a novel paradigm for the molecular

- mechanism of membrane fusion. *Structure*. 2001; 9:255-266.
16. Yin HS, Wen X, Paterson RG, Lamb RA, Jardetzky TS. Structure of the parainfluenza virus 5 F protein in its metastable, prefusion conformation. *Nature*. 2006; 439:38-44.
  17. Waterhouse A, Bertoni M, Bienert S, Studer G, Tauriello G, Gumienny R, Heer FT, de Beer TAP, Rempfer C, Bordoli L, Lepore R, Schwede T. SWISS-MODEL: homology modelling of protein structures and complexes. *Nucleic Acids Res*. 2018; 46:W296-w303.
  18. Navaratnarajah CK, Oezguen N, Rupp L, Kay L, Leonard VH, Braun W, Cattaneo R. The heads of the measles virus attachment protein move to transmit the fusion-triggering signal. *Nat Struct Mol Biol*. 2011; 18:128-134.
  19. Jardetzky TS, Lamb RA. Activation of paramyxovirus membrane fusion and virus entry. *Curr Opin Virol*. 2014; 1:24-33.
  20. Blumenthal R, Gallo SA, Viard M, Raviv Y, Dri M, Puri A. Fluorescent lipid probes in the study of viral membrane fusion. *Chem Phys Lipids*. 2002; 116:39-55.
  21. Bagai S, Lamb RA. Quantitative measurement of paramyxovirus fusion: differences in requirements of glycoproteins between simian virus 5 and human parainfluenza virus 3 or Newcastle disease virus. *J Virol*. 1995; 69:6712-6719.
  22. Ji Y, Liu T, Jia Y, Liu B, Yu Q, Cui X, Guo F, Chang H, Zhu Q. Two single mutations in the fusion protein of Newcastle disease virus confer hemagglutinin-neuraminidase independent fusion promotion and attenuate the pathogenicity in chickens. *Virology*. 2017; 509:146-151.
  23. Russell CJ, Kantor KL, Jardetzky TS, Lamb RA. A dual-functional paramyxovirus F protein regulatory switch segment: activation and membrane fusion. *J Cell Biol*. 2003; 163:363-374.
  24. Bose S, Heath CM, Shah PA, Alayyoubi M, Jardetzky TS, Lamb RA. Mutations in the parainfluenza virus 5 fusion protein reveal domains important for fusion triggering and metastability. *J Virol*. 2013; 87:13520-13531.
  25. Poor TA, Jones L, Sood A, Leser GP, Plasencia MD, Rempel DL, Jardetzky TS, Woods RJ, Gross ML, Lamb RA. Probing the paramyxovirus fusion (F) protein-refolding event from pre- to postfusion by oxidative footprinting. *Proc Natl Acad Sci USA*. 2014; 111:E2596-E2605.
  26. Welch BD, Liu Y, Kors CA, Leser GP, Jardetzky TS, Lamb RA. Structure of the cleavage-activated prefusion form of the parainfluenza virus 5 fusion protein. *Proc Nat Acad Sci USA*. 2012; 109:16672-16677.
  27. Swanson K, Wen X, Leser GP, Paterson RG, Lamb RA, Jardetzky TS. Structure of the Newcastle disease virus F protein in the post-fusion conformation. *Virology*. 2010; 402:372-379.
  28. Li J, Melanson VR, Mirza AM, Iorio RM. Decreased dependence on receptor recognition for the fusion promotion activity of L289A-mutated newcastle disease virus fusion protein correlates with a monoclonal antibody-detected conformational change. *J Virol*. 2005; 79:1180-1190.
  29. Young JK, Li D, Abramowitz MC, Morrison TG. Interaction of peptides with sequences from the Newcastle disease virus fusion protein heptad repeat regions. *J Virol*. 1999; 73:5945-5956.
  30. Song AS, Poor TA, Abriata LA, Jardetzky TS, Dal Peraro M, Lamb RA. Immobilization of the N-terminal helix stabilizes prefusion paramyxovirus fusion proteins. *Proc Natl Acad Sci U S A*. 2016; 113:E3844-3851.
  31. Stewart-Jones GBE, Chuang GY, Xu K, *et al*. Structure-based design of a quadrivalent fusion glycoprotein vaccine for human parainfluenza virus types 1-4. *Proc Natl Acad Sci U S A*. 2018; 115:12265-12270.

(Received March 17, 2019; Revised April 21, 2019; Accepted May 17, 2019)

# Knockdown expression of *MECR*, a novel gene of mitochondrial FAS II inhibits growth and colony-formation, promotes apoptosis of hepatocellular carcinoma cells

Yulong Cai, Yixin Lin, Xianze Xiong, Jiong Lu, Rongxing Zhou, Yanwen Jin, Zhen You, Hui Ye, Fuyu Li, Nansheng Cheng\*

Department of Biliary Surgery, West China Hospital, Sichuan University, Chengdu, Sichuan Province, China.

## Summary

Mitochondrial trans-2-enoyl-CoA reductase (*MECR*) is a protein-coding gene, and the protein encoded by this gene is an oxidoreductase that catalyzes the last step in mitochondrial fatty acid synthesis (mtFASII). Numerous studies have shown disorder of lipid metabolism is closely related with malignance, especially in liver cancer. Through pre-experiment, we found that the expression of *MECR* gene was highly expressed in hepatocellular carcinoma (HCC) cell lines *in vitro*. This suggests that the *MECR* gene may play a role of oncogene in HCC. Therefore, we conducted a preliminary experimental study on the role of *MECR* gene in HCC cells *in vitro*. Objective to explore whether the *MECR* gene can affect the malignant biological behavior of HCC. We selected HCC cell line BEL-7404 as experimental cell, which involves the highest expression of *MECR* in the pre-experiment. We constructed *MECR* knockdown lentivirus vector, and then infected HCC cell lines to down-regulate *MECR* expression, and establish negative control group (NC). Through various experiments of cytology, our study showed that knockdown of *MECR* inhibited cell proliferation and colony formation, promoted apoptosis, and inhibited metastasis in HCC cell lines BEL-7404. *MECR* might serve as a novel gene therapeutic target for the treatment of HCC. Further study is needed to elucidate the signaling pathway through which *MECR* functions in HCC.

**Keywords:** Hepatocellular carcinoma, *MECR*

## 1. Introduction

Hepatocellular carcinoma (HCC) arises from hepatocytes and represents the most frequent type of primary liver cancer, occupying more than 90% (1). Worldwide, there are more than 700,000 new HCC patients each year, ranking fifth and seventh in the incidence of malignant tumors in men and women, respectively (2). At present, the overall prognosis rate of liver malignant tumors is still low. According to statistics, the 5-year survival rate of liver cancer in the United States is only 16.6%. Due to

the continuous improvement of HCC treatment methods, the prognosis of HCC is relatively improved (3,4). Poor prognosis means finding more accurate biomarkers to predict a patient's prognosis and finding a more effective therapeutic gene targets are top priority for current research (5,6). Although some carcinogenic mechanisms and molecular mechanisms of HCC have been studied and proved, including genomic instability (7,8), gene mutation (9,10), carcinogenic and tumor suppressor gene expression (11), signaling pathways and so on (12-15), the overall and exact molecular pathology of HCC remains unclear. Still need a lot of basic scientific research and studies.

Despite the presence of a cytosolic fatty acid synthesis pathway, mitochondria have retained their own means of creating fatty acids *via* the mitochondrial fatty acid synthesis (mtFASII) pathway. Mitochondrial enoyl-CoA reductase (*MECR*), the last enzyme in the mtFASII

Released online in J-STAGE as advance publication June 10, 2019.

\*Address correspondence to:

Dr. Nansheng Cheng, Department of Bile Duct Surgery, West China Hospital, Sichuan University, No. 37 GuoXue Xiang, Chengdu 610041, Sichuan Province, China.  
E-mail: nanshengcheng2012@163.com

pathway, is a 2-enoyl thioester reductase that acts as a dimer, with a pocket forming between the two monomers that can accommodate fatty acid chains up to 16 carbons in length (16-18). The initial study of the *MECR* gene was found to be associated with peroxisome proliferator-activated receptor alpha (*PPARα*). Recent studies further elucidate that overexpression of the *MECR* gene activates the *PPARα* transcriptional pathway, possibly as a coactivator, or by increasing mtFASII activity (19,20). *PPARα* is a transcription factor whose main role is to participate in liver fat metabolism and adipocyte differentiation. Studies have also shown that *PPARα* plays a role in promoting metabolic pathways in the development of liver cancer (21). There are few studies on the relationship between *MECR* gene and disease. According to the literature, mutations in *MECR* gene can cause dystonia and optic atrophy in children (22). Animal experiments show that overexpression of *MECR* leads to cardiac dysfunction in mouse (23). In addition, it may be related to small airway obstruction (24). In terms of tumors, the *MECR* gene has not yet been reported.

A large number of studies have shown that lipid metabolism disorders are closely related to tumor cells, especially liver malignancies (25). However, studies on mitochondrial fat metabolism and HCC are still lacking. Therefore, we conducted a preliminary experimental study on the role of the *MECR* gene (encoding a key protein for mtFASII) in HCC cells *in vitro*. Objective to explore whether *MECR* gene can affect the malignant biological function of HCC.

Through pre-experiment, we found that *MECR* gene was highly expressed in four HCC cell lines, BEL7404, BEL7402, SMMC7721, and HepG2. This suggests that the *MECR* gene may play a role as oncogene in the HCC cell lines. Therefore, we further explored the effects of *MECR* gene on the malignant biological behavior of HCC cells by knocking down the *MECR* gene and establishing a negative control group, laying a foundation for future molecular pathway research.

## 2. Materials and Methods

### 2.1. Cell Culture

Human HCC cell lines, BEL-7402, BEL-7404, SMMC-7721, HepG2 and human renal epithelial 293T cells were purchased from the Shanghai Cell Bank (Shanghai, China). Cell lines were cultured in RPMI-1640 medium, supplemented with 10% fetal bovine serum FBS (Gibco®, Shanghai, China), 1% penicillin and 1% streptomycin at 37°C in a 5% CO<sub>2</sub> incubator.

### 2.2. Quantitative RT-PCR

Total RNA from the 4 cell lines, BEL-7402, BEL-7404, SMMC-7721, HepG2, was extracted using the TRIzol reagent (Invitrogen, Shanghai, China), according to the

manufacturer's instructions and was then used for RT reaction. Briefly, 2 µg of total RNA from each sample was reverse transcribed to single-stranded cDNA. One microliter of cDNA was used as a template for the following PCR. The primers used were as follows: for *MECR* forward, 5'-GTTGGAGGGAACGAAGGTGT-3' and reverse, 5'-CGCTCTGAAGAGGGATGTCA-3'; for *TP53* forward, 5'-GAG GTTGGCTCTGACTGTACC-3' and reverse, 5'-TCCGTCCCAGTAGATTACCAC-3'; and for *GAPDH* forward, 5'-TGACTTCAACAGCG ACACCCA-3', and reverse, 5'-CACCTGTTGCTGTA GCCAAA-3'. The quantitative RT-PCR comprised an initial denaturation at 95°C for 15 sec, then 45 cycles at 95°C for 5 sec and 60°C for 30 sec. The PCR products of *MECR*, *TP53* and *GAPDH* were 175, 133 and 121 bp. All samples were examined in triplicates.

### 2.3. Recombinant lentiviral vector production and cell infection

The complementary DNA sequence (TCATAT CTTCAAAGCAGAT) of *MECR* was designed from the full-length *MECR* sequence (NIM: 608205, GenBank: NM\_016011.3) by GeneChem Co. Ltd. (Shanghai, China). After testing knockdown efficiencies, the stem-loop oligonucleotides were synthesized and inserted into the lentivirus-based PSCSI-GFP (GeneChem Co. Ltd.) with *AgeI/EcoRI* sites. Lentivirus particles were prepared as previously described (26).

For lentivirus infection, BEL-7404 cells were cultured into 6-well plates and then the *MECR*-shRNA-lentivirus or negative control (NC) lentivirus was added according to a multiplicity of infection (MOI). After 72 h of infection, the cells were observed under a fluorescence microscope (MicroPublisher 3.3RTV; Olympus, Tokyo, Japan). After 120 h of infection, the cells were harvested to determine knockdown efficiency by quantitative RT-PCR.

### 2.4. Western blot analysis

After protein quantization by the Coomassie brilliant blue assay, 20 µg of protein was loaded in loading buffer, resolved on 10% SDS-polyacrylamide gels, electrotransferred to nitrocellulose membranes, and incubated overnight with antibodies against *MECR* (1:2000 dilution; Sigma), *TP53* (1:500 dilution; CST) and *BAX* (1:500 dilution; Abcam). Secondary antibody was applied, and the relative content of the target proteins was detected by chemiluminescence. *GAPDH* was used as loading control.

### 2.5. Cell growth assay

BEL-7404 cells at the logarithmic phase after infection with *MECR*-shRNA-lentivirus and scrambled shRNA lentivirus were digested, resuspended, counted and

inoculated in 96-well plates. From the second day, cells with green fluorescence were taken photos and counted by Cellomics ArrayScan VT1 Readers once a day. Cell growth was observed continuously for 5 days, and cell growth curves were drawn.

#### 2.6. Colony formation assay

Cells at the logarithmic phase after infection were inoculated in 6-well plates at the density of 800 cells/well. Culture medium was changed every three days. Cells were allowed to grow for 11 days to form colonies. When the cell numbers in most single colonies were greater than 50, cells were washed with PBS once and fixed in paraformaldehyde (Sangon Biotech Shanghai Co. Ltd) for 30 min. Cells were then washed with PBS and stained with Giemsa dye (Chemicon) for 20 min. After washing with ddH<sub>2</sub>O for several times, the number of colonies was counted under fluorescence microscope (Olympus, Japan).

#### 2.7. FACS (fluorescence assisted cell sorting) cell cycle analysis

Cells were cultured in 6-well plates and were infected with *MECR*-shRNA-lentivirus or control. When the cells grew to 80% confluence, they were collected by trypsinization and centrifugation at 1500 rpm for 5 min, washed once with PBS, and fixed in 70% alcohol for 1 h. Then, cells were rehydrated and resuspended in PBS containing Rnase (100 mg/mL) on ice, stained with propidium iodide (PI), filtered through a 50- $\mu$ m nylon mesh, and then analyzed using a BD FACS Calibur Flow Cytometer (BD Biosciences, San Diego, CA, USA). All experiments were performed in triplicate.

#### 2.8. Detection of apoptosis by FACS

Cell apoptosis was assayed by staining with Annexin V-APC and detected by FACS. For analysis of apoptosis, the cells were harvested, washed with 1  $\times$  binding buffer and resuspended in 1 mL 1  $\times$  staining buffer. Then 5 mL Annexin V-APC was added into 100 mL of the above cell suspension (about 1  $\times$  10<sup>5</sup>–1  $\times$  10<sup>6</sup> cells), and incubated at room temperature in the dark for 10-15 min. After incubation, cells were analyzed using the BD FACS Calibur Flow Cytometer (BD Biosciences, San Diego, CA, USA). All experiments were performed in triplicate.

#### 2.9. Transwell assay

The upper surface of Transwell invasion assay filters (Corning Costar, Shanghai, China) was coated by matrigel at 37°C for 30 min. Then cell culture medium (600 mL) was added into the basolateral chamber, and the apical chamber was added with serum-free medium

containing 5  $\times$  10<sup>4</sup> transfected cells. After 24h culture at 37°C, the serum-free medium was absorbed, and the adherent cells in upper surface were removed. Next, the rest cells were fixed with 100% methanol and stained with crystal violet. The number of cells penetrating through matrigel was the standard to evaluate the invasive ability. Three high power fields were randomly chosen to calculate the cell number. Each experiment was independently performed in triplicate.

#### 2.10. Immunofluorescence detection

Cells of each group, which were incubated for 48 hours in 24-well plates, were fixed with 2.5% glutaraldehyde for 15 minutes after the upper residual liquid was removed. Then they were incubated with 0.25% Triton X-100 for 15 minutes at room temperature, followed by blocking with 4% goat serum for 30 minutes at room temperature. *TP53* antibody (1:100) was added and incubated for 12 hours at 4°C. After washing with PBS for three times, rhodamine-labeled fluorescent secondary antibody (1:400) was added and incubated in a 37°C incubator for 40 minutes. 4',6-Diamidino-2-phenylindole was added to stain for 5 minutes. At last, the cells were observed under a fluorescence microscope and the number of positive cells was counted. Cells that exhibited blue immunofluorescence were *TP53*-positive cells.

#### 2.11. Statistical analysis

SPSS 21.0 statistical software was used to analysis. The data shown are presented as the mean  $\pm$  standard deviation (SD) of three independent experiments. Statistical significance was determined with Student's *t* test. A *P* value of less than 0.05 was considered significant.

### 3. Results

#### 3.1. *MECR* mRNA detection in four HCC cell lines

In order to find out whether there is a relationship between *MECR* and HCC, we detected the *MECR* mRNA in four HCC cell lines BEL-7402, BEL-7404, SMMC-7721, HepG2 by PCR. *GAPDH* gene was amplified as internal control. The relative expression of target gene was calculated with 2<sup>- $\Delta\Delta C_t$</sup>  method (27). The results showed that *MECR* mRNA was expressed in all four cell lines and the *MECR* gene expression abundance in these cell lines was high (Figure 1).

#### 3.2. Knockdown efficiency determined by western blot analysis

Human embryonic kidney 293T cells were infected with *MECR*-shRNA lentivirus or NC lentivirus. Western blot was used to detect the *MECR* protein expression. As

shown in Figure 2, compared with NC group the content of *MECR* protein was greatly reduced in the *MECR*-shRNA lentivirus group. This result indicated effective knockdown of the target sequence.

### 3.3. Lentivirus-mediated knockdown of *MECR* in the human HCC cell line BEL-7404

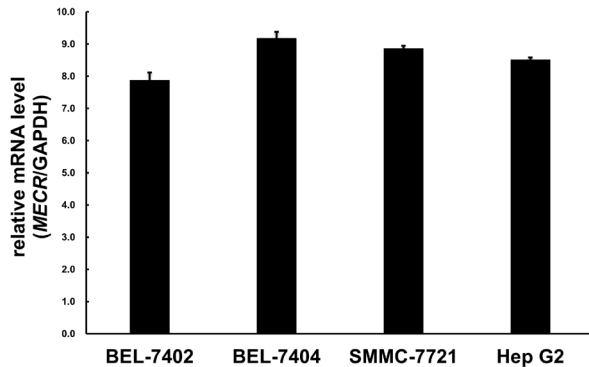


**Figure 1. *MECR* mRNA levels in four HCC cell lines.** Expression of *MECR* mRNA was measured by RT-PCR in the indicated cell lines. A constitutively expressed GAPDH gene was used as an internal control.

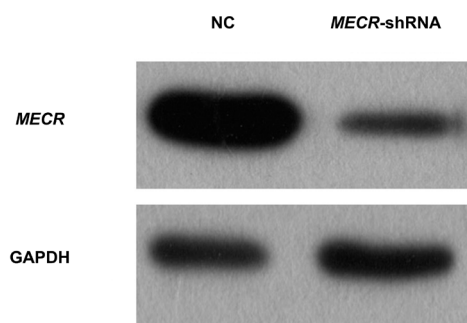


**Figure 2. Knockdown of *MECR* protein expression in 293T cells.** *MECR* protein expression was analyzed by western blotting in control-transfected (NC) and *MECR*-shRNA-transfected 293T cells. GAPDH was used as a loading control.

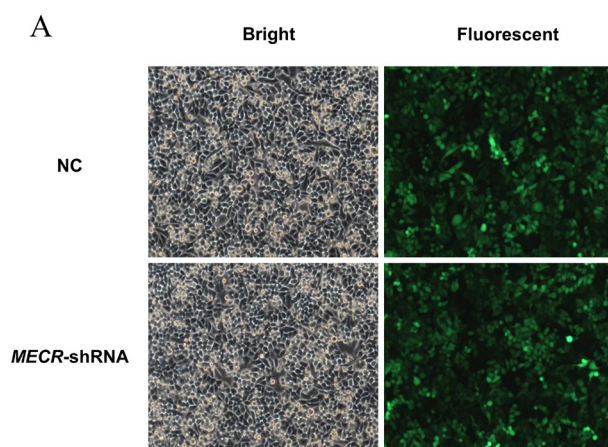


**Figure 3. *MECR* silencing efficiency by shRNA lentivirus.** (A) Lentivirus infection in BEL-7404 HCC cell line. Bright and fluorescent photomicrographs of BEL-7404 cells were taken 72 h after lentivirus infection at a magnification of  $\times 100$ ; (B) Identification of *MECR* knockdown efficiency using shRNA lentivirus by real-time PCR in BEL-7404 cells (\*\* $P < 0.01$ ).

HCC cell line BEL-7404, which involved the highest relative expression of *MECR*, was adopted to explore the role of *MECR*. Knockdown of *MECR* gene BEL-7404 cell line group and NC group were established by infected with *MECR*-shRNA lentivirus and NC lentivirus. As shown in Figure 3A, by day 3 post infection, the proportion of infected cells was  $> 80\%$  for both groups. And at day 5 post infection, *MECR* mRNA was assessed by real-time PCR. In the experiment group, the expression level of *MECR* mRNA was significantly lower than NC group (Figure 3B).

### 3.4. Knockdown of *MECR* in BEL-7404 cells inhibited cell proliferation

To investigate the effect of *MECR* on cell growth, BEL-7404 cells were infected by either the *MECR*-shRNA or NC lentivirus, and then were seeded into 96-well plates and analyzed by Cellomics Arrayscan with time-dependent manner for 5 days. As showed in Figure 4A, fluorescently stained cells were greatly increased in the NC group, and the cell-count confirmed our observation (Figure 4B). By analysis, the growth rate was also higher in the NC group while the number of *MECR*-shRNA-transfected cells did not change much. The results showed *MECR* knockdown significantly inhibited proliferation of the BEL-7404 cells ( $P < 0.05$ ).

### 3.5. Knockdown of *MECR* inhibited BEL-7404 cells colony formation

We then studied the colony-formation ability of knockdown *MECR* in BEL-7404 cells. BEL-7404 cells treated with *MECR*-shRNA or control lentivirus were allowed to grow for 11 days to form colonies. As shown in Figure 5, *MECR* knockdown resulted in significant decrease in the number of colonies in BEL-7404 cells ( $P < 0.01$ ), compared with the control groups. These results

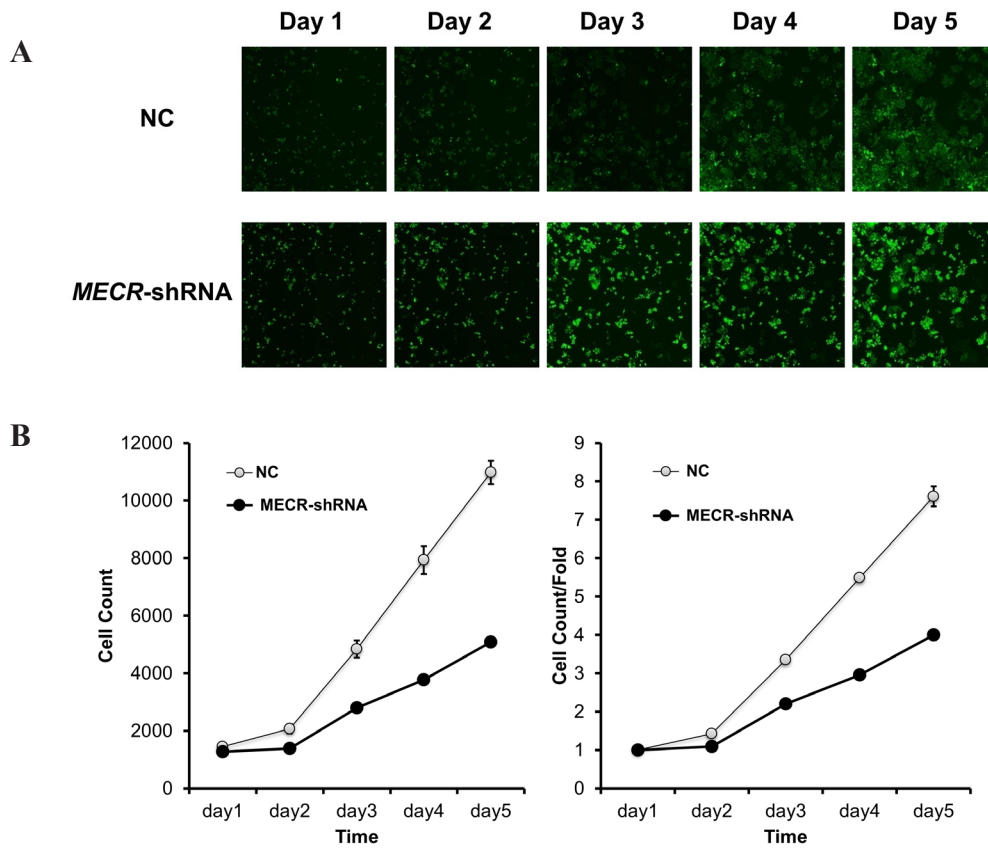


**Figure 4. MECR silencing inhibited HCC cell proliferation.** (A) Cells were infected with the control or *MECR*-shRNA lentivirus and high content cell imaging was applied every day as indicated to acquire raw images of cell growth. (B) *MECR* silencing by shRNA lentivirus significantly inhibited the growth rate of BEL-7404 cells, as shown by cell count for 5 days ( $P < 0.05$ ).

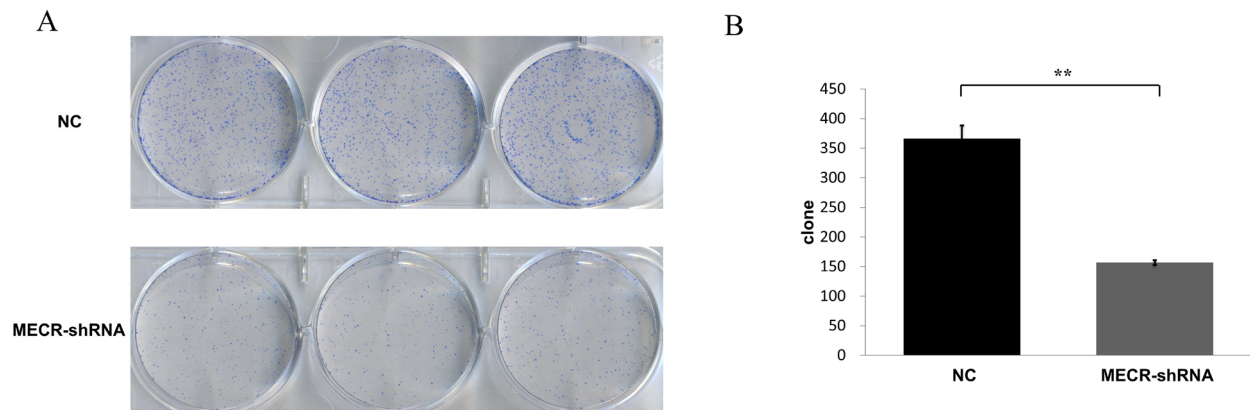


**Figure 5. MECR silencing inhibited HCC cell colony formation.** (A) Photomicrographs of Giemsa-stained colonies of BEL-7404 cells growing in 6-well plates for 11 days after infection; (B) The number of cells in colony of BEL-7404 cells was counted. Cell number in *MECR* shRNA group was significantly reduced, as compared with the control group (\*\* $P < 0.01$ ).

suggested that the *MECR* gene is associated with colony forming ability of HCC cells.

### 3.6. Knockdown of *MECR* in BEL-7404 cells do not affect cell cycle

In this experiment, it was detected that *MECR* can inhibit the proliferation and colony-formation of HCC cells after knockdown. To explore whether *MECR* can affect cell

cycle progression in BEL-7404 cells, the experimental group and control group cells were assessed the cell cycle phase by flow cytometry after 5 days of transfection. The results showed that the proportion of cells in the G1 phase after *MECR* knockdown was 46.3%, which was lower than that in the NC group (48.76%), and the difference was statistically significant ( $P < 0.01$ ). However, in the S phase (17.77% vs 17.79%) and the G2/M phase (35.93% vs 33.45%), there was no

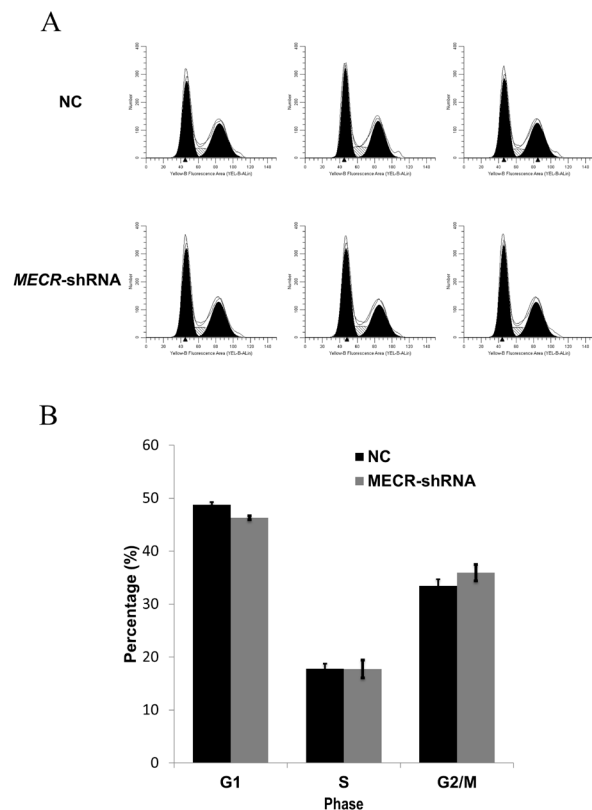


**Figure 6. The effects of MECR on cell cycle. (A)** The result of flow cytometry; **(B)** The proportion of cells in the G1 phase after *MECR* knockdown was decreased, but there were no significant difference between two groups in S phase and G2/M phase.

significant difference in cell proportion (Figure 6). From the results, it was shown that although knockdown of the *MECR* gene significantly inhibited the proliferation of HCC BEL-7404 cells, it did not affect the cell cycle.

### 3.7. Knockdown of *MECR* in BEL-7404 cells promoted cell apoptosis

We first used Annexin V-APV to stain and culture the experimental group and the control group for 5 days, and then used flow cytometry to detect apoptosis of the two groups. After repeated three experiments, the results showed that the apoptosis rate of BEL-7404 cells in the experimental group after *MECR* knockdown was 9.38%, 9.66%, and 9.68%, and the mean value was 9.57%, while the apoptosis rate of BEL-7404 cells in NC group was 3.80 %, 3.56%, 3.69%, with an average of 3.68%. It can be seen that after *MECR* gene knockdown, the apoptosis rate of cells increased significantly, and the difference was statistically significant ( $P < 0.01$ , Figures 7A and 7B). In addition, we further detect and verify apoptosis by measuring the activity of Caspase 3-7. The results showed that compared with the NC group, the activity of Caspase 3-7 in the experimental group increased, suggesting that apoptotic cells increased, and the difference was statistically significant ( $P < 0.01$

Figure 7C). The results showed that *MECR* knockdown significantly promoted apoptosis of the BEL-7404 cells.

### 3.8. Knockdown of *MECR* inhibited BEL-7404 cells migration

In this experiment, the *MECR* gene is a mitochondrial metabolism-related gene, and the mitochondria is a cell "energy plant". *MECR* knockdown may have an effect on cancer cells athletic ability. Therefore, in this experiment, the migrating ability of BEL-7404 cells knocking down the *MECR* gene was explored. This experiment was performed using the Transwell method to detect the migration ability of HCC cells. After 24 hours incubation in a transwell chamber, the transfected cells were stained and counted. As shown in Figure 8, the results showed that compared with the NC group, the number of metastatic cells in the experimental group knocking down the *MECR* was significantly decreased, and the difference was statistically significant ( $P < 0.01$ ). The results indicated that knockdown of *MECR* gene can inhibit the migration of HCC BEL-7404 cells *in vitro*.

### 3.9. Preliminary study on the regulation mechanism of *MECR* on HCC apoptosis

This experiment has initially confirmed that knockdown of *MECR* gene can effectively promote apoptosis of HCC cells. Since this experiment is the first to report that the *MECR* gene is associated with tumors, there is currently no available reference to analyze its specific molecular biological mechanisms. Therefore, we have a preliminary exploration of the mechanism of apoptosis induced by *MECR* in HCC cells. Whether *MECR* gene knockdown can affect the expression of proteins associated with HCC apoptosis has been confirmed. We tested BAX and *TP53* proteins by means of western blot assay. As shown in Figure 9, the BAX protein showed no significant difference between the two groups, while the *TP53* protein showed a downward trend in the experimental group. Therefore, *TP53* gene and protein expression were further verified by qRT-PCR and immunofluorescence staining. The results showed that there was no significant difference in mRNA expression of *TP53* gene between the experimental group and the NC group, and there was no difference in expression between the two groups of *TP53* proteins by immunofluorescence detection. The results showed that knockdown of the *MECR* gene did not affect the expression of BAX and *TP53* proteins.

## 4. Discussion

According to WHO data, HCC is currently the fifth most common malignant tumor and is the second tumor-killing disease worldwide (28). Although

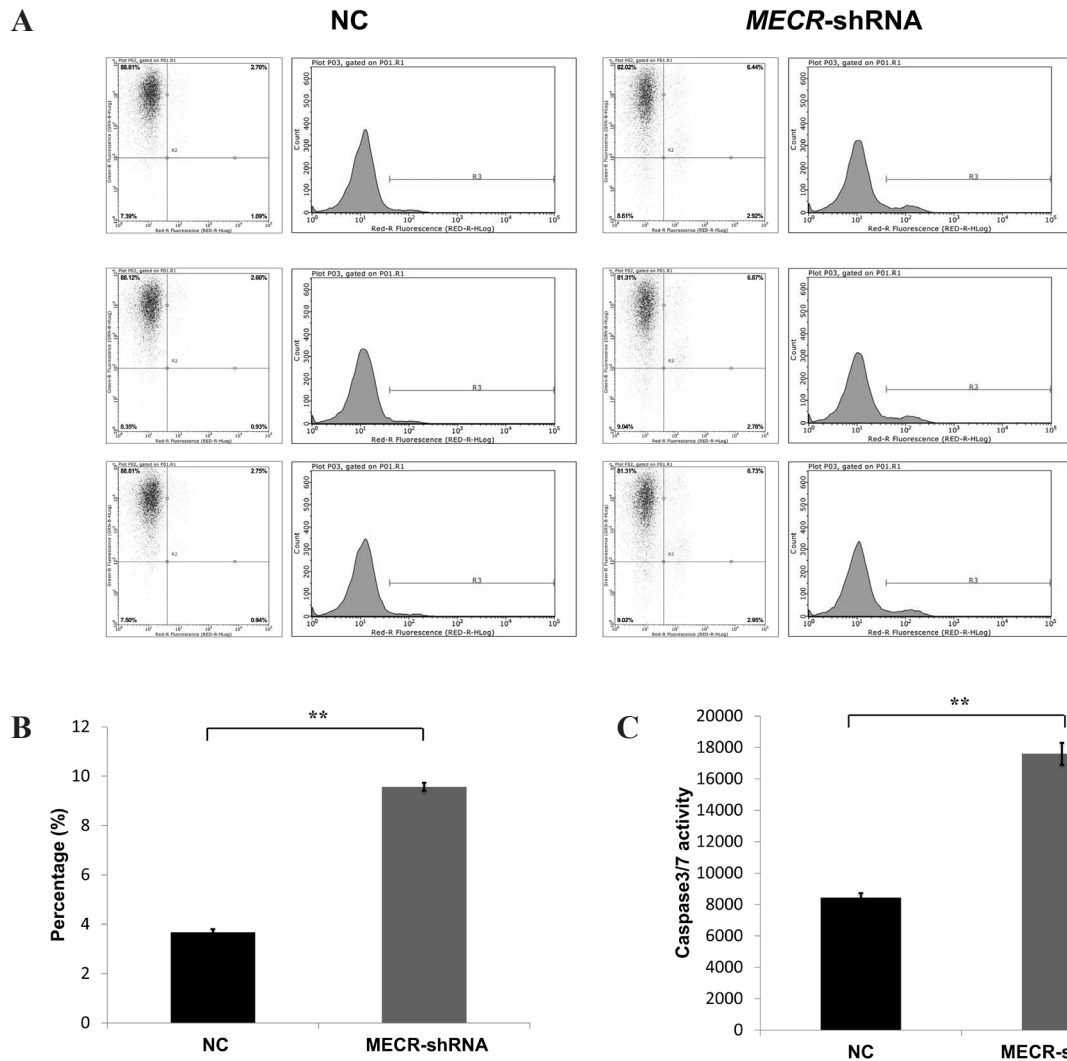


**Figure 7. *MECR* silencing promoted HCC cell apoptosis.** (A) Cell death was determined by Annexin V staining and flow cytometry; (B) Quantification of results showed the significant increase in apoptosis in the *MECR*-shRNA cultures compared with the NC (\*\* $P < 0.01$ ); (C) The results showed that the activity of Caspase 3-7 in the experimental group increased significantly (\*\* $P < 0.01$ ).

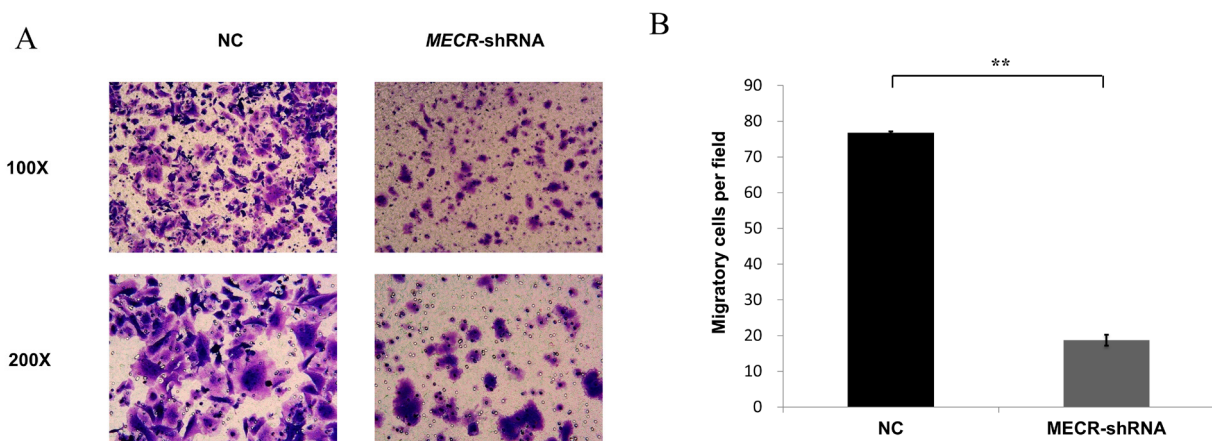


**Figure 8. *MECR* silencing inhibited HCC cell migration.** (A) Representative images of migration assays of BEL-7404 HCC cells transfected with *MECR*-shRNA or control lentivirus; (B) Quantification of results showed the number of metastatic cells in the experimental group knocking down the *MECR* was significantly decreased, and the difference was statistically significant (\*\* $P < 0.01$ ).

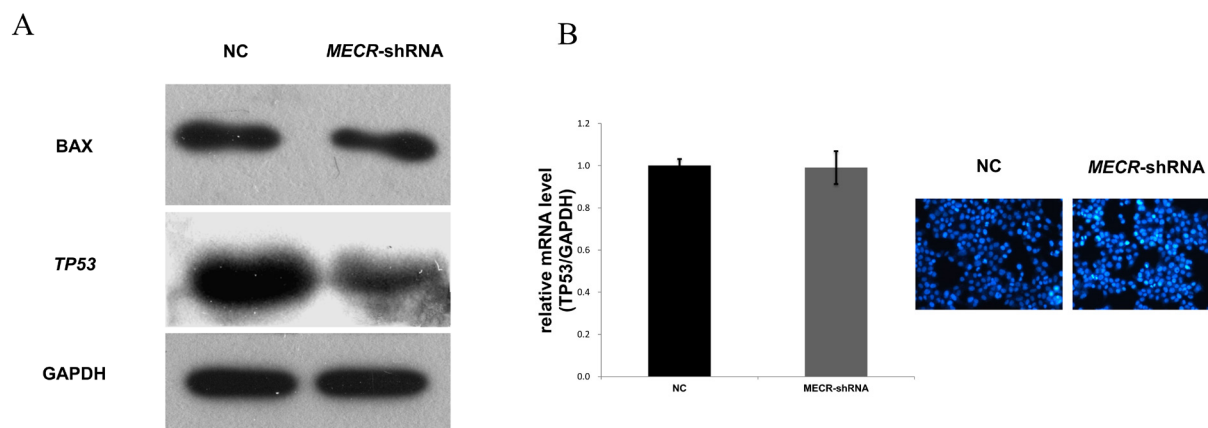


**Figure 9.** The expression of *BAX* and *TP53* proteins after knockdown *MECR*. (A) The protein levels of *BAX* and *TP53* were determined by western blot assays; (B) RT-PCR was used to assess the mRNA levels of *TP53* and immunofluorescence was applied to verify the protein levels of *TP53*.

the current treatment of surgery, TACE, RFS and chemotherapy has improved the patient's 5 year survive rate, its high recurrence and metastasis rate make the overall therapeutic effect of HCC still unsatisfactory (6,29). With the expectation of more effective and thorough treatment, gene therapy is considered as a possible treatment (30). Therefore, it is particularly important to identify key genes and corresponding molecular mechanisms that affect tumor growth and recurrence (31).

The *MECR* gene is a protein-coding gene, and its expressed protein is a reductase that regulates the final step of mitochondrial lipid metabolism. It has not been reported in other tumors. This experiment found that the expression abundance of *MECR* gene in four HCC *in vitro* cell lines was high, suggesting that there is a link between high expression of *MECR* gene and HCC.

Lentivirus is a highly efficient gene vector (32). This experiment uses shRNA as an interference vector to transfect BEL-7404 cell line knockdown *MECR* gene with lentivirus as vector, and transfected with negative lentiviral shRNA as NC Control, a series of cytological tests to study the effect of *MECR* gene on the malignant behavior of HCC cell lines.

The results of this experiment show that *MECR*-shRNA lentivirus effectively knocks down the mRNA and protein expression of the *MECR* gene. On the basis of this, using cell-count by Cellomics Arrayscan with time-dependent manner, it was found that the knockdown of the *MECR* revealed that the growth of the HCC cell line BEL-7404 was inhibited.

In order to explore the reasons for knockdown of the *MECR* gene to induce cell growth inhibition, the cells were further assayed for apoptosis, cell cycle and cell clone formation. One of the important features of early apoptosis is the activation of the cysteine-specific protease Caspase family of proteins. This type of enzyme can participate in a series of biochemical reactions, respond to early signs of apoptosis and cause

the corresponding protein substrate to cleave, which in turn triggers cell disintegration. Activation of the Caspase family can effectively promote apoptosis (33,34). Apoptosis-related experiments found that knockdown of the *MECR* gene effectively activated apoptosis, and the number of apoptotic cells in the experimental group increased and the caspase 3/7 activity was significantly increased. Cell cycle refers to the activity of cells from the end of the previous division to the end of the next division, divided into G0/G1 phase (diploid, DNA content is 2N), S phase (DNA content between G1 and G2) And G2/M phase (tetraploid, DNA content 4N). The results of cell cycle experiments in this experiment showed that although the number of cells in the G1 phase was small, the number of cells in the S phase was the same, and the number of cells in the G2/M phase was increased, only the G1 phase was statistically significant. The results indicate that knockdown of the *MECR* gene did not affect the HCC cell cycle. In addition, the results of colony formation experiments showed that after knockdown of *MECR* gene, the viability of individual cells decreased significantly, and the ability to form clones in experiment group was significantly inhibited. The above experiments show that *MECR* knockdown may increase the apoptosis by activating the apoptotic system, and inhibit the cell cloning ability, thereby inhibiting cell proliferation.

Although the 5-year overall survival rate of HCC patients can be as high as about 50% after surgery, its extremely high metastasis and recurrence is the main obstacle to further improve the survival of patients with HCC, and the recurrence rate can reach more than 60% after 5 years (35). In order to investigate whether the *MECR* gene affects the metastatic ability of HCC cells after affecting the metabolism of mitochondria, this experiment used transwell assay to test cell migration ability. The results showed that the migration ability of BEL-7404 cells in the experimental group knocking

down the *MECR* gene was significantly decreased, indicating that silencing the *MECR* gene can effectively inhibit the metastatic ability of HCC cells.

It is the next experimental research direction of this experiment to determine which signal pathway of *MECR* gene affects HCC cells. We underwent a preliminary exploration of proteins that have been closely related to tumor cell apoptosis. *TP53* has been widely studied and found to be an extremely important tumor suppressor gene. *TP53* gene mutation is found in many human cancer patients (36,37). Several studies have also shown that *TP53* protein plays an important role in HCC, regulating the apoptotic process of cells (38,39). BAX protein is another important protein in the regulation of tumor apoptosis, which can promote the release of cytochrome C and activate Caspase 9 and Caspase 3, which has been confirmed as one of the major proteins regulating apoptosis in HCC (40,41). This experiment explored the expression of these two important proteins of apoptosis exploratorily. Unfortunately, there was no difference in the expression of *TP53* and BAX between the experimental group and the NC group. The mechanism of *MECR* gene in apoptosis needs further exploration. In addition, according to the current literature reports, the only clearer is that the high expression of the *MECR* gene can significantly activate *PPAR $\alpha$* . *PPAR $\alpha$*  is a ligand of *PPARs*, which is mainly expressed in tissues with strong fatty acid metabolism such as liver, muscle and heart. It participates in lipid breakdown and oxidation to regulate lipid metabolism balance (42). Chang *et al.* found that miRNA-33a can promote Huh7 cell proliferation and inhibit apoptosis *in vitro*. The main target of this gene is *PPAR $\alpha$*  (43). In addition, the Shah team found that activation of *PPAR $\alpha$*  promoted HCC cell proliferation and induced hepatocarcinogenesis, and was associated with miRNA-let7C. In addition, mice with congenital deficiency of *PPAR $\alpha$*  fed *PPAR $\alpha$*  agonist Wy-14,643 did not induce liver cancer (44). In addition, there are a large number of studies in recent years that clarify that *PPAR $\alpha$*  plays an important regulatory role in the development of HCC (45-47). The effect of *MECR* gene knockdown on HCC cells may be related to the *PPAR $\alpha$*  pathway and have corresponding effects, which needs further experiments in this experimental group to verify.

## 5. Conclusion

The Warburg effect states that tumor cells provide function primarily through glycolysis even under aerobic conditions (48). In addition, due to the low glycolysis efficiency of tumor cells under aerobic conditions, it is a very important way for tumor cells to activate and strengthen lipid metabolism during the process of maintaining high-speed replication (49). Whether the metabolic abnormality of mitochondrial mtFASII dominated by *MECR* gene-

coding protein is related to tumor diseases has not been reported yet. This experiment has confirmed the close relationship between *MECR* gene and HCC proliferation, apoptosis and metastasis through a series of cytological experiments. In conclusion, the results of this experiment show that the knockdown of the *MECR* gene can be effectively silenced by lentiviral transfection of the HCC cell line BEL-7404 *in vitro*. Knockdown of *MECR* can inhibited cell proliferation and colony formation, promoted apoptosis, and inhibited metastasis in HCC cell lines BEL-7404. Therefore, knockdown of *MECR* gene-targeted therapy can be a possible therapeutic approach in patients with high expression of the *MECR* gene. How the specific *MECR* gene affects the molecular pathway of the signaling pathway of HCC cell lines needs further experimental research.

## Acknowledgements

This study was supported by the Post-Doctor Research Project, West China Hospital, Sichuan University. And we would like to acknowledge the support of the Department of Bile Duct Surgery, West China Hospital, Sichuan University, China.

## References

- Wallace MC, Preen D, Jeffrey GP, Adams LA. The evolving epidemiology of hepatocellular carcinoma: A global perspective. *Expert Rev Gastroenterol Hepatol.* 2015; 9:765-779.
- Torre LA, Bray F, Siegel RL, Ferlay J, Lortet-Tieulent J, Jemal A. Global cancer statistics, 2012. *CA Cancer J Clin.* 2015; 65:87-108.
- Laursen L. A preventable cancer. *Nature.* 2014; 516:S2-3.
- Song P, Cai Y, Tang H, Li C, Huang J. The clinical management of hepatocellular carcinoma worldwide: A concise review and comparison of current guidelines from 2001 to 2017. *Biosci Trends.* 2017; 11:389-398.
- Hoshida Y, Villanueva A, Kobayashi M, *et al.* Gene expression in fixed tissues and outcome in hepatocellular carcinoma. *N Engl J Med.* 2008; 359:1995-2004.
- Forner A, Llovet JM, Bruix J. Hepatocellular carcinoma. *Lancet.* 2012; 379:1245-1255.
- Zhang SH, Cong WM, Xian ZH, Dong H, Wu MC. Genomic instability in hepatocellular carcinoma revealed by using the random amplified polymorphic DNA method. *J Cancer Res Clin Oncol.* 2004; 130:757-761.
- Sun Z, Zhu Y, Aminbuhe, Fan Q, Peng J, Zhang N. Differential expression of APE1 in hepatocellular carcinoma and the effects on proliferation and apoptosis of cancer cells. *Biosci Trends.* 2018; 12:456-462.
- Lee JS. The mutational landscape of hepatocellular carcinoma. *Clin Mol Hepatol.* 2015; 21:220-229.
- Darcy DG, Chiaroni-Clarke R, Murphy JM, Honeyman JN, Bhanot U, LaQuaglia MP, Simon SM. The genomic landscape of fibrolamellar hepatocellular carcinoma: Whole genome sequencing of ten patients. *Oncotarget.* 2015; 6:755-770.

11. Li M, Zhao H, Zhang X, *et al.* Inactivating mutations of the chromatin remodeling gene *ARID2* in hepatocellular carcinoma. *Nat Genet.* 2011; 43:828-829.
12. Zhou SL, Zhou ZJ, Hu ZQ, Li X, Huang XW, Wang Z, Fan J, Dai Z, Zhou J. CXCR2/CXCL5 axis contributes to epithelial-mesenchymal transition of HCC cells through activating PI3K/Akt/GSK-3beta/Snail signaling. *Cancer Lett.* 2015; 358:124-135.
13. Lan Y, Han J, Wang Y, *et al.* STK17B promotes carcinogenesis and metastasis *via* AKT/GSK-3beta/Snail signaling in hepatocellular carcinoma. *Cell Death Dis.* 2018; 9:236.
14. Yu M, Xue H, Wang Y, Shen Q, Jiang Q, Zhang X, Li K, Jia M, Jia J, Xu J, Tian Y. miR-345 inhibits tumor metastasis and EMT by targeting IRF1-mediated mTOR/STAT3/AKT pathway in hepatocellular carcinoma. *Int J Oncol.* 2017; 50:975-983.
15. Qi F, Wang J, Zhao L, Cai P, Tang W, Wang Z. Cinobufacini inhibits epithelial-mesenchymal transition of human hepatocellular carcinoma cells through c-Met/ERK signaling pathway. *Biosci Trends.* 2018; 12:291-297.
16. Clay HB, Parl AK, Mitchell SL, Singh L, Bell LN, Murdock DG. Altering the Mitochondrial Fatty Acid Synthesis (mtFASII) Pathway Modulates Cellular Metabolic States and Bioactive Lipid Profiles as Revealed by Metabolomic Profiling. *PLoS One.* 2016; 11:e0151171.
17. Chen ZJ, Pudas R, Sharma S, Smart OS, Juffer AH, Hiltunen JK, Wierenga RK, Haapalainen AM. Structural enzymological studies of 2-enoyl thioester reductase of the human mitochondrial FAS II pathway: New insights into its substrate recognition properties. *J Mol Biol.* 2008; 379:830-844.
18. Miinalainen IJ, Chen ZJ, Torkko JM, Pirila PL, Sormunen RT, Bergmann U, Qin YM, Hiltunen JK. Characterization of 2-enoyl thioester reductase from mammals. An ortholog of YBR026p/MRF1'p of the yeast mitochondrial fatty acid synthesis type II. *J Biol Chem.* 2003; 278:20154-20161.
19. Masuda N, Yasuno H, Furusawa T, Tsukamoto T, Sadano H, Osumi T. Nuclear receptor binding factor-1 (NRBF-1), a protein interacting with a wide spectrum of nuclear hormone receptors. *Gene.* 1998; 221:225-233.
20. Parl A, Mitchell SL, Clay HB, Reiss S, Li Z, Murdock DG. The mitochondrial fatty acid synthesis (mtFASII) pathway is capable of mediating nuclear-mitochondrial cross talk through the PPAR system of transcriptional activation. *Biochem Biophys Res Commun.* 2013; 441:418-424.
21. Misra P, Reddy JK. Peroxisome proliferator-activated receptor-alpha activation and excess energy burning in hepatocarcinogenesis. *Biochimie.* 2014; 98:63-74.
22. Heimer G, Keratar JM, Riley LG, *et al.* MECR Mutations Cause Childhood-Onset Dystonia and Optic Atrophy, a Mitochondrial Fatty Acid Synthesis Disorder. *Am J Hum Genet.* 2016; 99:1229-1244.
23. Chen Z, Leskinen H, Liimatta E, Sormunen RT, Miinalainen IJ, Hassinen IE, Hiltunen JK. Myocardial overexpression of Mecer, a gene of mitochondrial FAS II leads to cardiac dysfunction in mouse. *PLoS One.* 2009; 4:e5589.
24. van der Plaats DA, de Jong K, Lahousse L, Faiz A, Vonk JM, van Diemen CC, Nedeljkovic I, Amin N, Obeidat M, van Duijn CM, Boezen HM, Postma DS. The Well-Known Gene HHIP and Novel Gene MECR Are Implicated in Small Airway Obstruction. *Am J Respir Crit Care Med.* 2016; 194:1299-1302.
25. Furuta E, Okuda H, Kobayashi A, Watabe K. Metabolic genes in cancer: Their roles in tumor progression and clinical implications. *Biochim Biophys Acta.* 2010; 1805:141-152.
26. Lois C, Hong EJ, Pease S, Brown EJ, Baltimore D. Germline transmission and tissue-specific expression of transgenes delivered by lentiviral vectors. *Science.* 2002; 295:868-872.
27. Lin CZ, Ou RW, Hu YH. Lentiviral-mediated microRNA-26b up-regulation inhibits proliferation and migration of hepatocellular carcinoma cells. *Kaohsiung J Med Sci.* 2018; 34:547-555.
28. Heimbach JK, Kulik LM, Finn RS, Sirlin CB, Abecassis MM, Roberts LR, Zhu AX, Murad MH, Marrero JA. AASLD guidelines for the treatment of hepatocellular carcinoma. *Hepatology.* 2018; 67:358-380.
29. Colombo M, Sangiovanni A. Treatment of hepatocellular carcinoma: Beyond international guidelines. *Liver Int.* 2015; 35 Suppl 1:129-138.
30. Guinn BA, Mulherkar R. International progress in cancer gene therapy. *Cancer Gene Ther.* 2008; 15:765-775.
31. Ludwig JA, Weinstein JN. Biomarkers in cancer staging, prognosis and treatment selection. *Nat Rev Cancer.* 2005; 5:845-856.
32. Lever AM, Strappe PM, Zhao J. Lentiviral vectors. *J Biomed Sci.* 2004; 11:439-449.
33. Le DA, Wu Y, Huang Z, Matsushita K, Plesnila N, Augustinack JC, Hyman BT, Yuan J, Kuida K, Flavell RA, Moskowitz MA. Caspase activation and neuroprotection in caspase-3- deficient mice after *in vivo* cerebral ischemia and *in vitro* oxygen glucose deprivation. *Proc Natl Acad Sci U S A.* 2002; 99:15188-15193.
34. Mooney LM, Al-Sakkaf KA, Brown BL, Dobson PR. Apoptotic mechanisms in T47D and MCF-7 human breast cancer cells. *Br J Cancer.* 2002; 87:909-917.
35. Yang LY, Fang F, Ou DP, Wu W, Zeng ZJ, Wu F. Solitary large hepatocellular carcinoma: A specific subtype of hepatocellular carcinoma with good outcome after hepatic resection. *Ann Surg.* 2009; 249:118-123.
36. Hong B, van den Heuvel AP, Prabhu VV, Zhang S, El-Deiry WS. Targeting tumor suppressor p53 for cancer therapy: Strategies, challenges and opportunities. *Curr Drug Targets.* 2014; 15:80-89.
37. Haupt S, Haupt Y. Importance of p53 for cancer onset and therapy. *Anticancer Drugs.* 2006; 17:725-732.
38. Wu W, Liu S, Liang Y, Zhou Z, Bian W, Liu X. Stress Hormone Cortisol Enhances Bcl2 Like-12 Expression to Inhibit p53 in Hepatocellular Carcinoma Cells. *Dig Dis Sci.* 2017; 62:3495-3500.
39. Zhang G, Zeng X, Zhang R, Liu J, Zhang W, Zhao Y, Zhang X, Wu Z, Tan Y, Wu Y, Du B. Dioscin suppresses hepatocellular carcinoma tumor growth by inducing apoptosis and regulation of TP53, BAX, BCL2 and cleaved CASP3. *Phytomedicine.* 2016; 23:1329-1336.
40. Miao R, Xu X, Wang Z, Liu S, Qu K, Chen W, Liu C. Synergistic effect of nutlin-3 combined with aspirin in hepatocellular carcinoma HepG2 cells through activation of Bcl-2/Bax signaling pathway. *Mol Med Rep.* 2018; 17:3735-3743.
41. Lee SY, Choe YJ, Park JY, Lee SS, Kim YH, Shin SJ, Chung YJ, Kim HS. Wilms' tumor gene 1 enhances

- nutlin-3-induced apoptosis. *Oncol Rep.* 2014; 31:131-136.
42. Jeng LB, Velmurugan BK, Hsu HH, Wen SY, Shen CY, Lin CH, Lin YM, Chen RJ, Kuo WW, Huang CY. Fenofibrate induced PPAR alpha expression was attenuated by oestrogen receptor alpha overexpression in Hep3B cells. *Environ Toxicol.* 2018; 33:234-247.
43. Chang W, Zhang L, Xian Y, Yu Z. MicroRNA-33a promotes cell proliferation and inhibits apoptosis by targeting PPARalpha in human hepatocellular carcinoma. *Exp Ther Med.* 2017; 13:2507-2514.
44. Shah YM, Morimura K, Yang Q, Tanabe T, Takagi M, Gonzalez FJ. Peroxisome proliferator-activated receptor alpha regulates a microRNA-mediated signaling cascade responsible for hepatocellular proliferation. *Mol Cell Biol.* 2007; 27:4238-4247.
45. Drakaki A, Hatzia Apostolou M, Polytaichou C, Vorvis C, Poultsides GA, Souglakos J, Georgoulas V, Iliopoulos D. Functional microRNA high throughput screening reveals miR-9 as a central regulator of liver oncogenesis by affecting the PPARA-CDH1 pathway. *BMC Cancer.* 2015; 15:542.
46. Li J, Huang Q, Long X, Zhang J, Huang X, Aa J, Yang H, Chen Z, Xing J. CD147 reprograms fatty acid metabolism in hepatocellular carcinoma cells through Akt/mTOR/SREBP1c and P38/PPARalpha pathways. *J Hepatol.* 2015; 63:1378-1389.
47. Zhang N, Chu ES, Zhang J, Li X, Liang Q, Chen J, Chen M, Teoh N, Farrell G, Sung JJ, Yu J. Peroxisome proliferator activated receptor alpha inhibits hepatocarcinogenesis through mediating NF-kappaB signaling pathway. *Oncotarget.* 2014; 5:8330-8340.
48. Warburg O. On the origin of cancer cells. *Science.* 1956; 123:309-314.
49. Maan M, Peters JM, Dutta M, Patterson AD. Lipid metabolism and lipophagy in cancer. *Biochem Biophys Res Commun.* 2018; 504:582-589.

(Received April 25, 2019; Revised May 25, 2019; Accepted June 3, 2019)

# Higher $\beta$ -human chorionic gonadotropin and estrogen levels during the first 6 weeks of pregnancy are associated with threatened abortion

Ling Xu<sup>1,§</sup>, Qun Wei<sup>2,§</sup>, Qiong Wu<sup>1</sup>, Yanbo Zhong<sup>1</sup>, Yangfang Li<sup>1</sup>, Jun Xu<sup>1,\*</sup>, Yunheng Zhu<sup>1,\*</sup>

<sup>1</sup> Department of Obstetrics and Gynecology, Minhang Hospital, Fudan University, Shanghai, China;

<sup>2</sup> Songjiang Maternity & Child Health Hospital of Shanghai, Shanghai, China.

## Summary

The associations of human chorionic gonadotropin (hCG), estrogen, and progesterone levels with threatened abortion have not been fully studied. Eighty women with threatened abortion were recruited sequentially, and the levels in their pregnancy hormones during the first trimester were compared with that of 160 normal early pregnancy controls. The natural logarithm transformed (Ln) hCG and Lnestrogen of women with threatened abortion and gestational age  $\leq 6$  weeks were significantly higher than values for the normal controls of the same gestational age ( $8.6 \pm 1.2$  vs.  $7.4 \pm 1.7$  mIU/mL and  $5.8 \pm 0.4$  vs.  $5.4 \pm 0.5$  pg/mL); the two hormones reached similar levels in the groups of gestational age  $> 6$  weeks. Among the group with gestational age  $\leq 6$  weeks, a univariate logistic regression showed that LnhCG and Lnestrogen were associated with threatened abortion, with odds ratios (ORs) of 1.85 [95% confidence interval (CI): 1.30-2.64] and 4.62 (95% CI: 1.67-12.80), respectively. The multivariate logistic regression model revealed that hCG and estrogen were mutually confounding factors, and only hCG was an independent factor for threatened abortion (OR 1.56; 95% CI: 1.06-2.28). None of the variables in the univariate or multivariate logistic regression was a factor associated with threatened abortion after 6 weeks gestational age. In conclusion,  $\beta$ -hCG and estrogen levels in the first half of the first trimester are factors associated with threatened abortion.

**Keywords:** Early pregnancy, cross-sectional study, gestational week

## 1. Introduction

The complex interaction among luteinizing hormone (LH), follicle-stimulating hormone (FSH), estrogen, and progesterone regulates the follicular, ovulatory, and luteal phases of the menstrual cycle spatiotemporally (1-3). Levels of estrogen and progesterone are low at the beginning of the follicular phase, and then estrogen peaks and progesterone starts to increase during the ovulatory phase (1-3). Estrogen and progesterone

levels are high during most of the luteal phase, which causes the lining of the uterus to thicken to prepare for possible fertilization (1-3). If no egg is fertilized, the corpus luteum degenerates and no longer produces progesterone, the estrogen level decreases, and a new menstrual cycle starts (1-3). This repertoire lasts throughout a woman's reproductive life, except during pregnancy (1-4).

A new repertoire occurs once a sperm meets an egg. Human chorionic gonadotropin (hCG) is synthesized, mainly by the syncytiotrophoblast of the newly developing placenta, 1 day after implantation. hCG replaces the function of LH on about day 8 after ovulation and rescues the corpus luteum from involution (5). This maintains progesterone and estrogen secretion by the ovarian granulosa cells during the first trimester (6). hCG is at its peak (about 100,000 IU/L) between weeks 8 and 10 of gestation, and tends to plateau at a lower level for the remainder

Released online in J-STAGE as advance publication May 24, 2019.

<sup>§</sup>These authors contributed equally to this work.

\*Address correspondence to:

Drs. Jun Xu and Yunheng Zhu, Department of Obstetrics and Gynecology, Minhang Hospital, Fudan University, 170 Xinsong Road, Minhang District, Shanghai 201199, China.  
E-mail: xlartical@163.com (Xu J), henghengalex@hotmail.com (Zhu YH)

of the pregnancy (4,7). Progesterone and estrogen are largely produced by the corpus luteum until about 10 weeks of gestation; after the first trimester, the placenta synthesizes and secretes these two hormones (8-10). Progesterone levels gradually increase to 100-200 ng/mL when the pregnancy reaches term gestation. Estrogen levels increase steadily during pregnancy and reach their peak in the third trimester (8-10).

Progesterone and estrogen play significant roles during a normal pregnancy (8-10). The gradually increasing level of estrogen during pregnancy enhances the formation of blood vessels and transfer of nutrients, and supports the developing fetus (8-10). Progesterone keeps the placenta functioning properly and the uterine lining healthy and thick, as well as stimulating growth of breast tissue (4,7,8-10). It also prevents natural pre-pregnancy contractions of the uterine smooth muscle, allowing the fetus to grow in the expanding womb. Progesterone stimulates secretion of Th2 and reduces secretion of Th1 cytokines, reducing maternal immunological rejection of the fetus (11,12).

Any change in the homeostasis of these hormones impacts a normal pregnancy (13-15). A low hCG level is always observed in women who eventually miscarried in their first trimester and can indicate a blighted ovum or an ectopic pregnancy, whereas a high hCG level can indicate a molar pregnancy or a multiple pregnancy (13-15). Threatened abortion often occurs during the period of luteal-placental shift (8 to 12 weeks of gestation) due to a limited corpus luteum function or an abnormality in placental progesterone production and secretion (14). A reduction in the rate of spontaneous miscarriage with the use of dydrogesterone was also observed (14). Lower estrogen level was found in women with threatened abortion and historically estrogen was also commonly used to save threatened pregnancies in these women (16,17). However, evidence from randomised controlled trials to assess the use of estrogen and/or progesterone for preventing miscarriages is insufficient (6,13,17,18). Thus, the associations of these hormones levels with abnormal pregnancy remain undefined, some theories are controversial (6,13,17,18), and further studies are needed. In this report, the associations of hCG, estrogen, and progesterone levels with threatened abortion were evaluated in 80 women with threatened abortion and 160 normal controls. Our results showed that  $\beta$ -hCG and estrogen levels in the first half of the first trimester are higher in women with threatened abortion than women with normal early pregnancy and no significant difference in progesterone level observed between two groups.

## 2. Materials and Methods

### 2.1. Design and participants

This study was carried out in accordance with the

recommendations of the Declaration of Helsinki for medical research involving human subjects, the World Medical Association with written informed consent from all subjects. All subjects gave written informed consent in accordance with the Declaration of Helsinki. The protocol was approved by The Review Board of the Ethics Committee of Medical Research at Minhang Hospital, Fudan University.

A cross-sectional study was conducted on continuously registered outpatients visiting our Department of Obstetrics and Gynecology, between January 2016 and February 2017. Integrating the current consensus on diagnosis of threatened abortion (19-21), in this report, threatened abortion (threatened miscarriage) referred to a bloody vaginal discharge or bleeding other than spotting during the first trimester of completed gestation with evidence of a progressive viable pregnancy on ultrasound.

For differential diagnosis of threatened abortion; a pelvic exam was performed on women suspected of threatened abortion to identify the source of bleeding and to determine whether the amniotic sac was ruptured; a transvaginal ultrasound was performed to determine the amount of bleeding, to learn intrauterine pregnancy, and to monitor the heartbeat and development of the fetus; serial quantitative serum  $\beta$ -hCG and progesterone levels were measured to monitor the dynamic changes of pregnancy hormones; in addition, gonorrhea and chlamydia testing were also performed to exclude infection. Since there is no reliable approach to diagnose threatened abortion, women suspected of threatened abortion, whose intrauterine fetus survived over first trimester, were identified as threatened abortion. All subjects were assembled by four experienced obstetricians with cross validation; any uncertainties in inclusion criteria were resolved by discussion among chief obstetricians in our department.

As showed in Figure 1, subjects with early pregnancy loss (the loss of a pregnancy during the first 13 weeks of pregnancy,  $N = 9$ ), ectopic pregnancy ( $N = 8$ ), twin or multiple pregnancy ( $N = 2$ ), prophylactic hormonal supplementation ( $N = 2$ ), and supportive hormonal care ( $N = 3$ ) were excluded from this study. Exclusion criteria also include women with inevitable, incomplete, or complete abortion ( $N =$ ); women with septic abortion ( $N = 0$ ); and women with non-threatened abortion-related bleeding (such as extragenital bleeding,  $N = 3$ ). Finally, 80 women with threatened abortion were included in this study.

The normal controls of early pregnancy were selected from every tenth women with an early pregnancy but no complications continuously (Figure 1). 14 subjects refuse to participate; 10 subjects with incomplete data; 3 subjects were ectopic pregnancy; and 3 subjects were twin/multiple were excluded from the control group. Finally, 160 subjects with early pregnancy were involved as normal controls.

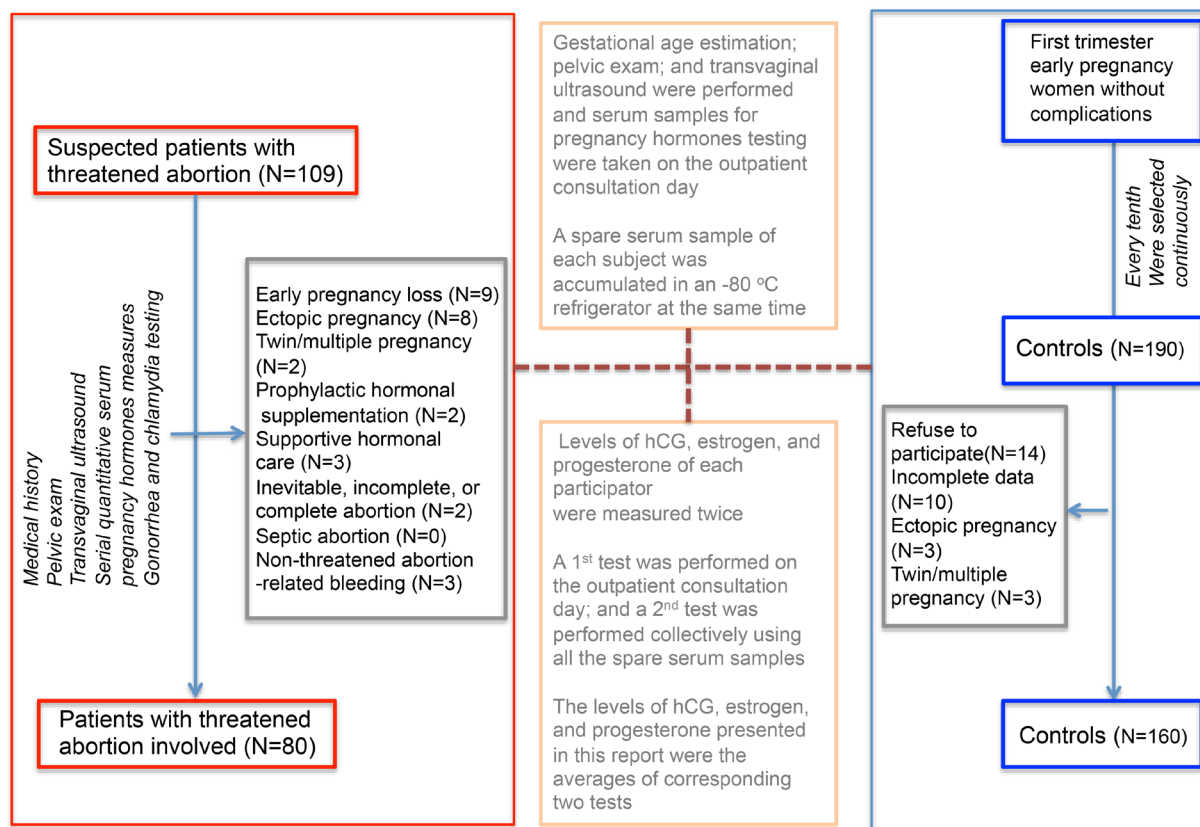


**Figure 1. A diagram of the study subjects involved, measurements of pregnancy hormones and gestational age estimation.** This is a cross-sectional study conducted on continuously registered outpatients visiting our Department of Obstetrics and Gynecology. Right panel, flowchart of controls involved; left panel, flowchart of cases involved; middle panel, diagnosis process.

Their levels of serum hCG, progesterone, and estrogen were measured according to the principle of ethical voluntariness. Gestational age was calculated from the last normal menstrual period if the mother had a regular period and knew the first day of her last menstrual period or according to the "Determination of Gestational Age by Ultrasound" recommendation from the American College of Obstetricians and Gynecologists (19) on the day visiting our department.

## 2.2. Levels of serum hCG, progesterone, and estrogen

The levels of hCG, progesterone, and estrogen were determined in the clinical laboratory of our hospital. Briefly, blood samples were drawn in all the women upon admission and centrifuged at 3,000 rpm at  $4^{\circ}\text{C}$  in time; serum samples were stored at  $-20^{\circ}\text{C}$  before daily centralized and unified routine testing. For this study, a spare serum sample of each patient with strict records was accumulated in an  $-80$  degree refrigerator at the same time. Levels of hCG, estrogen, and progesterone of each participant were measured twice; a 1<sup>st</sup> test was performed on the outpatient consultation day; and a 2<sup>nd</sup> test was performed collectively using all the spare serum samples; the levels presented in this report were the averages of corresponding twice tests (Figure 1). All measurements were carried out in the same laboratory.

hCG, progesterone, and estrogen concentrations were measured using the ARCHITECT Total Beta hCG Reagent Kit (Longford, Ireland), the ARCHITECT PROGEST RGT, and the ARCHITECT Estrogen Reagent Kit according to the manufacturer's instructions. The inter-assay coefficients of variation were calculated from the mean values for the high and low controls (reference reagents provided by Abbott Architect) on each plate; the inter-assay coefficients of variation for estrogen, progesterone and hCG were 9.2%, 10.3% and 11.1%, respectively. The intra-assay coefficients variation were calculated from the individual coefficients variation for all of the duplicates; and the intra-assay coefficients variation for estrogen, progesterone and hCG were 7.9%, 6.8% and 8.3%, respectively.

## 2.3. Statistical analysis

The distribution of all variables is assessed using a histogram; variables with a skewed distribution were transformed by natural logarithm (Ln) and further presented by histogram. The Ln-transformed variables were used instead of the original clinical values. Ln-transformed and normally distributed variables are presented as means  $\pm$  standard deviations (SDs). Differences between groups were evaluated using the independent-samples Mann-Whitney *U*-test. Spearman's

rank correlation coefficient array analysis was performed to determine the collinearity and interior relationships among the variables. Binary logistic regression analysis was adopted to understand how the pregnancy hormones were associated with threatened abortion. Variables in the models were selected according to Spearman's rank correlation coefficient and physiological and biochemical principles. All statistical analyses were performed with SPSS software (ver. 13.0; SPSS, Inc., Chicago, IL, USA), and the significance level was set to  $\alpha = 0.05$ .

### 3. Results

#### 3.1. hCG and estrogen levels are significantly higher in women with a threatened abortion

Variables of pooled subjects (without stratification by gestational age) were compared first to detect differences in the pregnancy hormone levels between women with threatened abortion and those with normal early pregnancy. hCG, estrogen, and progesterone displayed skewed distributions, so the concentrations were natural log-transformed before statistical analyses. As shown in Table 1, the average Lnestrogen and LnhCG levels were significantly higher in women with threatened abortion than in those with normal pregnancy. No differences in age, gestational age, or progesterone levels were observed between the two groups. In conclusion, hCG and estrogen levels were significantly higher in women with threatened abortion.

#### 3.2. hCG and estrogen levels of women with a threatened abortion are higher in the first half of the first trimester

The levels of hCG, estrogen, and progesterone were stratified by gestational age to further understand their distributions in women with threatened abortion and women with normal pregnancy. As shown in Figure 2A, the LnhCG level of women with threatened abortion and gestational age  $\leq 6$  weeks was  $8.6 \pm 1.2$  mIU/mL, which was significantly higher than that of the normal controls ( $7.4 \pm 1.7$  mIU/mL) from the same gestational age group. Interestingly, the hCG level of women with

threatened abortion was similar to that of normally pregnant women with gestational age  $> 6$  weeks ( $10.8 \pm 1.2$  vs.  $10.7 \pm 1.2$  mIU/mL). A similar trend in estrogen levels was observed: the Lnestrogen of women with threatened abortion and the normal controls of gestational age  $\leq 6$  weeks and  $> 6$  weeks were  $5.8 \pm 0.4$  vs.  $5.4 \pm 0.5$  pg/mL and  $6.4 \pm 0.5$  vs.  $6.4 \pm 0.6$  pg/mL, respectively. The estrogen level of women with threatened abortion was significantly higher than that of the normal controls in the gestational age  $\leq 6$  weeks group (Figure 2B). The Lnprogesterone level of women with threatened abortion was similar between the two gestational age stratifications ( $2.9 \pm 0.3$  and  $2.9 \pm 0.3$  ng/mL, respectively), whereas, the Lnprogesterone level of the normal controls tended to differ between the two gestational age stratifications ( $2.8 \pm 0.5$  and  $3.0 \pm 0.3$  ng/mL, respectively;  $P > 0.05$ ) (Figure 2C). Taken together, these data showed that the hCG and estrogen levels of women with threatened abortion were higher during the first half of the first trimester and reached levels similar to those of controls thereafter.

#### 3.3. Factors associated with threatened abortion without stratification by gestational age

A multivariate logistic regression analysis was performed without the gestational age stratification to understand how hCG and estrogen levels were associated with threatened abortion. To exclude any impact of collinearity of these hormone indices on the statistical model, the relationships between individual variables were quantified by the Spearman's rank correlation coefficient array analysis. As shown in Figure 2D, hCG and gestational age, estrogen and gestational age, hCG and estrogen, and estrogen and progesterone were significantly correlated, with correlation coefficients of 0.871, 0.762, 0.787, and 0.255, respectively. Similar correlation coefficients were observed in women with threatened abortion, except for estrogen and progesterone (Figure 2E). Univariate analyses showed that LnhCG and Lnestrogen were possible factors associated with threatened abortion (Table 2). However, the multivariate logistic regression

**Table 1. Differences between women with a threatened abortion and normal early pregnancy with no stratification by gestational age**

Variables	Threatened abortion, $N = 80$	Early pregnancy, $N = 160$	$P$
Age	$29.4 \pm 5.3$	$28.9 \pm 5.5$	0.443
Gestational week (range)	$6.7 \pm 1.4$ (4.6 - 11.0)	$6.6 \pm 1.6$ (4.4 - 12.1)	0.217
hCG, mIU/mL	29,503.0 (10,825.0, 80,360.0)	12,026.6 (1,404.5, 52,255.8)	/
LnhCG, mIU/mL	$10.0 \pm 1.6$	$9.0 \pm 2.2$	$< 0.001$
Progesterone, ng/mL	19.2 (15.7, 21.0)	18.4 (14.9, 22.9)	/
LnProgesterone, ng/mL	$2.9 \pm 0.3$	$2.9 \pm 0.4$	0.570
Estrogen, pg/mL	480.0 (329.5, 844.0)	375.0 (220.0, 652.0)	/
LnEstrogen, pg/mL	$6.2 \pm 0.5$	$5.9 \pm 0.7$	0.001

Normally distributed data are presented as mean  $\pm$  SD; skewed data are presented as median (interquartile range). Differences between groups were examined using an independent-samples Mann-Whitney  $U$ -test. hCG, human chorionic gonadotropin; Ln, natural logarithm.

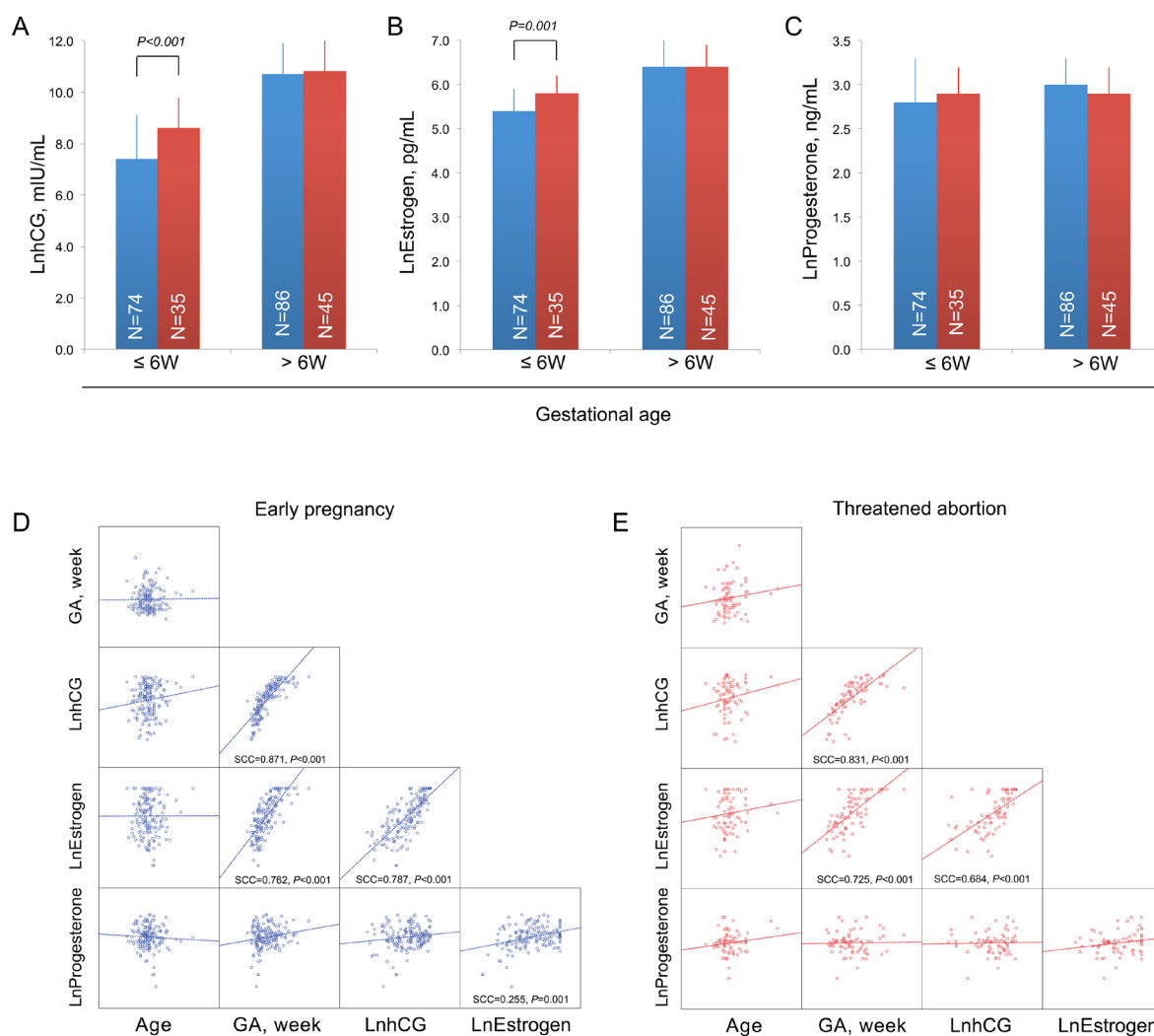


**Figure 2.** The levels in pregnancy hormones stratified by gestational age and Spearman's rank correlation coefficient array analysis. (A) to (C), average LnhCG, LnEstrogen and Lnprogesterone of women with gestational age  $\leq 6$  weeks (numbers of threatened abortion and early pregnancy were 35 and 74, respectively) and  $> 6$  weeks (numbers of threatened abortion and early pregnancy were 45 and 86, respectively). Red histograms in (A) to (C), women with threatened abortion; blue histograms in (A) to (C), women with normal early pregnancy. (A), average LnhCG with SD; (B), average LnEstrogen with SD; (C), average Lnprogesterone with SD. (D), collinearity and relationships between variables of women with early pregnancy were quantified by Spearman's rank correlation coefficient array analysis. (E), collinearity and relationships between variables of women with threatened abortion were quantified by Spearman's rank correlation coefficient array analysis. SCC, Spearman's rank correlation coefficient; SD, standard deviation.

**Table 2.** Factors associated with threatened abortion without stratification by gestational age

Items	OR	95% CI	P
Univariate analyses			
Gestational week	1.34	0.97 - 1.55	0.213
LnProgesterone, ng/mL	1.24	0.59 - 2.58	0.569
LnhCG, mIU/mL	1.31	1.13 - 1.52	< 0.001
LnEstrogen, pg/mL	2.06	1.32 - 3.21	0.001
Multivariate logistic regression modeling			
LnEstrogen, pg/mL	1.89	0.91 - 2.31	0.235
LnhCG, mIU/mL	1.28	1.10 - 1.49	0.001

Backward stepwise (Wald) multivariate logistic regression analysis was adopted. hCG, human chorionic gonadotropin; Ln, natural logarithm; OR, odds ratio; CI, confidence interval.

model showed that hCG and estrogen were mutually confounding factors, and only LnhCG remained an independent factor positively associated with threatened abortion (OR 1.28; 95% CI 1.10-1.49; Table 2).

#### 3.4. Factors associated with a threatened abortion with stratification by gestational age

The preceding analysis showed that hCG and estrogen

**Table 3. Factors associated with a threatened abortion using stratification by gestational age**

Items	Gestational age $\leq$ 6 weeks, $N = 109$			Gestational age $>$ 6 weeks, $N = 131$		
	OR	95% CI	$P$	OR	95% CI	$P$
Univariate analyses						
Gestational week	2.35	0.93 - 5.72	0.521	0.95	0.70 - 1.28	0.739
LnProgesterone, ng/mL	2.11	0.71 - 6.31	0.188	0.49	0.15 - 1.64	0.252
LnhCG, mIU/mL	1.85	1.30 - 2.64	0.001	1.07	0.79 - 1.44	0.656
LnEstrogen, pg/mL	4.62	1.67 - 12.80	0.003	1.27	0.64 - 2.55	0.491
Multivariate logistic regression modeling						
LnEstrogen, pg/mL	2.59	0.86 - 7.79	0.091	1.38	0.62 - 3.07	0.437
LnhCG, mIU/mL	1.56	1.06 - 2.28	0.023	0.94	0.65 - 1.34	0.718

hCG, human chorionic gonadotropin; Ln, natural logarithm; OR, odds ratio; CI, confidence interval.

levels of women with threatened abortion were higher in the first half, but not in the second half, of the first trimester. To study the factors associated with threatened abortion more precisely, subjects were divided into two groups: gestational age  $\leq$  6 weeks and  $>$  6 weeks. A logistic regression analysis was performed on these two groups. The univariate analysis showed that LnhCG and Lnestrogen were factors for threatened abortion in the group with gestational age  $\leq$  6 weeks. The multivariate logistic regression model showed that hCG and estrogen were mutually confounding factors, and only LnhCG remained an independent factor positively associated with threatened abortion (OR 1.56; 95% CI 1.06-2.28; Table 3). As expected, none of the hormone levels was a factor associated with threatened abortion for the group of gestational age  $>$  6 weeks in the univariate or multivariate logistic regression model (Table 3).

#### 4. Discussion

Abnormal early pregnancy is common and has numerous clinicopathological characteristics (21,22). In this study, we focused on threatened abortion and evaluated the associations of three hormones with threatened abortion. The LnhCG and Lnestrogen levels of pooled subjects with threatened abortion were significantly higher than those of gestational age-matched controls with normal pregnancy. A further gestational age stratification showed that LnhCG and Lnestrogen levels were significantly higher than the normal controls only in women with threatened abortion at gestational age  $\leq$  6 weeks. Univariate analyses revealed that LnhCG and Lnestrogen were factors associated with threatened abortion. Although hCG and estrogen were mutually confounding factors and only LnhCG remained an independent risk for threatened abortion in the multivariate logistic regression model, we incline to results of univariable analyses to annotate the role of hCG and estrogen in association with threatened abortion based on following physiological principle: hCG is synthesized and secreted by the syncytiotrophoblast of the developing placenta,

whereas, progesterone and estrogen is synthesized and secreted by corpus luteum (4,7,8-10); although hCG is a dominant hormone to maintain corpus luteum to secrete progesterone and estrogen during the first trimester, the role of estrogen in association with threatened abortion could not be erased by the high collinearity between hCG and estrogen levels.

As serum hCG levels normally double every 1.8-3 days for the first 6-7 weeks of pregnancy, any error in the gestational age calculation may have affected our comparative analysis (23,24). However, no significant difference in average gestational age was observed between the case and control groups. The univariate analysis also showed no association between gestational age and threatened abortion. Thus, the matched gestational age excluded any possible effects of gestational age on these hormone levels between the groups. Although hCG increases sharply during the first half of the first trimester, estrogen increases at a steady and slow rate (8-10), so a higher estrogen level in the threatened abortion group was not likely caused by an error in the gestational age calculation. The average Lnprogesterone level was stable between  $\leq$  6 weeks and  $>$  6 weeks of gestational age, which also suggested that the higher estrogen level was not a secondary error associated with higher hCG. Thus, higher Lnestrogen and steady Lnprogesterone levels might reflect an inherent pathophysiological characteristic of the corpus luteum associated with threatened abortion.

Current knowledge on high hCG levels is very limited. Existing hypotheses posit an error in the gestational age calculation, a signal of a twin or multiple pregnancy, and a result of fertility drugs (22). Molar pregnancy or trisomy 21 may cause excessive beta-hCG (21,25,26); since all participants had undergone ultrasound examination to monitor the heartbeat and development of the fetus; a possibility that the presence of molar pregnancy in the threatened abortion group could be excluded. While, trisomy 21 screening has not been carried out in our hospital, so, we could not exclude a possibility that the presence of trisomy 21 in the threatened abortion group was responsible for higher hCG partially. Nonetheless, all of our subjects

were singleton pregnancies, and women taking fertility drugs were excluded from this study. We also excluded the possibility of error in gestational age calculation in the preceding paragraph. Thus, a higher level of hCG in the first 6 weeks likely represents an abnormal pathophysiological characteristic in the synthesis and secretion of hCG associated with threatened abortion.

The definition of miscarriage includes types of inevitable, complete, missed and recurrent miscarriages in addition to threatened abortion. As a type with relatively good prognosis, threatened abortion is not studied enough. Commonly used estrogen and/or progesterone supplements had not approved by randomised controlled trials (6,13,17,18) suggesting that our knowledge in this topic is insufficient. Our data showed that higher, not lower, hCG and/or estrogen levels associated with threatened abortion. Although a cross-sectional study could not reveal the pathological mechanism of these associations, these clinical evidences will enlighten studies on the mechanism.

As we know, LH, FSH, and hCG are heterodimers consisting of a common glycoprotein  $\alpha$ -subunit and a unique  $\beta$ -subunit; and the  $\beta$ -subunits of LH and hCG shared 80% similarity in their amino acid sequences (27). During early pregnancy, hCG could control the function of corpus luteum through hypothalamic-pituitary-ovarian axis (27). The mechanisms underlying the elevation of hCG and estrogen in threatened abortion might be the following: higher hCG level might reflect the excessive development of placenta in women with threatened abortion, which altered the normal spatio-temporal interaction process between endometrium and placenta and cause bleeding; higher hCG level stimulates LH/hCG receptors on the granulosa-lutein cells (estrogen secreting), which are in a high steroidogenesis state of 18 carbon atoms steroids during the first 6 weeks of pregnancy (27), to produce and secrete more estrogen; whereas the thecal-lutein cells (progesterone secreting) maintain a normal rhythm of progesterone synthesis and secretion; alternatively, the above pathological processes will trigger the maternal injury repair mechanisms, elevated estrogen level may be a manifestation of the maternal injury repair mechanisms (28). As hCG level peaked at 6-8 weeks and followed by a relatively sharp decline in the first trimester, the above physiological changes will thus be regressed in the 2<sup>nd</sup> half of first trimester; this might be why hCG and estrogen levels were significantly higher than the normal controls only in women with threatened abortion at gestational age  $\leq 6$  weeks, but not at gestational age  $> 6$  weeks.

During the first trimester, most factors that cause a miscarriage are genetic (21). Although other reasons for miscarriage are varied and most often cannot be identified (21); the synthesis and secretion of hCG and luteal-placental shift are main endocrinological repertoire occurred in first trimester pregnancy, abnormality in the

series of rigorous physiological processes are believed to be a causer of threatened abortion (6,14,21). This is why our study focused on the three hormones levels only in the first trimester pregnancy. Although all fetuses of women with threatened abortion survived over first trimester, some of them might end with spontaneous abortion after 13 weeks (21,29). Meanwhile, miscarriage after first trimester might also occur in our control subjects. Since the pathophysiology of miscarriage differed by trimesters (19-22), factors associated with miscarriage within remain two trimesters need to be evaluated in further study.

In conclusion, our data showed that higher  $\beta$ -hCG and estrogen levels during the first 6 weeks of gestation were associated with threatened abortion. These results will advance our understanding of hormone supportive care in women participating in assisted reproduction techniques.

### Acknowledgements

This study was supported by a grant from the WU JIEPING MEDICAL FOUNDATION (grant number 320.6750.13152) and a grant of the Shanghai Municipal Commission of Health and Family Planning (Serial number: 201840340).

### References

1. Stricker R, Eberhart R, Chevaller MC, Quinn FA, Bischof P, Stricker R. Establishment of detailed reference values for luteinizing hormone, follicle stimulating hormone, estradiol, and progesterone during different phases of the menstrual cycle on the Abbott ARCHITECT analyzer. *Clin Chem Lab Med.* 2006; 44:883-887.
2. Nader S. Reproductive endocrinology: Menstrual cycle lengths – what can they tell us? *Nat Rev Endocrinol.* 2012; 8:704-706.
3. Wira CR, Rodriguez-Garcia M, Patel MV. The role of sex hormones in immune protection of the female reproductive tract. *Nat Rev Immunol.* 2015; 15:217-230.
4. Kumar P, Magon N. Hormones in pregnancy. *Niger Med J.* 2012; 53:179-183.
5. Korevaar TIM, Medici M, Visser TJ, Peeters RP. Thyroid disease in pregnancy: New insights in diagnosis and clinical management. *Nat Rev Endocrinol.* 2017; 13:610-622.
6. Polliotti BM. Current progress in early pregnancy investigation. *Early Pregnancy.* 1997; 3:38-51.
7. Itskovitz J, Rubattu S, Levron J, Sealey JE. Highest concentrations of prorenin and human chorionic gonadotropin in gestational sacs during early human pregnancy. *J Clin Endocrinol Metab.* 1992; 75:906-910.
8. Messinis IE, Messini CI, Dafopoulos K. Luteal-phase endocrinology. *Reprod Biomed Online.* 2009; 19:4314.
9. Fatemi HM. The luteal phase after 3 decades of IVF: What do we know? *Reprod Biomed Online.* 2009; 19:4331.
10. Devoto L, Kohen P, Muñoz A, Strauss JF 3<sup>rd</sup>. Human corpus luteum physiology and the luteal-phase dysfunction associated with ovarian stimulation. *Reprod*

- Biomed Online. 2009; 18:19-24.
11. Piccinni MP, Scaletti C, Maggi E, Romagnani S. Role of hormone-controlled Th1- and Th2-type cytokines in successful pregnancy. *J Neuroimmunol.* 2000; 109:30-33.
  12. Perricone C, de Carolis C, Perricone R. Pregnancy and autoimmunity: A common problem. *Best Pract Res Clin Rheumatol.* 2012; 26:47-60.
  13. Sotiriadis A, Papatheodorou S, Makrydimas G. Threatened miscarriage: Evaluation and management. *BMJ.* 2004; 329:152-155.
  14. Schindler AE, Carp H, Druckmann R, Genazzani AR, Huber J, Pasqualini J, Schweppe KW, Szekeres-Bartho J. European Progestin Club Guidelines for prevention and treatment of threatened or recurrent (habitual) miscarriage with progestogens. *Gynecol Endocrinol.* 2015; 31:447-449.
  15. Goldstein SR. Early pregnancy: Normal and abnormal. *Semin Reprod Med.* 2008; 26:277-283.
  16. Dessaive R, de Hertogh R, Thomas K. Correlation between hormonal levels and ultrasound in patients with threatened abortion. *Gynecol Obstet Invest.* 1982; 14:65-78.
  17. Lim CE, Ho KK, Cheng NC, Wong FW. Combined oestrogen and progesterone for preventing miscarriage. *Cochrane Database Syst Rev.* 2013; CD009278.
  18. Pillai RN, Konje JC, Tincello DG, Potdar N. Role of serum biomarkers in the prediction of outcome in women with threatened miscarriage: A systematic review and diagnostic accuracy meta-analysis. *Hum Reprod Update.* 2016; 22:228-239.
  19. Butt K, Lim K, DIAGNOSTIC IMAGING COMMITTEE. Determination of gestational age by ultrasound. *J Obstet Gynaecol Can.* 2014; 36:171-181.
  20. Griebel CP, Halvorsen J, Golemon TB, Day AA. Management of spontaneous abortion. *Am Fam Physician.* 2005; 72:1243-1250.
  21. First-Trimester Abortion. In: Williams Gynecology (Hoffman BL, Schorge JO, Bradshaw KD, Halvorson LM, Schaffer JI, Corton MM, eds). McGraw-Hill Education, New York, USA, 2016; pp137-160.
  22. Committee on Practice Bulletins-Gynecology. The American College of Obstetricians and Gynecologists Practice Bulletin no. 150. Early pregnancy loss. *Obstet Gynecol.* 2015; 125:1258-1267.
  23. Larsen J, Buchanan P, Johnson S, Godbert S, Zinaman M. Human chorionic gonadotropin as a measure of pregnancy duration. *Int J Gynaecol Obstet.* 2013; 123:189-195.
  24. Cole LA. hCG, the wonder of today's science. *Reprod Biol Endocrinol.* 2012; 10:24.
  25. Cavaliere A, Ermito S, Dinatale A, Pedata R. Management of molar pregnancy. *J Prenat Med.* 2009; 3:15-17.
  26. Shiefa S, Amargandhi M, Bhupendra J, Moulali S, Kristine T. First Trimester Maternal Serum Screening Using Biochemical Markers PAPP-A and Free  $\beta$ -hCG for Down Syndrome, Patau Syndrome and Edward Syndrome. *Indian J Clin Biochem.* 2013; 28:3-12.
  27. Reproductive Endocrinology. In: Williams Gynecology (Hoffman BL, Schorge JO, Bradshaw KD, Halvorson LM, Schaffer JI, Corton MM, eds). McGraw-Hill Education, New York, USA, 2016; pp334-368.
  28. Wang X, Bao H, Liu X, Wang C, Hao C. Effects of endometrial stem cell transplantation combined with estrogen in the repair of endometrial injury. *Oncol Lett.* 2018; 16:1115-1122.
  29. The American College of Obstetricians and Gynecologists. Multiple Pregnancy. <https://www.acog.org/-/media/For%20Patients/faq188.pdf>. (Accessed July 15, 2018)
- (Received April 25, 2019; Revised May 8, 2019; Re-  
Revised May 16, 2019; Accepted May 18, 2019)

# Protection of paeonol against epirubicin-induced hepatotoxicity: A metabolomic study

Xu Jing<sup>1</sup>, Chao Sun<sup>2</sup>, Huigang Chen<sup>3</sup>, Jing Sun<sup>2</sup>, Ying Zhang<sup>2</sup>, Jing Wu<sup>2,\*</sup>

<sup>1</sup>Laboratory Medical Center, The Second Hospital of Shandong University, Ji'nan, China;

<sup>2</sup>Department of Pharmacy, The Second Hospital of Shandong University, Ji'nan, China;

<sup>3</sup>Department of Pathological Obstetrics, ZhuCheng Maternal and Child Health Hospital, Weifang, China.

## Summary

Paeonol extracted from the Moutan Cortex, possesses hepatoprotective activity against epirubicin (EPI)-induced liver damage. This study evaluated the protective effect of paeonol on EPI-induced hepatotoxicity and explored the underlying metabolomic mechanism. Breast tumor-bearing mice were randomly divided into three groups: control, EPI, and EPI + paeonol treatment. Mice received a tail *i.v.* injection of EPI every other day for 3 cycles or/and intragastrically (*i.g.*) administered paeonol daily for 6 days. Hematoxylin-eosin (HE) staining and biochemical detection were used to determine the degree of damage. A gas chromatography-mass spectrometry (GC-MS) technique was established to determine the metabolites. PLS-DA and PCA were used to investigate metabolic changes. HE staining and biochemical detection results showed that EPI caused serious liver damage while paeonol ameliorated it. The results of mass spectrogram, partial least squares-discriminate analysis (PLS-DA), and principal component analysis (PCA) demonstrated that lipid, amino acid, and energy metabolism involving seven metabolites were obviously changed by EPI and reversed by paeonol. Additionally, paeonol inhibited EPI-induced activation of adenosine monophosphate activated protein kinase/mammalian target of Rapamycin (AMPK/mTOR) signalling pathway. Our results demonstrated the hepatoprotective effect of paeonol on EPI-induced hepatotoxicity in mice, provided potential biomarkers for early assessment of EPI-induced liver injury and illuminated the metabolic mechanism underlying paeonol-related hepatic protection.

**Keywords:** Paeonol, liver injury, GC-MS, metabolomic, AMPK/mTOR

## 1. Introduction

Epirubicin (EPI), an effective anthracycline antibiotic, is mainly metabolized in the liver, and its metabolites are associated with oxidative stress toxicity (1). EPI-induced liver toxicity is one of the major causes of hepatic dysfunction (2). Paeonol (2-hydroxy-4-methoxyacetophenone) is an active constituent isolated from the Chinese herbal medicine Moutan Cortex and *Cynanchum paniculatum* (3). Paeonol has been reported

to have various biological activities, including anti-inflammatory, anti-allergic, and immune-regulation (4). In our previous studies, paeonol presented antioxidative stress activity, anti-inflammatory action, and apoptosis inhibition in EPI-induced liver damage by affecting the phosphatidylinositol 3-kinase/protein kinase B (PI3K/AKT) and nuclear factor (NF)-KB pathways (5).

EPI-induced hepatocyte oxidative stress and paeonol-related antioxidants change a series of biochemical parameters, which impact downstream metabolic processes (6,7). Conventional judgment of hepatotoxicity is principally according to the changes of aminopherases, including aspartate transaminase (AST), which increased after hepatonecrosis (8). Therefore, it is a priority to investigate potential indicators in initial liver injury induced by EPI and the treatment outcomes of paeonol.

With the development of analytical technologies, the metabolomic approach is widely used for the

Released online in J-STAGE as advance publication June 23, 2019.

\*Address correspondence to:

Dr. Jing Wu, Department of Pharmacy, The Second Hospital of Shandong University, 247# Beiyuan Road, Ji'nan 250033, China.

E-mail: wujing19830603@126.com

identification of biomarkers for disease investigation and toxicity assessment (2). The combined application of mass spectrometry and chromatography is gaining widespread use in metabolomic studies, and the most common technique is gas chromatography-mass spectrometry (GC-MS) for its strategic advantages (9). In the present work, GC-MS-based pairwise comparative metabolomic was applied to investigate the altered metabolites in serum and uncover the potential metabolic processes following EPI and paeonol treatment. The results demonstrate potential biomarkers for early assessment of EPI-induced hepatotoxicity and illuminate the metabolic mechanism underlying paeonol-related hepatic protection.

## 2. Materials and Methods

### 2.1. Materials

EPI and paeonol (purity, 99.12% by high-performance liquid chromatography: HPLC) were purchased from Sigma-Aldrich, Inc., St. Louis, MO, USA. Trimethylchlorosilane (TMCS) and n-heptadecanoic acid was purchased from Sinopharm Chemical Reagent Co., Ltd. (Shanghai, China). Methoxy pyridine was purchased from Tianjin Kermel Chemical Reagent Co., Ltd. (China). HPLC grade acetonitrile and n-hexane were purchased from J.T. Baker (USA).

### 2.2. Instruments

Agilent 7890A-5975C GC-MS (Agilent Technologies, Inc., USA), XW-80A vortex mixers (Jingke Industrial Co., Ltd., Shanghai, China), MS205 DU electronic scale (Mettler-Toledo, Shanghai, China), ABBOTT centrifuge (Abbott Laboratories, USA) and KD-500DE ultrasound cleaner (Kunshan Ultrasonic Instrument Co., Ltd., China) were used.

### 2.3. Animals

Female BALB/c mice (aged 6-8 weeks, weighing 18-22 g) were purchased from the Laboratory Animal Centre, of Shandong University in China. The animals were housed under specific-pathogen free conditions at the Animal Centre of the Department of Pharmacology of the School of Medicine of Shandong University in China. The protocol for the *in vivo* study with mice conforms to the Guide for the Care and Use of Laboratory Animals published by the US National (Permit Number: KYLL-2017(GJ)A-0028). All experiments were approved by the Ethics Committee of The Second Affiliated Hospital of Shandong University.

### 2.4. Experimental design

A breast tumor-bearing mice model was established as

previously described (8). In brief, BALB/c mice were subcutaneously injected with 4T1 cells (suspension, 100  $\mu$ L,  $5 \times 10^6$  cells/mL) in the right side of the fourth mammary gland. The tumor length and width were measured using a digital caliper, and the tumor volume was calculated using the following formula: tumor volume ( $\text{mm}^3$ ) = (length  $\times$  width<sup>2</sup>)/2. When the size of the tumors was approximately 100  $\text{mm}^3$ , the mice were randomly divided into three groups: control, EPI, and EPI + paeonol treatment:

Control group: mice received intragastrically (*i.g.*) administered saline daily for 6 days and a tail intravenous (*i.v.*) injection of saline every other day for three cycles;

EPI group: mice received *i.g.* saline daily for 6 days and a tail *i.v.* injection of EPI (6 mg/kg) every other day for 3 cycles;

Combined group: mice received *i.g.* paeonol (30 mg/kg) daily for 6 days and a tail *i.v.* injection of EPI (6 mg/kg) every other day for 3 cycles.

Blood was collected and the mice were sacrificed on day 8. The liver tissues were removed rapidly. Some livers were fixed in formalin for hematoxylin and eosin (HE) staining, whereas others were frozen in liquid nitrogen (stored at  $-80^\circ\text{C}$ ) for Western blot analysis.

### 2.5. Histopathological examination and assay of hepatic marker enzymes

Liver tissues were fixed in 10% buffered formalin, embedded in paraffin, sectioned (5 mm thick) and stained with HE for histopathological analysis under light microscope (CKX41, 170 Olympus, Tokyo, Japan). Samples were obtained after centrifugation (4,000 rpm, 5 min) to monitor the biochemistry index. The alanine aminotransferase (ALT), glutamic-oxalacetic transaminase (AST) and alkaline phosphatase (ALP) in plasma were assayed according to the manufacturer's instructions (Nanjing Jiancheng Biotechnology Institute, China).

### 2.6. Western blot analyses

Western blots were analyzed as described previously (8). All procedures followed the suppliers' instructions. Livers were cut into small pieces, homogenized in pyrolysis liquid (containing phenylmethylsulfonyl fluoride) on ice and centrifuged at 12,500 rpm for 5 min at  $4^\circ\text{C}$ . Supernatants were harvested to denature by boiling for 5 min in loading buffer.

Samples were electrophoresed, electro-transferred onto polyvinylidene difluoride (PVDF) membranes, incubated with primary antibodies and secondary antibodies, visualised using chemiluminescence reagent (Millipore, USA) and exposed to X-ray film. Data was quantitated by comparison to vehicle control using Image Jet software. Triplicate experiments with

triplicate samples were conducted. Primary antibodies were all from Cell Signalling Technology (Beverly, MA), including p-AMPK (adenosine monophosphate activated protein kinase, 1:900), AMPK (1:1000), p-mTOR (mammalian target of Rapamycin, 1:800), mTOR (1:1000), LC3(1:1000), Atg5(1:1000), Atg7(1:1000), Beclin1(1:1000) and  $\beta$ -actin (1:1000).

### 2.7. Blood sample preparation

Blood samples were collected and centrifuged for 5 min at 4,000 rpm. Plasma was separated and stored at  $-80^{\circ}\text{C}$  until analysis. Acetonitrile (250  $\mu\text{L}$ ) was added to 100  $\mu\text{L}$  of serum (ice-bath for 15 min), vortexed for 3 min, then centrifuged at 10,000 rpm for 10 min. The supernatant (150  $\mu\text{L}$ ) was transferred to a GC vial and evaporated under a stream of nitrogen gas to dryness. Fifty  $\mu\text{L}$  of methoxy pyridine (15 mg/mL) was added to the vial for 1 h at  $70^{\circ}\text{C}$ , and 50  $\mu\text{L}$  of derivatization reagent (N-methyl-N (trimethylsilyl) trifluoroacetamide : trimethylchlorosilane = 100:1, V/V) was then added. The combined solution was kept at  $70^{\circ}\text{C}$  for another hour, vortexed after adding 150  $\mu\text{L}$  n-hexane (0.10 mg/mL of heptadecanoic acid) as an internal standard and centrifuged to separation (3,000 rpm for 10 min). The liquid supernatant was drawn for GC-MS analysis (10).

### 2.8. GC-MS analysis

The derivative sample (2  $\mu\text{L}$ ) was injected into GC-MS. An HP-5MS column (0.25 mm  $\times$  30 m  $\times$  0.25 mm, Agilent, USA) was used in metabolite studies, and the helium carrier gas pressure was set at 10 psi. The GC oven was initially set at  $85^{\circ}\text{C}$  for 1 min, increased to  $180^{\circ}\text{C}$  at a rate of  $10^{\circ}\text{C}/\text{min}$  and then kept at  $260^{\circ}\text{C}$  for 15 min. MS detection was conducted in EI mode with an electron energy of 70 eV and full scan mode with m/z of 60 to 600, followed by splitless mode injection (10).

### 2.9. Metabolomic analysis

MSD Chemstation software (Version E02.00.493, Agilent Technologies) was used to process the GC-MS data. Endogenous metabolites were identified by matching the spectra against the reference library of NIST 08 Identification System. The metabolite data derived from the three groups were further analyzed using pattern recognition methods in software SIMCA-P+ 11.5 (UmetricsAB, Umea, Sweden). The dataset was subjected to normalization and pare to scaling prior to multivariate analysis. Partial least squares-discriminate analysis (PLS-DA) and principal component analysis (PCA) were used to explain the maximum variation and separation among the defined class samples. Variable importance in the projection (VIP) was used to interpret the specific metabolites among classes. Sixteen concentrations of potential

biomarkers in the control, EPI, and EPI + paeonol groups were introduced into SPSS/Win 11.0 software (SPSS Inc., Chicago, IL) for further *t*-tests, and a *p* value of  $< 0.05$  or  $< 0.01$  was considered statistically significant ( $*p < 0.05$ ,  $^{\#}p < 0.01$ ) (10,11).

## 3. Results

### 3.1. Changes of histopathology and biomarkers

4T1-tumor bearing mice were treated three times with EPI at 6 mg/kg, a cumulative dose that can cause hepatotoxicity in mice (5). In our present study, histopathology of HE staining from control mice livers showed normal architecture. HE-stained liver sections (Figure 1A) from mice treated with EPI had severe liver damage characterized by infiltration of inflammatory cells, interstitial hemorrhage and necrosis. However, samples from the combined group represented histopathological changes in mitigation compared to those receiving EPI alone.

The ALT, AST and ALP activities in plasma, the most widely adopted drug-induced liver injury biomarkers for hepatotoxicity, were measured to evaluate EPI-induced liver damage. Samples in EPI-treated mice demonstrated increased levels of ALT, AST and ALP. By contrast, the combination of EPI and paeonol resulted in an apparent reversal of the EPI-induced increase in liver function enzymes (Figure 1B).

### 3.2. Analysis of metabolite profiling

GC-MS analysis was performed to separate the complex endogenous metabolites. The typical total ion chromatography (TIC) of three groups of samples is displayed in Figure 2. Based on the metabolic profile data, more than 50 metabolites were detected in the plasma. After derivatization, normalization and filtering steps, 16 metabolites with a degree of matching above 80% were selected and identified by calculating on the basis of confirmed ion and fragmentation patterns and compared with the mass spectrum of the library, as shown in Table 1. The relative standard deviation (RSD) of each common peak was less than 15% ( $n = 5$ ), showing that the precision of analytical platforms was excellent.

GC-MS results suggested that the metabolite spectrum in the plasma mainly included contributions from amino acids and lipids, which are probably associated with oxidative stress induced by EPI. The concentrations of the substances inside the body are related to the energy metabolism and autophagy activity.

### 3.3. Multivariate statistical analysis

To illustrate the differences in metabolic profiles, the

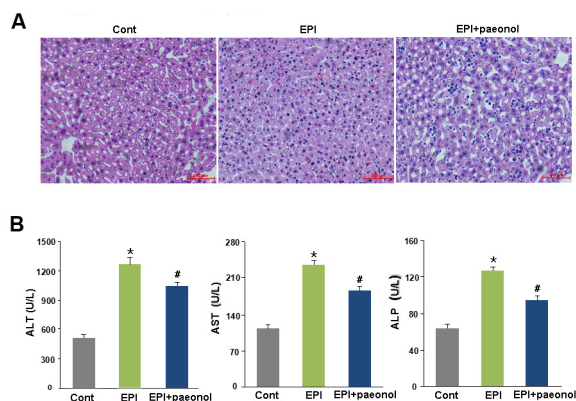


**Figure 1. Effects of paeonol on EPI-induced hepatic dysfunction.** Mice were treated with saline, EPI (6 mg/kg) every other day for 3 cycles and/or paeonol (30 mg/kg) daily for 6 days. Then, electrocardiographs (A) and myocardial enzymes (B) were examined, and the data were statistically significant (mean ± S.E.M.; \* $p < 0.05$  versus control, # $p < 0.05$  versus EPI-treated mice).

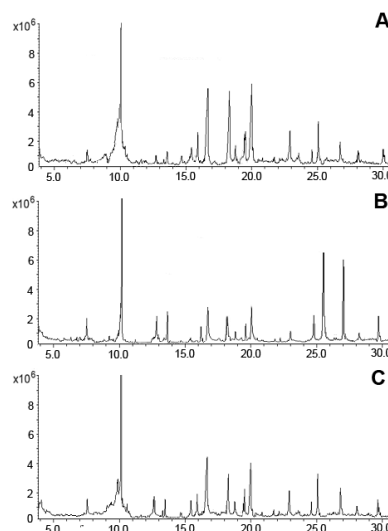


**Figure 2. The typical total ion current chromatograms (TIC) of three samples.** The TIC of (A) control samples, (B) EPI group and (C) EPI+paeonol group by GC-MS analysis.

**Table 1. Summary of the changes in relative levels of metabolites in mice plasma indicated by the PLS-DA loading plots and statistical analysis**

No.	Metabolites compounds	Retention time/min	EPI vs. CONT	EPI+PAE vs. EPI
1	Lactic acid	7.51	↑	↓
2	L-Alanine	12.85	↓	↑
3	Glycine	15.92	↓#	↑#
4	L- Serine	16.49	↑#	↓#
5	L-Valine	13.28	↑*	↓*
6	L- Leucine	15.37	↑*	↓*
7	L- Threonine	18.26	↓	↑
8	L-Aspartic acid	18.93	↓	↑
9	Palmitic acid	19.50	↓#	↑#
10	Oleic acid	20.83	↓#	↑#
11	Galactose	22.95	↓	↑
12	Succinic acid	24.63	↑#	↓#
13	Malic acid	25.14	↑*	↓*
14	Citric acid	26.87	↑	↓
15	Stearic acid	28.14	↓	↑
16	Cholesterol	30.02	↑	↓

Marks indicate the direction of the change, *i.e.*, ↓ for decrease, ↑ for increase; # $p < 0.05$  and \* $p < 0.01$ , as indicated by the statistical analysis *t*-test.

GC-MS spectra were further segmented and subjected to PCA. The score plot clearly discriminated the distinct separation of the three groups: control, EPI, and EPI + paeonol (Figure 3). The control group was clustered to the under-right section, while EPI-treated groups generally clustered in the opposite region. The combined group was located between the control and EPI-treated groups.

PLS-DA was performed to further identify the metabolites underlying the differences among the groups. As shown in Figure 4, the score plots show a complete separation between the control and EPI-treated groups, in which the control group clustered to the right, while locations of the EPI-treated group generally moved to the lower-left region. The combined group moved away from the EPI-treated group, tending

to move toward the controls. The results implied that the overall metabolism of the EPI-treated mice changed significantly, and the metabolites in co-treated mice represented a tendency to move closer to the controls. In addition, the outliers in the groups were probably caused by individual differences.

On the basis of the cross-validated PLS-DA model and *t*-test analysis, the VIP was calculated. Seven endogenous metabolites whose VIP values were larger than 1 were selected as the candidates of the potential biomarkers for EPI-induced liver injury. Serum levels of glycine and oleic acid were lower in the EPI group than those in the controls, while amounts of malic acid, L-leucine, L-valine, succinic acid and serine were higher. The coefficient column plot of the latent variables using PLS-DA is shown in Figure 5.

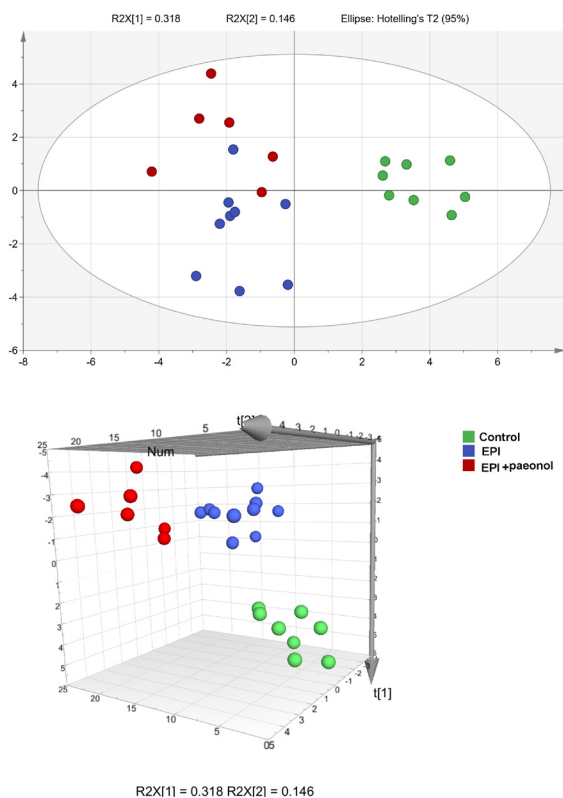


**Figure 3. The PCA statistical analysis results.** The PCA scores plot mapping GC-MS spectra of control, EPI, and EPI+paeonol groups.

### 3.4. Relative signalling pathway

To verify that the protective effect against EPI-induced hepatotoxicity afforded by paeonol requires autophagy inhibition. The efficiency of the autophagy was confirmed by Western blot analysis. As shown in Figure 6, the EPI treatment significantly reduced p-mTOR level, and increased p-AMPK, LC3II/LC3I, Atg5, Atg7, Beclin1 levels in livers. We next exposed EPI-treated and then subjected them to scrambled or paeonol. The results showed that paeonol significantly attenuated the autophagy activation, the protective effects of paeonol, indicating paeonol-dependent protection against EPI-induced autophagy activation in liver.

## 4. Discussion

EPI is an effective anthracycline antibiotic that is widely used to treat various malignancies. Nevertheless, EPI-induced liver injury is a concern depending on the dosage and duration of therapy, resulting in hepatic dysfunction and acute liver failure. EPI has been shown to be metabolized by the liver, and its metabolites are related to oxygen-free radicals, which lead to liver toxicity (1). In our previous research, EPI was able to activate the PI3K/Akt/NF- $\kappa$ B pathway to enhance oxidative stress and induce hepatocyte apoptosis in 4T1-tumor mice. Despite much research, the precise mechanism underlying the EPI-induced acute and

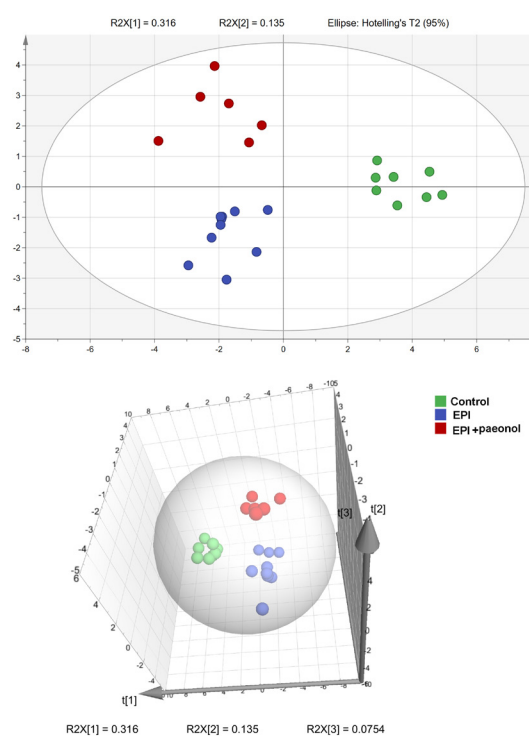


**Figure 4. The PLS-DA statistical analysis results.** The PLS-DA scores plot mapping GC-MS spectra of control, EPI, and EPI+paeonol groups.

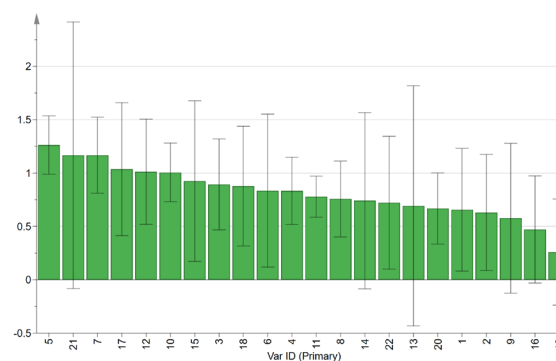


**Figure 5. The VIP statistical analysis results.** The VIP was calculated on the basis of the cross-validated PLS-DA model and t-test analysis.

chronic normal liver tissue damage should be further explored.

In the current study, we observed that the serum ALT, AST and ALP, as well as HE staining confirmed EPI-induced liver damage and paeonol-related hepatoprotective effects, which are consistent with published literature (12). In addition, a metabolomic analysis of systemic variation following EPI and paeonol treatment was also investigated in mice. The metabolic markers of EPI and paeonol were distinguishable in a well-established plasma GC-MS-based metabolomic profile. A panel of candidate endogenous metabolites was identified as potential biomarkers.

The results indicated that the metabolic alteration,

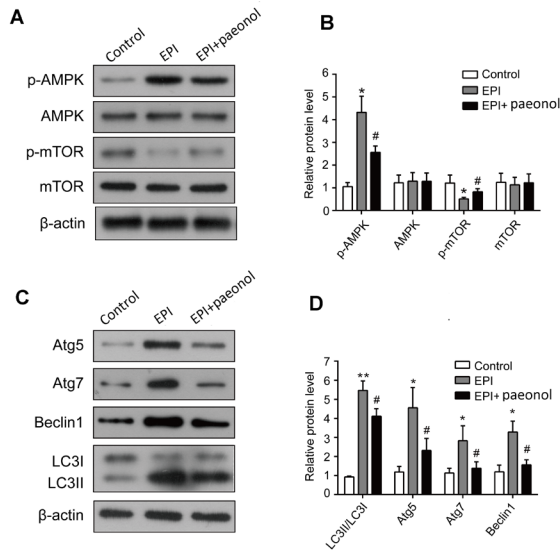


**Figure 6. Paeonol mitigates the EPI-induced hepatotoxicity via the AMPK/mTOR pathway.** (A) The expression levels of p-AMPK, AMPK, p-mTOR and mTOR in livers were inspected by Western blotting. (B) Data were quantitated to represent mean  $\pm$  S.E.M. ( $n \geq 3$ ). (C) The expression levels of LC3II/LC3I, Atg5, Atg7 and Beclin1 in livers were inspected by Western blotting. (D) Data were quantitated to represent mean  $\pm$  S.E.M. ( $n \geq 3$ ). (\* $p < 0.05$  versus control, # $p < 0.05$  versus EPI-treated mice).

including increments of 5 metabolites in plasma, and decrements of 2 metabolites in plasma occurred after EPI treatment. It is noteworthy that all metabolite alteration could be reversed by paeonol treatment, suggesting possible pharmacological mechanisms of the hepatoprotective effect of paeonol. The changed metabolites related to some potential metabolic pathways: lipid metabolism (palmitic acid and oleic acid), amino acid metabolism (serine, valine, leucine, and glycine) and energy metabolism (succinic acid and malic acid).

Our previous study demonstrated that the generation of reactive oxygen species (ROS) is one of the major proposed mechanisms of EPI-induced liver injury, which leads to cell membrane damage and results in the release of marker enzymes of hepatotoxicity. Under the condition of oxidative stress, the tricarboxylic acid (TCA) cycle is slowed down, resulting in decreased production of ROS (13,14). The two crucial energy supply substances for the mitochondrial TCA cycle, succinic acid and malic acid are increased due to the dysfunction of mitochondria (15). Furthermore, gluconeogenesis is also inhibited under oxidative stress, resulting in an increase of serine, which is able to synthesize hepatic glucose (16). In addition, the synthesis of very low-density lipoproteins (VLDL) is significantly affected in transporting lipids from liver to plasma by dysfunction of hepatic enzymes, contributing to a decrease of palmitic acid and oleic acid (17). Furthermore, a mass of ROS leads to the consumption of antioxidants, such as glutathione (GSH), which is synthesized with glycine, glutamate and cysteine in the

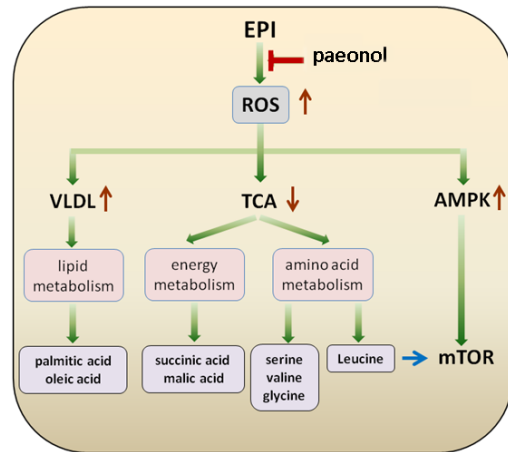


**Figure 7. The possible molecular mechanism of the hepatoprotective effect of paeonol on EPI-induced hepatotoxicity in mice.**

liver (18). Therefore, the decrease of glycine in the EPI-treated group is closely associated with the large amount of GSH synthesis. We previously found that paeonol was able to exert its anti-oxidative stress activity in EPI-induced hepatotoxicity (8). In our present study, compared to EPI-treatment, succinic acid, malic acid and serine are reduced and palmitic acid, oleic acid and glycine are elevated in the paeonol-treated group.

The branched-chain amino acids (BCAAs), including valine, leucine, and isoleucine, have been reported in liver, renal and other tissue injuries (19,20). Holeček *et al.* observed that the BCAAs are extremely decreased both in carbon tetrachloride and ischaemic acute liver damage. As essential amino acids, valine and leucine not only participate in protein metabolism, but also have various physiological and metabolic functions (21). After being converted into  $\alpha$ -ketoisovalerate (KIV, ketovaline) and  $\alpha$ -ketoisocaproate (KIC, ketoleucine), valine and leucine can be oxidized by the liver and then be catabolized to succinyl-CoA and acetyl-CoA, which enter into the TCA cycle (22). The elevation of BCAA levels may result from amino acids leaking from the dying hepatocytes into the circulatory system (19). In our study, valine and leucine increased dramatically in the EPI group compared to the controls.

The AMP-activated protein kinase (AMPK) is a central regulator of cellular and organismal metabolism (23). In eukaryotes, AMPK plays a crucial role in metabolism, especially in energy homeostasis in the liver and other dedicated tissues (24,25). It is activated when ATP production is lower, resulting in a relatively increased AMP/ATP ratio (26). The activation of AMPK can suppress the mTOR pathway by directly phosphorylating raptor (15). In addition, leucine was shown to enhance AMPK activity to promote palmitate uptake both *in vitro* and *in vivo* (27). On the other hand, leucine has been shown to function as a regulator to activate the mTOR signalling pathway, involved in the stimulation of protein synthesis (28). In our study, we

found that the expression of p-AMPK is augmented, and p-mTOR is distinctly decreased in EPI treatment compared to the controls. Furthermore, the activation of AMPK inducing the inhibition of mTOR-dependent signalling may be expected to stimulate autophagy. Figure 7 shows the possible molecular mechanism of the hepatoprotective effect of paeonol on EPI-induced hepatotoxicity. Therefore, whether the autophagy level is changed in EPI-induced hepatotoxicity should be studied further in future research.

In conclusion, our results demonstrate the hepatoprotective effect of paeonol on EPI-induced hepatotoxicity in mice. The underlying metabolomic mechanisms refer to lipid metabolism (palmitic acid and oleic acid), amino acid metabolism (serine, valine, leucine and glycine), energy metabolism (succinic acid and malic acid) and the AMPK/mTOR signalling pathway. Our study is not only beneficial to the understanding of the pathogenetic mechanism of EPI-induced hepatotoxicity, but also provides experimental data and a theoretical foundation for the hepatoprotective effect of paeonol.

#### Acknowledgements

This work was supported by Shandong Key Research and Development Program (2018GSF118075), National Natural Science Foundation of China (81703617), National Natural Science Foundation of China (81801163).

#### References

- Weenen H, van Maanen JM, de Planque MM, McVie JG, Pinedo HM. Metabolism of 4'-modified analogs of doxorubicin. unique glucuronidation pathway for 4'-epidoxorubicin. *Eur J Cancer Clin Oncol.* 1984; 20:919-926.
- Henninger C, Huelsenbeck J, Huelsenbeck S, Grosch S, Schad A, Lackner KJ, Kaina B, Fritz G. The lipid lowering drug lovastatin protects against doxorubicin-induced hepatotoxicity. *Toxicol Appl Pharmacol.* 2012; 261:66-73.
- Lee H, Lee G, Kim H, Bae H. Paeonol, a major compound of moutan cortex, attenuates Cisplatin-induced nephrotoxicity in mice. *Evid Based Complement Alternat Med.* 2013; 2013:310989.
- Li H, Wang SW, Zhang BL. Pharmacological action and pharmacokinetics of paeonol. *Asia-Pacific Tradit. Med.* 2010b; 6:110-112.
- Wu J, Xue X, Zhang B, Jiang W, Cao H, Wang R, Sun D, Guo R. The protective effects of paeonol against epirubicin-induced hepatotoxicity in 4T1-tumor bearing mice *via* inhibition of the PI3K/Akt/NF-kB pathway. *Chem Biol Interact.* 2016; 244:1-8.
- Sun Z, Du J, Hwang E, Yi TH. Paeonol extracted from *Paeonia suffruticosa* Andr. ameliorated UVB-induced skin photoaging *via* DLD/Nrf2/ARE and MAPK/AP-1 pathway. *Phytother Res.* 2018; 32:1741-1749.
- Zhang A, Sun H, Wang X. Serum metabolomics as a novel diagnostic approach for disease: a systematic review. *Anal Bioanal Chem.* 2012; 404:1239-1245.
- Wu J, Xue X, Zhang B, Cao H, Kong F, Jiang W, Li J, Sun D, Guo R. Enhanced antitumor activity and attenuated cardiotoxicity of Epirubicin combined with Paeonol against breast cancer. *Tumour Biol.* 2016; 37:12301-12313.
- Deng M, Zhang M, Sun F, Ma J, Hu L, Yang X, Lin G, Wang X. A gas chromatography-mass spectrometry based study on urine metabolomics in rats chronically poisoned with hydrogen sulfide. *Biomed Res Int.* 2015; 2015:295241.
- Wei C, Li Y, Yao H, Liu H, Zhang X, Guo R. A metabolomics study of epilepsy in patients using gas chromatography coupled with mass spectrometry. *Mol Biosyst.* 2012; 8:2197-2204.
- Lu X, Zhao Q, Tian Y, Xiao S, Jin T, Fan X. A metabolomic characterization of (+)-usnic acid-induced liver injury by gas chromatography-mass spectrometry-based metabolic profiling of the plasma and liver in rat. *Int J Toxicol.* 2011; 30:478-491.
- Wu J, Xue X, Zhang B, Jiang W, Cao H, Wang R, Sun D, Guo R. The protective effects of paeonol against epirubicin-induced hepatotoxicity in 4T1-tumor bearing mice *via* inhibition of the PI3K/Akt/NF-kB pathway. *Chem Biol Interact.* 2016; 244:1-8.
- Liu J, Litt L, Segal MR, Kelly MJ, Pelton JG, Kim M. Metabolomics of oxidative stress in recent studies of endogenous and exogenously administered intermediate metabolites. *Int J Mol Sci.* 2011; 12:6469-6501.
- OuYang Q, Tao N, Zhang M. A damaged oxidative phosphorylation mechanism is involved in the antifungal activity of citral against *penicillium digitatum*. *Front Microbiol.* 2018; 9:239.
- Shin DJ, Kim JE, Lim TG, Jeong EH, Park G, Kang NJ, Park JS, Yeom MH, Oh DK, Bode AM, Dong Z, Lee HJ, Lee KW. 20-O-beta-D-glucopyranosyl-20(S)-protopanaxadiol suppresses UV-Induced MMP-1 expression through AMPK-mediated mTOR inhibition as a downstream of the PKA-LKB1 pathway. *J Cell Biochem.* 2014; 115:1702-1711.
- Huang X, Shao L, Gong Y, Mao Y, Liu C, Qu H, Cheng Y. A metabolomic characterization of CCl4-induced acute liver failure using partial least square regression based on the GC/MS metabolic profiles of plasma in mice. *J Chromatogr B Analyt Technol Biomed Life Sci.* 2008; 870:178-185.
- Martin P. The oxford textbook of clinical hepatology. *Gastroenterology.* 2000; 118:449.
- Abeti R, Baccaro A, Esteras N, Giunti P. Novel Nrf2-inducer prevents mitochondrial defects and oxidative stress in Friedreich's Ataxia models. *Front Cell Neurosci.* 2018; 12:188.
- Holecck M, Mráz J, Tilšer I. Plasma amino acids in four models of experimental liver injury in rats. *Amino Acids.* 1996;10:229-241.
- Teplan V, Schuck O, Horackova M, Skibova J, Holecck M. Effect of a keto acid-amino acid supplement on the metabolism and renal elimination of branched-chain amino acids in patients with chronic renal insufficiency on a low protein diet. *Wien Klin Wochenschr.* 2000; 112:876-881.
- Bifari F, Nisoli E. Branched-chain amino acids differently modulate catabolic and anabolic states in mammals: A pharmacological point of view. *Br J Pharmacol.* 2017;

- 174:1366-1377.
22. Holecek M. Branched-chain amino acids in health and disease: Metabolism, alterations in blood plasma, and as supplements. *Nutr Metab (Lond)*. 2018; 15:33.
  23. Hardie DG. AMP-activated protein kinase: An energy sensor that regulates all aspects of cell function. *Genes Dev*. 2011; 25:1895-1908.
  24. Hardie DG, Ross FA, Hawley SA. AMPK: A nutrient and energy sensor that maintains energy homeostasis. *Nat Rev Mol Cell Biol*. 2012; 13:251-262.
  25. Ki SH, Choi JH, Kim CW, Kim SG. Combined metadoxine and garlic oil treatment efficaciously abrogates alcoholic steatosis and CYP2E1 induction in rat liver with restoration of AMPK activity. *Chem Biol Interact*. 2007; 169:80-90.
  26. Gowans GJ, Hawley SA, Ross FA, Hardie DG. AMP is a true physiological regulator of AMP-activated protein kinase by both allosteric activation and enhancing net phosphorylation. *Cell Metab*. 2013; 18:556-566.
  27. Bruckbauer A, Zemel MB, Thorpe T, Akula MR, Stuckey AC, Osborne D, Martin EB, Kennel S, Wall JS. Synergistic effects of leucine and resveratrol on insulin sensitivity and fat metabolism in adipocytes and mice. *Nutr Metab (Lond)*. 2012; 9:77.
  28. Murgas Torrazza R, Suryawan A, Gazzaneo MC, Orellana RA, Frank JW, Nguyen HV, Fiorotto ML, El-Kadi S, Davis TA. Leucine supplementation of a low-protein meal increases skeletal muscle and visceral tissue protein synthesis in neonatal pigs by stimulating mTOR-dependent translation initiation. *J Nutr*. 2010; 140:2145-2152.

(Received April 19, 2019; Revised May 28, 2019; Accepted June 9, 2019)

## Analysis of mutations in the *FOXI1* and *KCNJ10* genes in infants with a single-allele *SLC26A4* mutation

Xuelei Zhao<sup>1,2,3,§</sup>, Xiaohua Cheng<sup>1,2,3,§</sup>, Lihui Huang<sup>1,2,3,\*</sup>, Xianlei Wang<sup>1,2,3</sup>, Cheng Wen<sup>1,2,3</sup>, Xueyao Wang<sup>1,2,3</sup>, Liping Zhao<sup>1,2,3</sup>

<sup>1</sup> Beijing Tongren Hospital, Capital Medical University, Beijing, China;

<sup>2</sup> Beijing Institute of Otolaryngology, Beijing, China;

<sup>3</sup> Key Laboratory of Otolaryngology, Head and Neck Surgery, Ministry of Education, Beijing, China.

### Summary

The current study investigated how the *FOXI1* and *KCNJ10* genes were affected in infants with a single-allele mutation in the *SLC26A4* gene, and it determined the audiological phenotypes of infants with double heterozygous mutations (DHMs) in the three genes. Subjects were 562 infants with a single-allele *SLC26A4* mutation detected during neonatal deafness genetic screening; the infants were seen as outpatients by Otology at Beijing Tongren Hospital. All subjects underwent *SLC26A4* sequencing. Twenty infants had a second-allele variant while the remaining 542 had an *SLC26A4* single-allele mutation. Infants also underwent *FOXI1* and *KCNJ10* sequencing. All patients with double heterozygous mutations in the aforementioned genes underwent an audiological evaluation and a limited imaging study; variants and audiological phenotypes were analyzed. Of 562 patients, 20 had *SLC26A4* bi-allelic mutations; 8 carried single mutations in both *SLC26A4* and *KCNJ10*. No pathogenic mutations in the *FOXI1* gene were found. Four missense mutations in *KCNJ10* were detected, including c.812G>A, c.800A>G, c.53G>A, and c.1042C>T. Eight individuals with a DHMs all passed universal newborn hearing screening, and all were found to have normal hearing. These data suggest that individuals with an *SLC26A4* single-allele mutation, combined with *FOXI1* or *KCNJ10* gene mutations, do not suffer hearing loss during infancy, though this finding is worthy of further follow-up and in-depth discussion.

**Keywords:** Infants, *SLC26A4* gene, *FOXI1* gene, *KCNJ10* gene, audiological evaluation

### 1. Introduction

*SLC26A4* gene mutations are associated with deafness. In China, the rate of mutation in the *SLC26A4* gene in patients with an enlarged vestibular aqueduct (EVA) is approximately 97%. The most common variant is c.919-2A>G (I). According to Chinese studies, 11.6-38% of patients with EVA were unable to be identified based on

pathogenic factors. Of those, 7.4-24% had an *SLC26A4* mono-allelic mutation (2-4). Foreign studies found that among patients with EVA the rate of *SLC26A4* bi-allelic and mono-allelic mutations was 16-83.9% and 16-36%, respectively (5-8).

A large number of individuals with a single-allele *SLC26A4* mutation have been identified as genetic screening for neonatal deafness has advanced in China. Clinicians are increasingly emphasizing the diagnosis of this condition and genetic counseling for patients. In China, Zhao *et al.* reported that the frequency of a second-allele variant in infants with a known single-allele mutation in the *SLC26A4* gene was 3.50% (13/371) for any type of variant and 2.96% (11/371) for pathogenic mutations (9). In other words, around 97% of these infants could not be genotyped using *SLC26A4* gene sequencing.

Several recent studies have indicated that mutations

Released online in J-STAGE as advance publication June 25, 2019.

§These authors contributed equally to this work.

\*Address correspondence to:

Dr. Lihui Huang, Key Laboratory of Otolaryngology, Head and Neck Surgery, Ministry of Education, Beijing Institute of Otolaryngology, Beijing Tongren Hospital, Capital Medical University, No.17 Hougou Lane, Chongnei Street, Beijing 100005, China.

E-mail: huangpub@126.com

in the *FOXI1* and *KCNJ10* genes might also be associated with PDS/DFNB4 and that these mutations are inherited with heterozygous mutations in *SLC26A4* (10,11). Most of the subjects in studies that analyzed mutations in *FOXI1* or *KCNJ10* were patients with sensorineural hearing loss (SNHL) or EVA.

One aim of the current study was to analyze mutations in the *FOXI1* and *KCNJ10* genes in infants with a single-allele *SLC26A4* mutation. Another aim of this study was to identify the audiological phenotypes of infants with DHMs in those three genes.

## 2. Methods

### 2.1. Subject recruitment

Subjects were 562 Chinese newborns with a single-allele *SLC26A4* mutation that was detected during neonatal deafness genetic screening between April 2015 and March 2019. Exonic and flanking splice site regions of the *SLC26A4* gene were sequenced in all subjects. Subjects were screened for 4 genes and 15 pathogenic variants. Sequencing of the *FOXI1* and *KCNJ10* genes was conducted for patients without an *SLC26A4* second-allele variant. All patients with DHMs in the aforementioned genes underwent an audiological evaluation and a limited imaging study.

### 2.2. DNA analysis

Genomic DNA was extracted from 2 mL of whole blood from each patient using the Blood DNA kit (Tiangen Biotech, Beijing, China). Exons (coding areas) and the flanking splice sites of the *SLC26A4*, *FOXI1*, and *KCNJ10* genes were screened for mutations *via* amplification with PCR and bidirectional sequencing. The American College of Medical Genetics (ACMG) guidelines were used for variant interpretation (12).

### 2.3. Bioinformatics and validation of the variants

Sequence data were analyzed by aligning sequences with NCBI reference sequences of *SLC26A4* (NG\_008489.1), *KCNJ10* (NG\_016411.1) and *FOXI1* (NG\_012068.2) using the software DNA Star 5.0. The 1000 Genomes Project database, ClinVar and dbSNP databases of the NCBI, and the Deafness Variation Database (DVD) were used as references to assess the novelty of the mutations found. Online tools including Mutation Taster, SIFT, CADD, and PolyPhen-2 were used to predict functional outcome of variants. GERP and PhyloP were used to determine predicted conservation scores for variants.

### 2.4. Audiological evaluation

A comprehensive audiological evaluation including ABR, DPOAE, auditory steady-state response (ASSR),

and acoustic immittance (AI) was performed. AI (226 Hz) was classified as A, B or C. AI (1,000 Hz) was classified as unimodal, bimodal, or flat (13,14).

Audiological evaluations were performed in accordance with the description of HSHL by Mazzoli *et al.* (15). The hearing threshold was calculated as the average hearing level at 0.5, 1.0, 2.0, and 4.0 kHz according to WHO standards (1997). Given the subjects' young age, the ABR threshold and ASSR were recorded, and mean thresholds at frequencies in the 0.5 to 4 kHz range were averaged to obtain an approximation for the behavioral hearing threshold (16,17).

### 2.5. Imaging study

Computed tomography of the temporal bone or magnetic resonance imaging of the inner ear was performed.

## 3. Results and Discussion

### 3.1. Demographic data

Of 562 subjects (359 males and 203 females), 20 had an *SLC26A4* second-allele variant while 542 had only an *SLC26A4* single-allele mutation. Subjects ranged in age from 3 to 34 months. The average age at first visit was  $5.16 \pm 3.21$  months. A flowchart of research procedures for patients undergoing neonatal deafness genetic screening and *SLC26A4*, *FOXI1*, and *KCNJ10* sequencing is shown in Figure 1. Eight subjects carried single mutations in both *SLC26A4* and *KCNJ10*. No pathogenic mutations in *FOXI1* were found.

### 3.2. Information on variants of the *KCNJ10* gene

*KCNJ10* sequencing identified 4 variants (Table 1), including a novel variant, c.800A>G (p.Asp267Gly), that was not found in the ClinVar, DVD, dbSNP, and HGMD databases and that had never been described in clinical reports. The proband (BJNS-6) was found to have normal hearing at 8 months; the His genotype was c.919-2A>G/c.800A>G DHMs. The c.1042C>T (rs137853074) mutation was found in the ClinVar, PubMed, and HGMD databases and was labeled 'pathogenic' in DVD. In the current study, however, BJNS-1 and 2 with a DHMs (twin sisters whose father and mother had a c.919-2A>G and c.1042C>T heterozygous mutation, respectively) were both found to have normal hearing. The genotype of the proband (BJNS-3) was also c.919-2A>G/c.1042C>T DHMs, and her hearing phenotype was normal as well. Two other variants, c.812G>A (rs3795339) and c.53G>A (rs115466046), were labeled as 'Benign' in ClinVar and DVD. Sequence electropherograms of abnormal sequences in the *SLC26A4* and *KCNJ10* genes from BJNS-1,2 and 3 are shown at Figure 2.

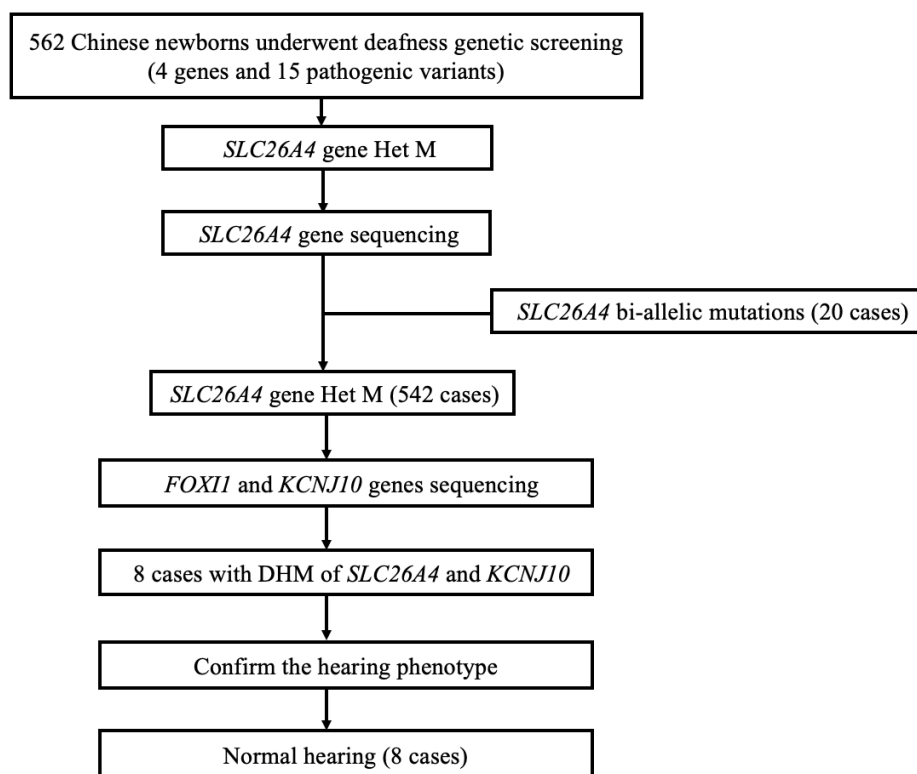


**Figure 1. Flowchart of the research procedures for subjects undergoing neonatal deafness gene screening and *SLC26A4*, *FOXI1*, and *KCNJ10* sequencing.** Abbreviations: Het M, heterozygous mutation; DHM, double heterozygous mutation.

**Table 1. Information on *KCNJ10* gene variants**

Variant	Amino acid	Location	Chromosomal position	Type of mutation	Pathogenicity*	CADD score	Mutant allele frequency
c.1042C>T	p.Arg348Cys	Exon 2	g.160011281:G>A	Missense	Pathogenic	23.6	18.75% (3/16)
c.812G>A	p.Arg271His	Exon 2	g.160011511:C>T	Missense	Benign	23.1	18.75% (3/16)
c.800A>G	p.Asp267Gly	Exon 2	g.160011523:T>C	Missense	No data	12.12	6.25% (1/16)
c.53G>A	p.Arg18Gln	Exon 2	g.160012270:C>T	Missense	Benign	22.6	6.25% (1/16)

\*As reported in the Deafness Variation Database (DVD)

### 3.3. Hearing phenotypes of the 8 subjects with DHMs of the *SLC26A4* and *KCNJ10* genes

Table 2 summarizes genotypes and phenotypes of subjects with DHMs of the *SLC26A4* and *KCNJ10* genes. Eight individuals all passed universal newborn hearing screening (UNHS) and they were all found to have normal hearing at different ages. Three of the individuals agreed to undergo a CT scan of the temporal bone, and results were normal.

### 3.4. Prediction of the functional outcome of variants

Prediction of the variant effect was performed using SIFT, Mutation Taster, Polyphen-2, GERP, and PhyloP. c.1042C>T was predicted to be "probably damaging" according to Polyphen-2 and SIFT, "disease causing" according to Mutation Taster, and "conserved"

according to GERP. c.800A>G was predicted to be "tolerated" according to SIFT, "benign" according to Polyphen-2, and "conserved" according to GERP and PhyloP.

The Cochrane Library, Pubmed, Embase and other databases were searched, and no studies were found to have analyzed mutations in the *FOXI1* and *KCNJ10* genes in infants with a single-allele *SLC26A4* mutation. Therefore, this may be the first study in China to analyze mutations in the two aforementioned genes in infants with a single-allele *SLC26A4* mutation.

### 3.5. Genetic testing

*KCNJ10* sequencing identified 4 variants, including a novel variant, c.800A>G(p.Asp267Gly). This is a missense variant, located in exon 2, that causes an amino acid substitution at position 267 from aspartic

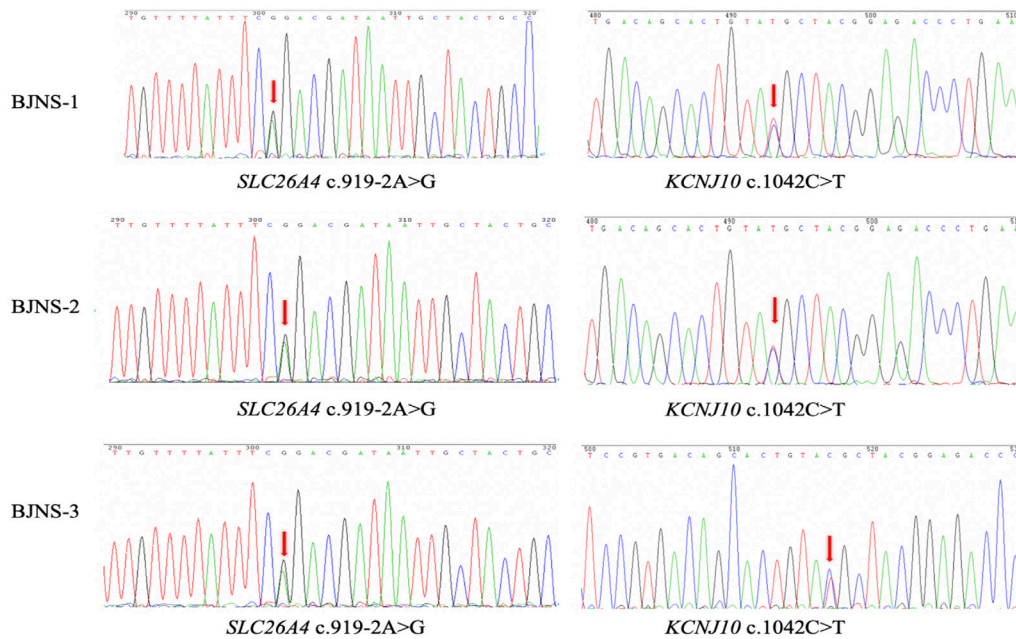


Figure 2. Sequence electropherograms of abnormal sequences in the *SLC26A4* and *KCNJ10* genes from three probands.

Table 2. Genotype and phenotype of subjects with DHMs

Patient No.	Age	Genotype	Phenotype	Imaging evaluation	UNHS results	
					R	L
BJNS-1	34 m	c.919-2A>G/c.1042C>T DHM	Normal	Normal	Pass	Pass
BJNS-2	34 m	c.919-2A>G/c.1042C>T DHM	Normal	Normal	Pass	Pass
BJNS-3	19 m	c.919-2A>G/c.1042C>T DHM	Normal	No data	Pass	Pass
BJNS-4	17 m	c.919-2A>G/c.53G>A DHM	Normal	Normal	Pass	Pass
BJNS-5	13 m	c.919-2A>G/c.812G>A DHM	Normal	No data	Pass	Pass
BJNS-6	10 m	c.919-2A>G/c.800A>G DHM	Normal	No data	Pass	Pass
BJNS-7	14 m	c.2168A>G/c.812G>A DHM	Normal	No data	Pass	Pass
BJNS-8	10 m	c.919-2A>G/c.812G>A DHM	Normal	No data	Pass	Pass

Abbreviations: DHMs, double heterozygous mutation; UNHS, universal newborn hearing screening.

acid to glycine. Online tools predicted this variant to be tolerated or benign. The proband (BJNS-6) was found to have normal hearing at 8 months and was advised to undergo a regular follow-up. Based on ACMG guidelines, c.800A>G is "likely benign." No pathogenic mutations in *FOXI1* gene were found. Only two known synonymous polymorphisms were identified in *FOXI1*; both were found in dbSNP (c.279G>A, rs2277944 and c.726C>T, rs35678180).

c.812G>A was previously reported by Chai *et al.*, who found it in 5% of controls with normal hearing, suggesting that this variant maybe a polymorphism in the Chinese population (18). Zhao *et al.* analyzed genotypes of *SLC26A4* and *KCNJ10* in 1,056 Chinese patients with NSEVA and found that the most frequently detected *KCNJ10* mutation was c.812G>A. The incidence of c.812G>A in patients with NSEVA does not differ significantly from that in control subjects with normal hearing (19). Subjects in the two aforementioned studies had EVA or hearing loss, while

subjects in the current study were all infants with an *SLC26A4* single-allele mutation. Three subjects (BJNS-5, 7 and 8) with c.919-2A>G/c.812G>A DHMs were identified. These subjects had normal hearing, which agrees with the findings of previous studies.

The mutation c.1042C>T was first reported by Yang, and he proposed that single mutations in both *SLC26A4* and *KCNJ10* (an inwardly rectifying potassium channel) lead to digenic NSEVA. c.1042C>T was found to reduce K<sup>+</sup> conductance activity and is regarded as a pathogenic SNV according to 1000 Genomes (11). However, the study by Zhao *et al.* (19) did not find c.1042C>T in patients with NSEVA with zero or one *SLC26A4* mutation, but c.1042C>T was found in a control subject with normal hearing and both *KCNJ10* c.1042C>T and *SLC26A4* pathogenic mutations were carried by parents with normal hearing who had children with NSEVA. These facts suggest that c.1042C>T might be a benign variant in the Chinese population. The current study also found three subjects

(BJNS1, 2, and 3) with c.919-2A>G/c.1042C>T DHMs, all of whom currently have normal hearing. Therefore, the pathogenicity of c.1042C>T still warrants further study.

### 3.6. Phenotypes and genotypes of individuals with DHMs

A meta-analysis indicated that, overall, 1.3% and 3.1% of patients suspected of having PDS/DFNB4 had variants in *FOXI1* and *KCNJ10*, respectively (20). In the current study, eight subjects with DHMs all passed UNHS and were found to have normal hearing. Three of those individuals agreed to undergo a CT scan of the temporal bone, and results were all normal. Together, these results suggest that individuals with *SLC26A4* single-allele mutation, combined with *FOXI1* or *KCNJ10* gene mutations, do not suffer hearing loss during infancy, though this finding is worthy of further follow-up and in-depth discussion. The actual contribution of *FOXI1* and *KCNJ10* mutations to SNHL may be more limited, *i.e.* maybe they affect only a relatively small number of patients with EVA, as suggested by a study that found no *FOXI1* or *KCNJ10* variants (21).

## 4. Conclusion

This may be the first study in China to analyze mutations in the *FOXI1* and *KCNJ10* genes in infants with a single-allele *SLC26A4* mutation. These data suggest that individuals with an *SLC26A4* single-allele mutation, combined with *FOXI1* or *KCNJ10* gene mutations, do not suffer hearing loss during infancy, though this finding is worthy of further follow-up and in-depth discussion.

## Acknowledgements

The authors wish to thank the patients and their family members for their participation in this study. This work was supported by grants from the National Key R&D Program of China [grant number 2018YFC1002204], the Beijing Natural Science Foundation [grant number 7172052], and the Fund to Foster the Scientific and Technological Foundation of Beijing Tongren Hospital, Capital Medical University [grant number 2016-YJJ-GGL-018].

## References

1. Wang Q, Zhao Y, Rao S, Guo Y, Yuan H, Zong L, Guan J, Xu B, Wang D, Han M, Lan L, Zhai S, Shen Y. A distinct spectrum of *SLC26A4* mutations in patients with enlarged vestibular aqueduct in China. *Clin. Genet.* 2007; 72:245-254.
2. Wu C, Lu Y, Chen P, Yeh P, Su Y, Hwu W, Hsu C. Phenotypic analyses and mutation screening of the

- SLC26A4* and *FOXI1* genes in 101 Taiwanese families with bilateral nonsyndromic enlarged vestibular aqueduct (DFNB4) or Pendred syndrome. *Audiol Neurootol.* 2010; 15:57-66.
3. Zhao J, Yuan Y, Chen J, Huang S, Wang G, Han D, Dai P. *SLC26A4* gene copy number variations in Chinese patients with non-syndromic enlarged vestibular aqueduct. *J Transl Med.* 2012; 10:82.
4. Pang XH, Chai YC, Chen P. The incidence and pathogenic correlation of *SLC26A4* mono-allelic mutations in deaf patients with enlarged vestibular aqueduct. *Chinese Scientific Journal of Hearing and Speech Rehabilitation.* 2015; 3:190-194. (in Chinese)
5. Rah YC, Kim AR, Koo JW, Lee JH, Oh SH, Choi BY. Audiologic presentation of enlargement of the vestibular aqueduct according to the *SLC26A4* genotypes. *Laryngoscope.* 2015; 125:216-222.
6. Tsukamoto K, Suzuki HD, Namba A, Namba A, Abe S, Usami S. Distribution and frequencies of PDS (*SLC26A4*) mutations in Pendred syndrome and nonsyndromic hearing loss associated with enlarged vestibular aqueduct: A unique spectrum of mutations in Japanese. *Eur J Hum Genet.* 2004; 11:916-922.
7. Pryor SP, Madeo AC, Reynolds JC, Sarlis NJ, Arnos KS, Nance WE, Yang Y, Zalewski CK, Brewer CC, Butman JA, Griffith AJ. *SLC26A4*/PDS genotype-phenotype correlation in hearing loss with enlargement of the vestibular aqueduct (EVA): Evidence that Pendred syndrome and non-syndromic EVA are distinct clinical and genetic entities. *J Med Genet.* 2005; 42:159-165.
8. Albert S, Blons H, Jonard L, *et al.* *SLC26A4* gene is frequently involved in nonsyndromic hearing impairment with enlarged vestibular aqueduct in Caucasian populations. *Eur J Hum Genet.* 2006; 14:773-779.
9. Zhao X, Huang L, Wang X, Wang X, Zhao L, Cheng X, Ruan Y. Genotyping and audiological characteristics of infants with a single-allele *SLC26A4* mutation. *Int J Pediatr Otorhinolaryngol.* 2019; 116:153-158.
10. Yang T, Vidarsson H, Blomqvist SR, Rosengren SS, Enerback S, Smith RJ. Transcriptional control of *SLC26A4* is involved in Pendred syndrome and nonsyndromic enlargement of vestibular aqueduct (DFNB4). *Am J Hum Genet.* 2007; 80:1055-1063.
11. Yang T, Gurrola JG, Wu H, Chiu SM, Wangemann P, Snyder PM, Richard JH. Mutations of *KCNJ10* together with mutations of *SLC26A4* cause digenic nonsyndromic hearing loss associated with enlarged vestibular aqueduct syndrome. *Am J Hum Genet.* 2009; 84:651-657.
12. Richards S, Aziz N, Bale S, Bick D, Das S, Gastier FS, Grody WW, Hegde M, Lyon E, Spector E, Voelkerding K, Rehm HL. Standards and guidelines for the interpretation of sequence variants: A joint consensus recommendation of the American College of Medical Genetics and Genomics and the Association for Molecular Pathology. *Genet. Med.* 2015; 17:405-424.
13. Lidén G. The scope and application of current audiometric tests. *J Laryngol Otol.* 1969; 83:507-520.
14. Jerger J. Clinical experience with impedance audiometry. *Arch Otolaryngol.* 1970; 92:311-324.
15. Mazzoli M, Camp GV, Newton V, Giarbini N, Declau F, Parving A. Recommendations for the description of genetic and audiological data for families with nonsyndromic hereditary hearing impairment. *Audiol. Med.* 2009; 1:148-150.
16. Kim SY, Park G, Han KH, Kim A, Koo JW, Chang

- SO, Seung HO, Park WY, Choi BY. Prevalence of p.V37I variant of GJB2 in mild or moderate hearing loss in a pediatric population and the interpretation of its pathogenicity. PLoS One. 2013; 8:e61592.
17. Liu J, Huang L, Fu X, Liu H, Yang Y, Cheng X, Ni T. The audiological characteristics of large vestibular aqueduct syndrome in infants and young children. J Clin Otorhinolaryngol Head Neck Surg (China). 2016; 30:1702-1709. (in Chinese)
  18. Chai Y, Huang Z, Tao Z, Li X, Li L, Li Y, Wu H, Yang T. Molecular etiology of hearing impairment associated with nonsyndromic enlarged vestibular aqueduct in East China. Am J Med Genet. 2013; 161:2226-2233.
  19. Zhao J, Yuan Y, Huang S, Huang B, Cheng Y, Kang D, Wang G, Han D, Dai P. *KCNJ10* may not be a contributor to n Chinese Subjects. PLoS One. 2014; 9:e108134.
  20. Pique LM, Brennan ML, Davidson CJ, Schaefer F, Greinwald J, Schrijver I. Mutation analysis of the *SLC26A4*, *FOXI1* and *KCNJ10* genes in individuals with congenital hearing loss. Peer J. 2014; 2:e384.
  21. Chen K, Wang X, Sun L, Jiang H. Screening of *SLC26A4*, *FOXI1*, *KCNJ10*, and *GJB2* in bilateral deafness patients with inner ear malformation. Otolaryngol Head Neck Surg. 2012; 146:972-978.

(Received June 2, 2019; Revised June 18, 2019; Accepted June 21, 2019)

# Design and synthesis of novel histone deacetylase 6 inhibitors with benzyl-triazole as the core skeleton

Zishuo Mou<sup>1,2,§</sup>, Jianjun Gao<sup>1,§,\*</sup>, He Miao<sup>2</sup>, Li Zhang<sup>2</sup>, Li Su<sup>2</sup>, Baolei Wang<sup>1</sup>, Yepeng Luan<sup>1,2,\*</sup>

<sup>1</sup>Department of Pharmacology, School of Pharmacy, Qingdao University, Qingdao, Shandong, China;

<sup>2</sup>Department of Medicinal Chemistry, School of Pharmacy, Qingdao University, Qingdao, Shandong, China.

## Summary

In the field of epigenetics, histone deacetylases (HDACs) are important members and well validated targets for anti-cancer drugs discovery. In this study, we designed and synthesized twenty-seven novel hydroxamic acid-based HDAC inhibitors (HDACis) with benzyl-triazole as the core skeleton. Most target compounds displayed excellent inhibition rates toward HDACs. Among them, compounds ZM-22 to ZM-27 with inhibition rates more than 90% toward HDACs exhibited potent inhibitory activity toward HDAC6, and ZM-23 possessed the best selectivity to HDAC6 over HDAC1. The high potency of compound ZM-23 toward HDAC6 was rationalized by molecular docking simulation. This series of compounds is worthy for further anti-cancer activity evaluation and structural optimization works.

**Keywords:** Histone deacetylase, isoform, selective, inhibitor, anti-tumor

## 1. Introduction

Modulating the activities of enzymes in the field of epigenetics including "writers", "erasers" and "readers" has emerged as an attractive therapeutic strategy fighting against human diseases (1). During the translation process, the "loosen" and "condensed" forms of DNA can be regulated by the acetylation level of lysine residues (2). As one kind of the most important epigenetic erasers, histone deacetylases (HDACs) are responsible for the removal of the acetyl group located on the lysine residues of histones (3), the progress frees the genetic component and triggers the transcriptions (4). Besides histones, HDACs can also act on numerous non-histone substrates such as  $\alpha$ -tubulin and p53 (5-

7). The crucial roles played by HDACs make them promising targets for various human diseases treatment, especially cancers.

Till now, 18 mammalian HDACs with different structures, locations and functions are reported, which can be categorized into four classes: class I (HDAC1, 2, 3, and 8), class II (class IIa: HDAC4, 5, 7, and 9 and class IIb: HDAC6 and 10), and class IV (HDAC11) are all zinc ion ( $Zn^{2+}$ ) dependent deacetylases that are mechanistically distinct from  $NAD^+$ -dependent class III HDACs (8). Following the function investigation of HDACs, numerous HDACs inhibitors (HDACis) are developed. Four HDACis, vorinostat (SAHA), romidepsin, belinostat, and panobinostat, have gained FDA approvals for the treatment of hematologic tumors (9). A survey of the results of clinical trials indicated that use of pan-HDACis or partially selective HDACis results in unwanted side effects such as fatigue, nausea/vomiting, diarrhea, cardiotoxicity and hematological toxicity, and thrombocytopenia (10,11), all of which severely limit their utilization in clinics.

With the purpose of eradicating the side effects, increasing number of researches are focusing on the development of isoform selective HDACis, especially HDAC6 selective inhibitors. In contrast to the lethal effect of HDAC1-3 genetic ablation, mice with HDAC6 knocked out are effectively normal (12). Several researches also demonstrated that HDAC6 selective

Released online in J-STAGE as advance publication May 31, 2019.

<sup>§</sup>These authors contributed equally to this work.

\*Address correspondence to:

Dr. Jianjun Gao, Department of Pharmacology, School of Pharmacy, Qingdao University, 38 Dengzhou Road, Qingdao 266021, Shandong, China.

E-mail: gaojj@qdu.edu.cn

Dr. Yepeng Luan, Department of Pharmacology and Department of Medicinal Chemistry, School of Pharmacy, Qingdao University, 38 Dengzhou Road, Qingdao 266021, Shandong, China.

E-mail: yluan@qdu.edu.cn

inhibitors have fewer side effects than pan-HDACis (13,14). So, the development of selective HDAC6 inhibitors should be advantageous as a therapeutic approach, which has encouraged scientists to develop potent and selective HDAC6 inhibitors (15-17). ACY-1215, a first-in-class selective HDAC6 inhibitor, exhibits anti-tumor effects alone or in combination with other drugs in various cancers and is currently undergoing clinical trials for the treatment of breast cancer (18).

The canonical pharmacophore of HDACis consists of three parts: a surface recognition region (cap) that interacts with the entrance of active pocket of HDACs; Zn<sup>2+</sup> binding group (ZBG) that chelates with Zn<sup>2+</sup>; a linker that conjugates the cap and ZBG and interacts with the hydrophobic channel of the active site (Figure 1) (19). It is well studied that the delicate design of "cap" and "linker" parts can contribute to the selectivity towards specific HDAC isoforms (2). In this study, with the aim of searching for novel selective HDAC6 inhibitors, a series of HDACis with benzyl-triazole as the core skeleton was designed and synthesized. Hydroxamic acid was selected as the ZBG. The linker length was fixed to 7 atoms according to the known structure-activity relationship (SAR) that 7-8 atoms long linker usually displays best HDACs inhibitory activity.

## 2. Materials and Methods

### 2.1. Chemistry

All of the chemical solvents and reagents, which were analytically pure without further purification, were purchased from Energy Chemical (Shanghai, China). Thin-layer chromatography was performed on 0.20 mm Silica Gel 60 F254 plates (Qingdao Haiyang Chemical, China). <sup>1</sup>H NMR and <sup>13</sup>C NMR spectra were recorded on a Bruker Avance 400 spectrometer (Bruker Company, Germany) or a Varian spectrometer (Varian, Palo Alto, CA, USA), using tetramethylsilane as an internal standard. Chemical shifts were given in parts per million. Mass spectra were recorded on a Q-TOF Premier mass spectrometer (Micromass, Manchester, U.K.).

### 2.2. In vitro HDAC inhibition fluorescence assay

In brief, 10 μL of enzyme solution (HeLa cell nuclear extract, HDAC1, or HDAC6) was mixed with different concentrations of tested compounds (50 μL). The mixture was incubated at 37°C for 5 min, followed by adding 40 μL fluorogenic substrate (Boc-Lys(acetyl)-AMC). After incubation at 37°C for 30 min, the mixture was quenched by addition of 100 μL of developer containing trypsin and trichostatin A (TSA). Over another incubation at 37°C for 20 min, fluorescence

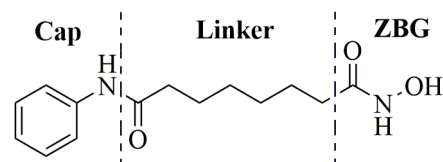


**Figure 1. The pharmacophore of HDACis with SAHA as an example.**

intensity was measured using a microplate reader at excitation and emission wavelengths of 390 and 460 nm, respectively. The inhibition ratios were calculated from the fluorescence intensity readings of tested wells relative to those of control wells, and the IC<sub>50</sub> values were calculated using a regression analysis of the concentration/inhibition data.

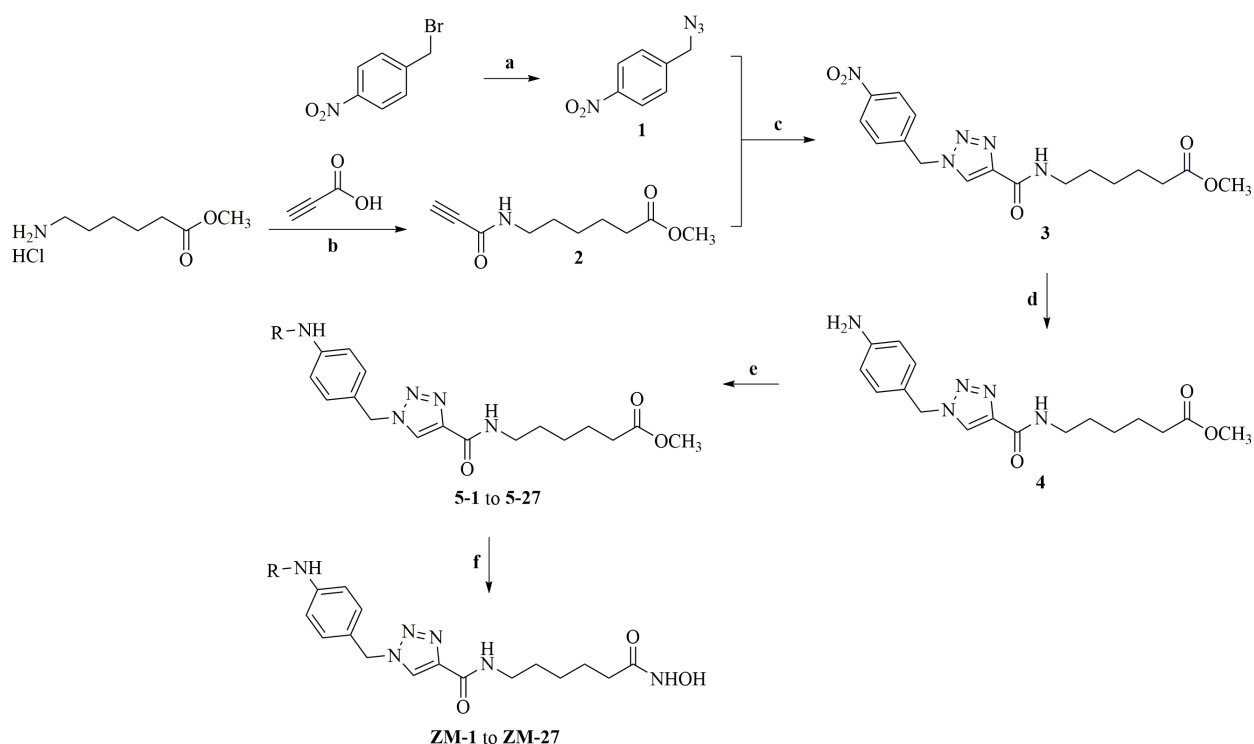
### 2.3. Molecular docking

Compounds were docked into the active site of HDAC6 (PDB entry: 5WGL) using Tripos SYBYL-X 2.1. Before docking process, the HDAC6 structure retrieved from PDB website was treated by deleting water molecules, adding FF99 charges. A 100-step minimization process was performed to further optimize the protein structure. The molecular structures were generated with Sybyl/Sketch module and optimized using Powell's method with the Tripos force field with convergence criterion set at 0.05 kcal/(Å mol) and assigned charges with the Gasteiger\_Hückel method. Molecular docking was carried out *via* the Sybyl/SurfexDock module. Other docking parameters were kept to the default values.

## 3. Results and Discussion

### 3.1. Chemical synthesis of target compounds

The synthesis route is outlined in Scheme 1. 4-Nitrobenzyl azide (**1**) was synthesized from mixture of 4-nitrobenzyl bromide and sodium azide (NaN<sub>3</sub>) using dimethyl sulfoxide (DMSO) as the solvent. In the other hand, the methyl 6-propiolamidohexanoate (**2**) was obtained by the condensation of methyl 6-aminocaproate hydrochloride and propiolic acid in the presence triethylamine (TEA) and dicyclohexylcarbodiimide (DCC). The Click reaction between **1** and **2** catalyzed by CuI could give the compound **3**. Reduction of the nitro group to amine group catalyzed by 5% Pd/C at the atmosphere of hydrogen could give the important intermediate **4**. In the next step, compound **4** reacted with various acyl chlorides or sulfonyl chlorides catalyzed by TEA to give compounds **5-1** to **5-27**. The methyl ester of compounds **5-1** to **5-27** was transferred to the hydroxamic acid by reacting with NH<sub>2</sub>OH in anhydrous MeOH to get the final products, ZM-1 to ZM-27. Specific synthetic



**Scheme 1. Reagents and conditions.** a.  $\text{NaN}_3$ , DMSO,  $30^\circ\text{C}$ , 24 h; b. DCC, TEA, dry DCM, RT, overnight; c. CuI, anhydrous THF, nitrogen, RT, overnight; d. 5% Pd/C, hydrogen,  $\text{CH}_3\text{OH}$ , RT, 10 h; e. TEA, DCM,  $0^\circ\text{C}$ , 1 h, then RT, 8 h; f.  $\text{NH}_2\text{OH}$ ,  $\text{CH}_3\text{OH}$ , RT, 2 h.

procedures and spectroscopy data of the all compounds see supplementary data (<http://www.biosciencetrends.com/action/getSupplementalData.php?ID=43>).

### 3.2. Activity of target compounds against HDACs extracted from Hela cell nucleus

We first screened the inhibitory activities of all 27 final products against Hela cell nucleus extracts whose main component is class I HDACs. Single concentration ( $1\ \mu\text{M}$ ) was used and the inhibition rate (%) was calculated. The results are presented in Table 1. All 27 compounds we obtained presented moderate to excellent inhibitory activities against HDACs demonstrating that both the benzyl-triazole fragment as the "cap" part and the linker length are appropriate for HDAC inhibition. Among all 27 compounds, six of them (ZM-22 to ZM-27) displayed robust inhibitory activity against HDACs with the inhibition rates higher than 90% at  $1\ \mu\text{M}$ . Notably, the compound ZM-26 is slightly more potent than the marketed drug SAHA. Surprisingly, these 6 compounds have a uniform sulfamide moiety in their structures, which is speculated to form extra interactions with HDAC compared with other amide-based compounds. This might be the reason why these 6 compounds possess higher inhibitory activities against HDACs than others.

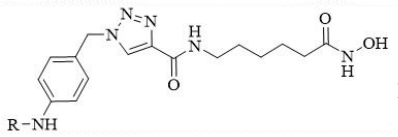
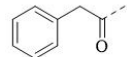
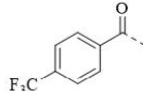
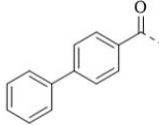
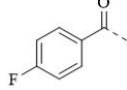
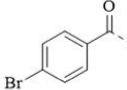
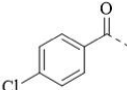
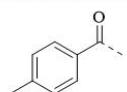
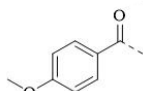
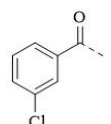
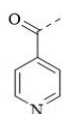
### 3.3. HDAC isoform specificity of compounds ZM-22 to ZM-27

With these 6 potent compounds in hand, their isoform selectivity was further investigated against HDAC1 (class I) and HDAC6 (class IIb). The pan-HDACi SAHA and HDAC6 selective inhibitor ACY1215 were utilized as the positive controls. The result is showed in Table 2. Consistent with published data, SAHA as a pan-HDACi is almost equipotent toward HDAC1 and 6 without conspicuous selectivity. ACY1215 as a well-studied HDAC6 selective inhibitor displayed high potency to HDAC6 with the  $\text{IC}_{50}$  value of 8.0 nM. Encouragingly, all of our 6 compounds are strong HDAC6 inhibitors with the  $\text{IC}_{50}$  values ranging from 8.4 to 50 nM. Compounds ZM-22 to ZM-25 display selectivity towards HDAC6 over HDAC1 with different degrees. The selectivity factor for HDAC6 over HDAC1 ( $\text{SF}_{6/1}$ ) of ZM-23 is 9.37, slightly better than that of ACY1215 ( $\text{SF}_{6/1} = 9.13$ ).

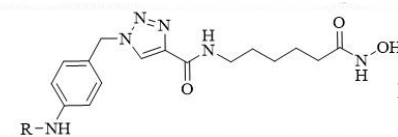
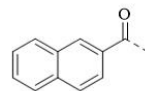
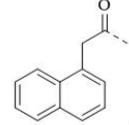
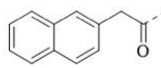
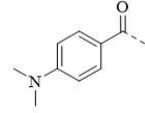
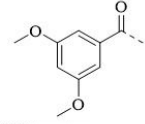
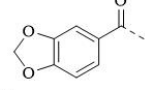
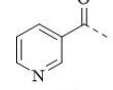
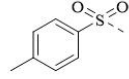
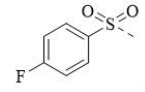
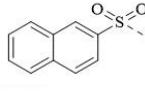
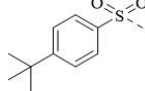
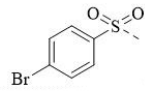
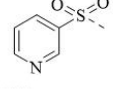
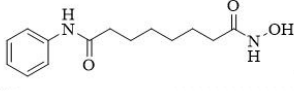
### 3.5. Molecular simulation result of compound ZM-23 towards HDAC6

To rationalize our biological experiment findings, molecular docking simulation was performed. Considering that compound ZM-23 displayed potent HDAC6 inhibitory activity as well as the best selectivity toward HDAC6 over HDAC1, we investigated the proposed binding mode of ZM-23 with HDAC6. The crystal structure of *Danio rerio* HDAC6 catalytic domain 2 in complex with ACY1215 (PDB code 5WGL) was used as the template. The result is showed

**Table 1. Structures all 27 target compounds and their inhibition rates against HDACs at 1  $\mu$ M**

Compd		Inhibition rate at 1 $\mu$ M
	R =	
ZM-1		84.9%
ZM-2		88.5%
ZM-3		71.4%
ZM-4		47.9%
ZM-5		53.9%
ZM-6		87.5%
ZM-7		64.5%
ZM-8		74.3%
ZM-9		67.7%
ZM-10		69.1%
ZM-11		71.4%
ZM-12		76.6%
ZM-13		86.0%
ZM-14		72.8%

**Table 1. Structures all 27 target compounds and their inhibition rates against HDACs at 1  $\mu$ M (continued)**

Compd		Inhibition rate at 1 $\mu$ M
	R =	
ZM-15		45.0%
ZM-16		88.0%
ZM-17		63.0%
ZM-18		80.0%
ZM-19		86.4%
ZM-20		71.0%
ZM-21		86.3%
ZM-22		93.1%
ZM-23		91.0%
ZM-24		92.3%
ZM-25		93.8%
ZM-26		97.1%
ZM-27		90.1%
SAHA		96.1%

**Table 2. The inhibitory activities of selected compounds against HDAC1 and HDAC6**

Compd	IC <sub>50</sub> <sup>a</sup> , nM		SF6/1 <sup>b</sup>
	HDAC1	HDAC6	
ZM-22	104.3	14.6	7.14
ZM-23	206.2	22.0	9.37
ZM-24	55.4	11.8	4.69
ZM-25	66.1	14.9	4.44
ZM-26	5.6	8.4	0.67
ZM-27	144.0	50.0	2.88
SAHA	43.2	20.7	2.09
ACY1215	73.0	8.0	9.13

<sup>a</sup>The IC<sub>50</sub> values are the means of three experiments. <sup>b</sup>SF6/1: selectivity factor for HDAC6 over HDAC1 (SF6/1 = IC<sub>50</sub>(HDAC1)/IC<sub>50</sub>(HDAC6)).

in Figure 2. From the docking result, we can see that the hydroxamic acid moiety of ZM-23 can smoothly chelate with the Zn<sup>2+</sup> in a monodentate manner. The oxygen atom of the carboxyl group in the hydroxamic acid formed a hydrogen bond with HIS614 residue. The fluorine atom on the terminal benzene ring formed a hydrogen bonds with ARG636 residue, and the oxygen atom of the amide group adjacent to the triazole formed another hydrogen bond with SER531 residue. All of these interactions can explain why ZM-23 possessed strong inhibitory activity toward HDAC6.

Different from other HDACs, HDAC6 is located mainly in cytoplasm and many non-histone proteins are its substrate (20). With regards to the structure, HDAC6 possess a wider entrance of the active pocket than other HDAC isoforms (21). This wide entrance can accommodate large size cap groups which make it possible to design specific HDAC6 inhibitors. With this in mind, we designed and synthesized a series of 27 novel compounds with large size cap groups by using benzyl-triazole as their core structures. Actually, many published potent HDACis contain the triazole fragment as the cap or linker part proving that it is favorable for binding with HDACs (22). In addition, triazole is a stable group that is able to resist metabolism and degradation under acidic/basic and oxidative/reductive conditions *in vivo*, and it can be used as the bioisostere of ester and amide groups (23). So, in this work, we also introduce a triazole moiety as the cap part. Hydroxamic acid was selected as the ZBG due to its high affinity to Zn<sup>2+</sup>. Out of all 27 compounds we obtained, compounds ZM-22 to ZM-27 containing a sulfamide moiety in their cap parts exhibited excellent inhibition rate to HDACs derived from the HeLa cell extracts. In the isoform selectivity assay, compound ZM-26 displayed the most potent HDAC6 inhibitory activity and compound ZM-23 possessed the best selectivity toward HDAC6 with the selective index slightly higher than ACY1215. In the docking study, the proposed binding mode of ZM-23 showed that the hydroxamic acid coordinated well

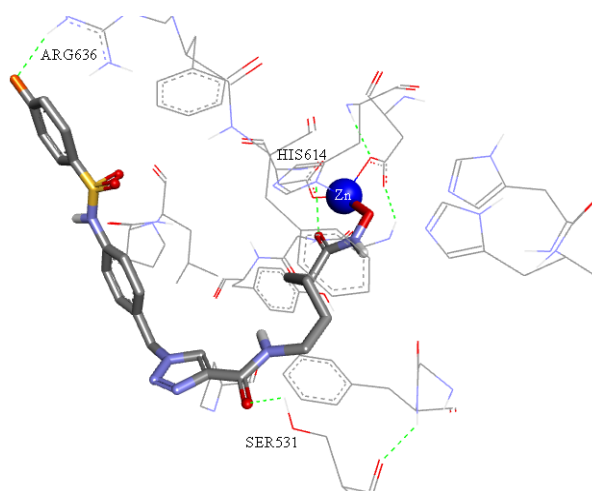


**Figure 2. Proposed binding model of compound ZM-23 with HDAC6 (by modification of PDB code 5WGL using Tripos SYBYL-X 2.1).** The Zn<sup>2+</sup> is presented as a blue sphere. Hydrogen bonds are shown as green dashed lines. The figure was generated by Discovery Studio Visualizer.

with the Zn<sup>2+</sup>. The sulfamide may provide a suitable angle for the cap part to interact with the rim of the HDAC6. The anticancer activities of novel HDAC6 inhibitors warrant further investigation.

#### 4. Conclusion

In this work, a series of 27 novel HDACis possessing benzyl-triazole as a central core were rationally designed based on the pharmacophore constituents of known HDACis. All of the target compounds displayed moderate to excellent inhibitory activities to HDACs. Out of them, compounds ZM-22 to ZM-27 with inhibition rates more than 90% toward HDACs exhibited potent inhibitory activity toward HDAC6, and ZM-23 possessed the best selectivity to HDAC6 over HDAC1. The proposed binding mode between ZM-23 and HDAC6 was also analyzed by docking simulation. All these results demonstrated that this series of compounds is worthy for further biological evaluation and structure optimization works.

#### Acknowledgements

We gratefully acknowledge the financial support from the National Science Foundation for Young Scientists of China to Y. L. (NSFC no. 81602947) and J. G. (NSFC no. 81503094), China Postdoctoral Science Foundation (no. 2016M600524), and Qingdao Postdoctoral Applied Research Project (no. 2016072; Jianjun Gao, Qingdao University).

#### References

1. Luan Y, Li J, Bernatchez JA, Li R. Kinase and Histone Deacetylase Hybrid Inhibitors for Cancer Therapy. *J Med*

- Chem. 2019; 62:3171-3183.
- Lee HY, Fan SJ, Huang FI, Chao HY, Hsu KC, Lin TE, Yeh TK, Lai MJ, Li YH, Huang HL, Yang CR, Liou JP. 5-Aroylindoles Act as Selective Histone Deacetylase 6 Inhibitors Ameliorating Alzheimer's Disease Phenotypes. *J Med Chem.* 2018; 61:7087-7102.
  - Boyault C, Sadoul K, Pabion M, Khochbin S. HDAC6, at the crossroads between cytoskeleton and cell signaling by acetylation and ubiquitination. *Oncogene.* 2007; 26:5468-5476.
  - Lee HY, Nepali K, Huang FI, Chang CY, Lai MJ, Li YH, Huang HL, Yang CR, Liou JP. (N-Hydroxycarbonylbenylamino)quinolines as selective histone deacetylase 6 inhibitors suppress growth of multiple myeloma *in vitro* and *in vivo*. *J Med Chem.* 2018; 61:905-917.
  - Hubbert C, Guardiola A, Shao R, Kawaguchi Y, Ito A, Nixon A, Yoshida M, Wang XF, Yao TP. HDAC6 is a microtubule-associated deacetylase. *Nature.* 2002; 417:455-458.
  - Luo J, Su F, Chen D, Shiloh A, Gu W. Deacetylation of p53 modulates its effect on cell growth and apoptosis. *Nature.* 2000; 408:377-381.
  - Vaziri H, Dessain SK, Ng Eaton E, Imai SI, Frye RA, Pandita TK, Guarente L, Weinberg RA. hSIR2(SIRT1) functions as an NAD-dependent p53 deacetylase. *Cell.* 2001; 107:149-159.
  - Bian J, Luan Y, Wang C, Zhang L. Discovery of N-hydroxy-4-(<sup>1</sup>H-indol-3-yl)butanamide as a histone deacetylase inhibitor. *Drug Discov Ther.* 2016; 10:163-166.
  - Li X, Xu W. HDAC1/3 dual selective inhibitors - new therapeutic agents for the potential treatment of cancer. *Drug Discov Ther.* 2014; 8:225-228.
  - Fraczek J, Vanhaecke T, Rogiers V. Toxicological and metabolic considerations for histone deacetylase inhibitors. *Expert Opin Drug Metab Toxicol.* 2013; 9:441-457.
  - Mackay HJ, Hirte H, Colgan T, Covens A, MacAlpine K, Greci P, Wang L, Mason J, Pham PA, Tsao MS, Pan J, Zwiebel J, Oza AM. Phase II trial of the histone deacetylase inhibitor belinostat in women with platinum resistant epithelial ovarian cancer and micropapillary (LMP) ovarian tumours. *Eur J Cancer.* 2010; 46:1573-1579.
  - Govindarajan N, Rao P, Burkhardt S, Sananbenesi F, Schluter OM, Bradke F, Lu J, Fischer A. Reducing HDAC6 ameliorates cognitive deficits in a mouse model for Alzheimer's disease. *EMBO Mol Med.* 2013; 5:52-63.
  - Kalin JH, Bergman JA. Development and therapeutic implications of selective histone deacetylase 6 inhibitors. *J Med Chem.* 2013; 56:6297-6313.
  - Seidel C, Schnekenburger M, Dicato M, Diederich M. Histone deacetylase 6 in health and disease. *Epigenomics.* 2015; 7:103-118.
  - Miao H GJ, Mou ZS, Wang BL, Zhang L, Su L, Han YT, Luan YP. Design, synthesis and biological evaluation of 4-piperidin-4-yltriazole derivatives as novel histone deacetylase inhibitors. *BioSci Trends.* 2019; 13:7.
  - Zhao C GJ, Zhang L, Su L, Luan Y. Novel HDAC6 selective inhibitors with 4-aminopiperidine-1-carboxamide as the core structure enhanced growth inhibitory activity of bortezomib in MCF-7 cells. *BioSci Trends.* 2019; 13:7.
  - Hsieh YL, Tu HJ, Pan SL, Liou JP, Yang CR. Anti-metastatic activity of MPT0G211, a novel HDAC6 inhibitor, in human breast cancer cells *in vitro* and *in vivo*. *Biochim Biophys Acta Mol Cell Res.* 2019; 1866:992-1003.
  - Cao J, Lv W, Wang L, Xu J, Yuan P, Huang S, He Z, Hu J. Ricolinostat (ACY-1215) suppresses proliferation and promotes apoptosis in esophageal squamous cell carcinoma *via* miR-30d/PI3K/AKT/mTOR and ERK pathways. *Cell Death Dis.* 2018; 9:817.
  - Kalin JH, Butler KV, Kozikowski AP. Creating zinc monkey wrenches in the treatment of epigenetic disorders. *Curr Opin Chem Biol.* 2009; 13:263-271.
  - Senger J, Melesina J, Marek M, Romier C, Oehme I, Witt O, Sippl W, Jung M. Synthesis and Biological Investigation of Oxazole Hydroxamates as Highly Selective Histone Deacetylase 6 (HDAC6) Inhibitors. *J Med Chem.* 2016; 59:1545-1555.
  - Butler KV, Kalin J, Brochier C, Vistoli G, Langley B, Kozikowski AP. Rational design and simple chemistry yield a superior, neuroprotective HDAC6 inhibitor, tubastatin A. *J Am Chem Soc.* 2010; 132:10842-10846.
  - Oyelere AK, Chen PC, Guerrant W, Mwakwari SC, Hood R, Zhang Y, Fan Y. Non-peptide macrocyclic histone deacetylase inhibitors. *J Med Chem.* 2009; 52:456-468.
  - Ding C, Chen S, Zhang C, Hu G, Zhang W, Li L, Chen YZ, Tan C, Jiang Y. Synthesis and investigation of novel 6-(1,2,3-triazol-4-yl)-4-aminoquinazolin derivatives possessing hydroxamic acid moiety for cancer therapy. *Bioorg Med Chem.* 2017; 25:27-37.

(March 2, 2019; Revised May 10, 2019; Accepted May 18, 2019)

## The epidemic of major sexually transmitted diseases in Shanghai, China, 2009-2018

Qi Tang<sup>1,2</sup>, Xuting Zhang<sup>3</sup>, Hongzhou Lu<sup>1,2,4,\*</sup>

<sup>1</sup>Scientific Research Center, Shanghai Public Health Clinical Center, Fudan University, Shanghai, China;

<sup>2</sup>Department of Infectious Diseases, Shanghai Public Health Clinical Center, Fudan University, Shanghai, China;

<sup>3</sup>Department of Dermatology, Sixth People's Hospital, Shanghai Jiao Tong University, Shanghai, China;

<sup>4</sup>Department of Infectious Disease, Huashan Hospital Affiliated to Fudan University, Shanghai, China.

### Summary

Acquired immune deficiency syndrome (AIDS), hepatitis B virus (HBV), hepatitis C virus (HCV), gonorrhea and syphilis are the major sexually transmitted diseases (STDs) in the world, which are the focus of epidemic prevention and control in China. The epidemiological trend analysis of STDs in Shanghai could reflect the epidemic situation of these diseases in high-income areas of China, providing a reference for how to control their epidemic. Although the overall incidence rate of infectious diseases levelled off after 2009, Shanghai still faces many new obstacles in the fight against STDs. Without effective prevention and control strategies for high-risk behaviors, such as active sexual activity without protection, for key susceptible populations, there may be a more serious epidemic of STDs in the future. Given these situations, strategies for controlling STDs in Shanghai should be more targeted with the development of epidemics, focusing on the following key areas for future work: *i*) attaching importance to health education; *ii*) strengthening epidemic surveillance; and *iii*) developing Community Health Service Centers (CHSC) as intervention subjects.

**Keywords:** HIV/AIDS, HBV, HCV, gonorrhea, syphilis

The prevalence and incidence of the curable sexually transmitted diseases (STDs) remain high according to global estimates, with more than 1 million infections acquired every day worldwide (1). Acquired immune deficiency syndrome (AIDS), hepatitis B virus (HBV), hepatitis C virus (HCV), gonorrhea and syphilis are the major STDs in the world, which are the focus of epidemic prevention and control in China (2-3). Shanghai Municipality represents the highest level of development in China, and STDs in Shanghai are close to the highest level in the country. The epidemiological trend analysis of STDs in Shanghai could reflect the epidemic situation of these diseases in high-income areas of China, providing a reference for how to control their epidemic.

Based on the data (4-24) from Shanghai Municipal

Health Commission (the incidence data for 2017 are not available), reported cases of AIDS increased from 106 in 2009 to 350 in 2018, while the reported incidence rate of AIDS from 0.77 cases per 100,000 individuals grew to 2.42 cases per 100,000 individuals (Figures 1-2). Although the number of people living with AIDS continues to increase, this may be because of the expansion of HIV testing rather than more new HIV infections occurring (25). Besides, benefiting from China's substantial progress, such as vaccination and drug discovery, in tackling its viral hepatitis epidemic, the reported incidence rate of HBV and HCV declined from 10.13 cases per 100,000 individuals and 2.09 cases per 100,000 individuals in 2009 to 2.17 cases per 100,000 individuals and 0.16 cases per 100,000 individuals in 2018, respectively (Figures 1-2). In addition, gonorrhea and syphilis epidemics are still serious, while showing a downward trend in the past three years, with a reported incidence rate of 16.27 cases per 100 000 individuals and 67.05 cases per 100 000 individuals in 2018, respectively (Figures 1-2).

As one of the most developed cities in China,

\*Address correspondence to:

Dr. Hongzhou Lu, Shanghai Public Health Clinical Center, Fudan University, No.2901, Caolang Road, Jinshan District, Shanghai 201508, China.

E-mail: luhongzhou@fudan.edu.cn

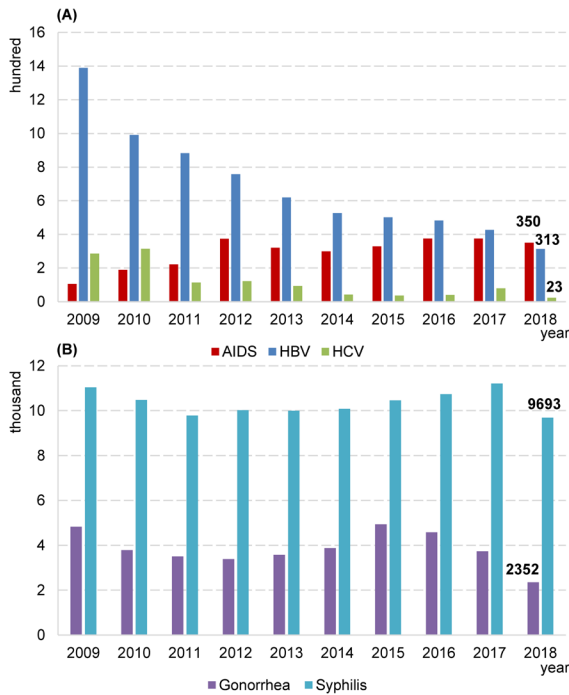


**Figure 1. Reported cases of sexually transmitted disease in Shanghai, China, 2009-2018.** Based on the data from Shanghai Municipal Health Commission, the reported cases of AIDS increased from 106 in 2009 to 350 in 2018, and the reported cases of HBV, HCV, gonorrhea and syphilis declined from 1389, 286, 4830 and 11041 in 2009 to 313, 23, 2352 and 9693 in 2018, respectively.

Shanghai Municipality was also once the one with the most prevalent venereal disease in China, with the highest rates (55.3 cases per 100,000 individuals) of total syphilis cases reported in 2005 (26). Although the overall incidence rate of infectious diseases levelled off after 2009, Shanghai still faces many new obstacles in the fight against STDs. As social activity developed and the economy increased, the main mode of STDs transmission has also changed in China. Men who have sex with men (MSM) has become one of the high-risk groups for AIDS infection and other sexually transmitted diseases in China (27-28). Without effective prevention and control strategies for high-risk behaviors, such as active sexual activity without protection, for these key populations, there may be a more serious epidemic of STDs in the future.

Given these situations, strategies for controlling STDs in Shanghai should be more targeted with the development of epidemics, focusing on the following key areas for future work: *i) Attaching importance to health education.* By giving full play to the role of non-governmental organizations (NGOs), to maximize health education for key populations, including publicity materials, behavioral intervention, condom distribution, testing mobilization, etc. *ii) Strengthening epidemic surveillance.* Relevant departments should improve management ability and work skills, providing STD-related services and continuously monitoring the

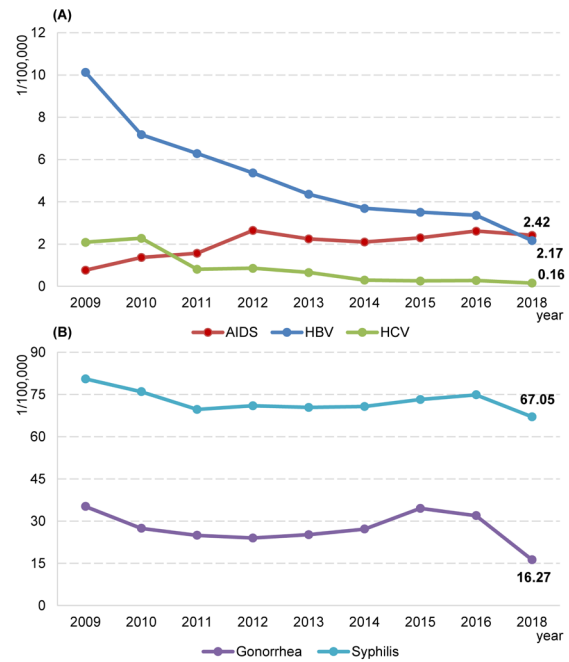


**Figure 2. Reported incidence rate of sexually transmitted disease in Shanghai, China, 2009-2016, 2018.** The reported incidence rate of AIDS from 0.77 cases per 100,000 individuals grew to 2.42 cases per 100,000 individuals. Besides, the reported incidence rate of HBV, HCV declined from 10.13 cases per 100,000 individuals and 2.09 cases per 100,000 individuals in 2009 to 2.17 cases per 100,000 individuals and 0.16 cases per 100,000 individuals in 2018, respectively. In addition, the reported incidence rate of 16.27 cases per 100,000 individuals and 67.05 cases per 100,000 individuals in 2018, respectively.

prevalence of STDs. On the basis of in-depth analysis of current STDs epidemic characteristics, more evidence-based decision-making is being adopted to better control the STDs epidemic. *iii) Developing Community Health Service Centers (CHSC)* as intervention subjects. Implementing the STDs prevention strategies with CHSC as the main body as soon as possible, so that CHSC can play a more important role in providing STD-related medical services, achieving early diagnosis and immediate treatment for STDs.

**Acknowledgements**

This research was funded by the 13th Five-Year National Major Science and Technology Project on Discovery of New Drugs from Ministry of Science and Technology of the People’s Republic of China (2017ZX09304027); Clinical Scientific Research Projects from Shanghai Public Health Clinical Center (KY-GW-2018-05).

**References**

1. World Health Organization. Sexually transmitted infections (STIs) Key facts. [https://www.who.int/en/news-room/fact-sheets/detail/sexually-transmitted-infections-\(stis\)](https://www.who.int/en/news-room/fact-sheets/detail/sexually-transmitted-infections-(stis)) (accessed May 16, 2019)

2. World Health Organization. Bulletin of the World Health Organization. [https://www.who.int/bulletin/online\\_first/en/](https://www.who.int/bulletin/online_first/en/) (accessed May 22, 2019)
3. World Health Organization. Progress report on HIV, viral hepatitis and sexually transmitted infections, 2019. <https://apps.who.int/iris/bitstream/handle/10665/324797/WHO-CDS-HIV-19.7-eng.pdf?ua=1> (accessed May 19, 2019)
4. Shanghai Municipal Health Commission. Statutory Reported Infectious Disease Epidemic in Shanghai in 2018. <http://wsjkw.sh.gov.cn/jbfbk2/20190423/63767.html> (accessed May 26, 2019)
5. Shanghai Municipal Health Commission. Statutory Reported Infectious Disease Epidemic in Shanghai in January 2017. <http://wsjkw.sh.gov.cn/jbfbk2/20180815/57000.html> (accessed May 26, 2019)
6. Shanghai Municipal Health Commission. Statutory Reported Infectious Disease Epidemic in Shanghai in February 2017. <http://wsjkw.sh.gov.cn/jbfbk2/20180815/57136.html> (accessed May 26, 2019)
7. Shanghai Municipal Health Commission. Statutory Reported Infectious Disease Epidemic in Shanghai in March 2017. <http://wsjkw.sh.gov.cn/jbfbk2/20180815/57306.html> (accessed May 26, 2019)
8. Shanghai Municipal Health Commission. Statutory Reported Infectious Disease Epidemic in Shanghai in April 2017. <http://wsjkw.sh.gov.cn/jbfbk2/20180815/57390.html> (accessed May 26, 2019)
9. Shanghai Municipal Health Commission. Statutory Reported Infectious Disease Epidemic in Shanghai in May 2017. <http://wsjkw.sh.gov.cn/jbfbk2/20180815/57489.html> (accessed May 26, 2019)
10. Shanghai Municipal Health Commission. Statutory Reported Infectious Disease Epidemic in Shanghai in June 2017. <http://wsjkw.sh.gov.cn/yqxx/20180815/57552.html> (accessed May 26, 2019)
11. Shanghai Municipal Health Commission. Statutory Reported Infectious Disease Epidemic in Shanghai in July 2017. <http://wsjkw.sh.gov.cn/jbfbk2/20180815/57647.html> (accessed May 26, 2019)
12. Shanghai Municipal Health Commission. Statutory Reported Infectious Disease Epidemic in Shanghai in August 2017. <http://wsjkw.sh.gov.cn/yqxx/20180815/57710.html> (accessed May 26, 2019)
13. Shanghai Municipal Health Commission. Statutory Reported Infectious Disease Epidemic in Shanghai in September 2017. <http://wsjkw.sh.gov.cn/yqxx/20180815/57856.html> (accessed May 26, 2019)
14. Shanghai Municipal Health Commission. Statutory Reported Infectious Disease Epidemic in Shanghai in October 2017. <http://wsjkw.sh.gov.cn/yqxx/20180815/57943.html> (accessed May 26, 2019)
15. Shanghai Municipal Health Commission. Statutory Reported Infectious Disease Epidemic in Shanghai in November 2017. <http://wsjkw.sh.gov.cn/yqxx/20180815/58066.html> (accessed May 26, 2019)
16. Shanghai Municipal Health Commission. Statutory Reported Infectious Disease Epidemic in Shanghai in December 2017. <http://wsjkw.sh.gov.cn/jbfbk2/20180815/58153.html> (accessed May 26, 2019)
17. Shanghai Municipal Health Commission. Statutory Reported Infectious Disease Epidemic in Shanghai in 2016. <http://wsjkw.sh.gov.cn/yqxx/20180815/57100.html> (accessed May 26, 2019)
18. Shanghai Municipal Health Commission. Statutory Reported Infectious Disease Epidemic in Shanghai in 2015. <http://wsjkw.sh.gov.cn/jbfbk2/20180815/59725.html> (accessed May 26, 2019)
19. Shanghai Municipal Health Commission. Statutory Reported Infectious Disease Epidemic in Shanghai in 2014. <http://wsjkw.sh.gov.cn/jbfbk2/20180815/59071.html> (accessed May 26, 2019)
20. Shanghai Municipal Health Commission. Statutory Reported Infectious Disease Epidemic in Shanghai in 2013. <http://wsjkw.sh.gov.cn/yqxx/20180815/58383.html> (accessed May 26, 2019)
21. Shanghai Municipal Health Commission. Statutory Reported Infectious Disease Epidemic in Shanghai in 2012. <http://wsjkw.sh.gov.cn/yqxx/20180815/57616.html> (accessed May 26, 2019)
22. Shanghai Municipal Health Commission. Statutory Reported Infectious Disease Epidemic in Shanghai in 2011. <http://wsjkw.sh.gov.cn/yqxx/20180815/56967.html> (accessed May 26, 2019)
23. Shanghai Municipal Health Commission. Statutory Reported Infectious Disease Epidemic in Shanghai in 2010. <http://wsjkw.sh.gov.cn/jbfbk2/20180815/60439.html> (accessed May 26, 2019)
24. Shanghai Municipal Health Commission. Statutory Reported Infectious Disease Epidemic in Shanghai in 2009. <http://wsjkw.sh.gov.cn/jbfbk2/20180815/60471.html> (accessed May 26, 2019)
25. Burki T. HIV in China: A changing epidemic. *Lancet Infect Dis.* 2018; 18:1311-1312.
26. Chen ZQ, Zhang GC, Gong XD, Lin C, Gao X, Liang GJ, Yue XL, Chen XS, Cohen MS. Syphilis in China: Results of a national surveillance programme. *Lancet.* 2007; 369:132-138.
27. Tang S, Tang W, Meyers K, Chan P, Chen Z, Tucker JD. HIV epidemiology and responses among men who have sex with men and transgender individuals in China: A scoping review. *BMC Infect Dis.* 2016; 16:588.
28. Xu JJ, Tang WM, Zou HC, et al. High HIV incidence epidemic among men who have sex with men in China: Results from a multi-site cross-sectional study. *Infect Dis Poverty.* 2016; 5:82.

(Received June 2, 2019; Revised June 24, 2019; Accepted June 28, 2019)

# Super-aged society: Constructing an integrated information platform of self-recording lifelogs and medical records to support health care in Japan

Kenji Karako<sup>1</sup>, Yu Chen<sup>1,\*</sup>, Peipei Song<sup>2,\*</sup>, Wei Tang<sup>3</sup>

<sup>1</sup> Department of Human and Engineered Environmental Studies, Graduate School of Frontier Sciences, The University of Tokyo, Chiba, Japan;

<sup>2</sup> The Institute for Global Health Policy Research, Bureau of International Health Cooperation, National Center for Global Health and Medicine, Tokyo, Japan;

<sup>3</sup> International Health Care Center, National Center for Global Health and Medicine, Tokyo, Japan.

## Summary

As the super-aged society, Japan is facing challenges in health care system. As one of measures to cope with challenges, the Ministry of Health, Labor, and Welfare started to construct an open medical information platform, named PeOPLE, in 2016 for personalized medical care, improvement of medical services, and the redistribution of medical resources. The Ministry plans to build the platform infrastructure by 2020 and put the platform into full-scale operation by 2025. PeOPLE collects only medical records, but it should collect lifelogs as well in order to better improve the health, especially for elderly. A lifelog is a record of a person's activity and it has potential to predict the probability a person will suffer a lifestyle-related disease as a result of the person's lifestyle. This prediction could help to maintain the health of the elderly. In addition, constructing a self-recording platform integrated with the medical platform is the best way to collect lifelogs since collecting a large amount of lifelogs for a long time from various people at public or medical agencies is difficult. A self-recording platform is a place where people can post and manage their lifelogs. In return for posting lifelogs, people will receive personalized health advice, which will attract more people.

**Keywords:** Japan, population aging, medical platform, deep learning

## 1. Introduction

According to the Cabinet Office, the current proportion of people aged 65+ years in the total population is 27.7% in Japan, and will reach 38.4% in 2016 (1). One of the big challenges faced by the super-aged society is the burden on the health care system. The types

of diseases that people develop change with age. A greater proportion of elderly will change the prevalence of diseases requiring specialized care. The elderly are likely to develop a lifestyle-related disease. In addition, the demand for health care in rural areas with a large percentage of elderly differs from that in urban areas. Doctor will need to be redeployed to meet local demand.

As one of measures to cope with above challenges, Japan is trying to construct a new medical information platform named PeOPLE (2,3). The Ministry of Health, Labor, and Welfare started the project in 2016. It plans to build the platform's infrastructure by 2020 and put the platform into full-scale operation by 2025. PeOPLE collects personal medical information from medical facilities such as hospitals and pharmacies as well as from local governments. A doctor can make a diagnosis and decide a treatment tailored to a

\*Address correspondence to:

Dr. Yu Chen, Department of Human and Engineered Environmental Studies, Graduate School of Frontier Sciences, The University of Tokyo, 5-1-5 Kashiwa-no-ha, Kashiwa Chiba, 227-8568, Japan.

E-mail: chen@edu.k.u-tokyo.ac.jp

Dr. Peipei Song, The Institute for Global Health Policy Research, Bureau of International Health Cooperation, National Center for Global Health and Medicine, Tokyo, 1-21-1 Toyama Shinjuku-ku, Tokyo 162-8655, Japan.

E-mail: psong@it.ncgm.go.jp

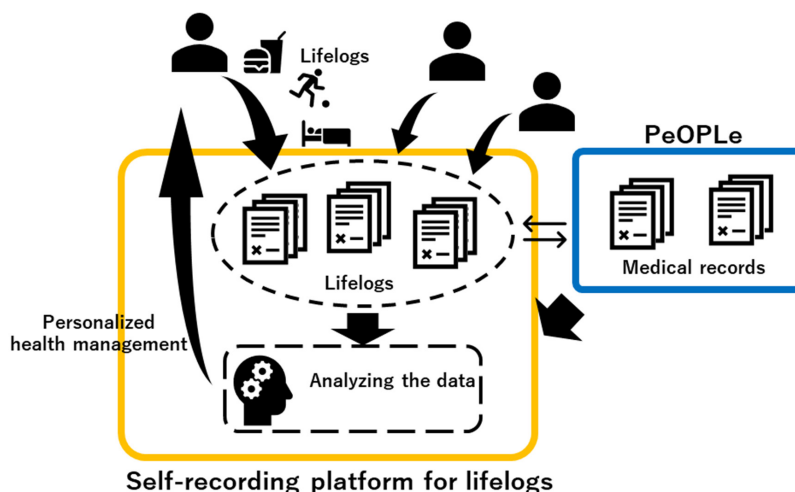


**Figure 1. Architecture of the self-recording platform for lifelogs.**

person by receiving the person's medical information from PeOPLE. Moreover, the massive amount of data collected by PeOPLE will be used to improve medical services and redistribute medical resources. Typically, the redistribution of medical resources plays a big role in addressing the medical problems faced by the super-aged society. Analyzing the collected data while focusing on the prevalence of diseases and patients in an area will help to resolve the uneven distribution of doctors (4).

In addition to collecting personal medical records, personal lifelogs should be collected to help maintain the health of elderly. A lifestyle-related disease develops as a result of lifestyle. A lifelog is the record of a person's daily activities, and it has the potential to predict the probability a person has of developing a lifestyle-related disease. The early prediction of disease based on lifelogs will help to manage the health of the elderly. In addition, predicting patients at risk of developing a lifestyle-related disease might improve the accuracy of the predicted demand for doctors in an area.

Here, the purposes of collecting lifelogs and the need for a new self-recording platform to collect a large amount of lifelogs to manage the health of the elderly will be described.

## 2. Purposes of collecting lifelogs

A lifelog has the potential to predict potential patients in an area, to predict lifestyle-related diseases, and to provide personally tailored information for health and disease prevention (5). A lifelog is a record of daily personal activities such as the amount of exercise, hours of sleep, and meals. Non-viral diseases such as lifestyle-related diseases are caused by lifestyle. Therefore, combining lifelogs with deep learning techniques

can help predict people who are likely to develop a disease. In medicine, deep learning has been studied in diagnostic imaging (6-9) as well as in predicting a patient's activities (10). Predicting a patient's activities based on medical records means predicting what will happen next to the patient, such as the worsening of symptoms, and when the patient will next visit the hospital. As with the prediction of a patient's activities, deep learning based on medical records and lifelogs will help to predict the development of lifestyle-related diseases. This provides people with the opportunity for prevention and early treatment.

Moreover, a lifelog helps a person to lead a healthier life. People can obtain information on living a healthier life by comparing their lifelogs to the lifelogs of healthy people. Analyzing the lifelogs of healthy people will reveal strategies to live healthier and longer.

## 3. A self-recording platform for lifelogs

A platform where people can post and manage the lifelogs they record will facilitate the collection of lifelogs. Lifelogs are records of a person's activities and are usually not preserved. To record their activities in logs, people should manually record their activities or use a device to automatically record their lifelogs. In addition, lifelogs should be continuously recorded by both healthy and unhealthy people for use in prediction and analysis. The government or a medical facility has difficulty collecting a large amount of lifelogs for a long time even though there are devices to help record lifelogs. That said, there are people who record lifelogs with recording devices to manager their health. They usually analyze the lifelogs themselves, but self-analysis has limitations since it only involves lifelogs and its does not involve medical records. If the government provides a platform where people can

post and manage all of the lifelogs they record, then the platform will provide integrated management of those lifelogs. In addition, combining lifelogs with medical records on PeOPLE will provide people with a comprehensive analysis. Therefore, the government should seek the cooperation of people who record their own lifelogs to manage their health.

The architecture of a self-recording platform for lifelogs is shown in Figure 1. The platform is a place where people can post their own lifelogs. The posted lifelogs are managed individually and linked to their own medical records on PeOPLE. Deep learning ascertains the causal relationships from posted logs and linked medical records to predict the probability of developing a lifestyle-related disease. Using trained deep learning models, the platform will provide people with personalized advice to prevent the development of a lifestyle-related disease.

There is another benefit provided by the self-recording platform for lifelogs. The platform provides a place for providing personal health advice. For example, a liver examination or better meals could be suggested to people who consume a large amount of alcohol. This benefit will attract the interest of people who actively manage their own health as well as people who are not interested in managing their health. The new service offering personalized health management will create the opportunity to obtain lifelogs from more people.

#### 4. Conclusion

Coping with the super-aged society, Japan is constructing an open medical information platform that will collect personal medical records and share those records with doctors for personalized diagnosis and treatment. The collected data will also be used to resolve the uneven distribution of doctors. Lifelogs should also be collected. A lifelog is a record of a person's activities, and it has potential to predict the probability of developing a lifestyle-related disease caused by a person's lifestyle. This prediction will help to maintain the health of the elderly. Constructing a self-recording platform integrated with the medical platform is the best way to collect lifelogs. A self-recording platform is a place where people can post and manage their lifelogs. In return for posting lifelogs,

people will receive personalized health advice, which will attract more people.

#### Acknowledgements

This work was supported by Grants-in-Aid from the Ministry of Education, Science, Sports, and Culture of Japan.

#### References

1. Annual report on aging of the population: 2019. [https://www8.cao.go.jp/kourei/whitepaper/w-2019/zenbun/01pdf\\_index.html](https://www8.cao.go.jp/kourei/whitepaper/w-2019/zenbun/01pdf_index.html). (accessed June 26, 2019). (in Japanese)
2. Round-table conference on the use of ICT in the field of health care. <https://www.mhlw.go.jp/file/05-Shingikai-12601000-Seisakutoukatsukan-Sanjikanshitsu-Shakaihoshoutantou/0000140305.pdf>. (accessed June 26, 2019). (in Japanese)
3. Construction of a "next-generation health care system" using ICT. <https://www.mhlw.go.jp/file/05-Shingikai-12601000-Seisakutoukatsukan-Sanjikanshitsu-Shakaihoshoutantou/0000140306.pdf>. (accessed June 26, 2019). (in Japanese)
4. Measures to deal with the uneven distribution of doctors through a plan to ensure the supply of doctors. <https://www.mhlw.go.jp/content/12601000/000504403.pdf>. (accessed June 28, 2019). (in Japanese)
5. Gurrin C, Smeaton AF, Doherty AR, Gurrin C, Smeaton AF, Doherty AR. LifeLogging: Personal big data. *Found Trends R Inf Retr.* 2014; 8:1-107.
6. Esteva A, Kuprel B, Novoa RA, Ko J, Swetter SM, Blau HM, Thrun S. Dermatologist-level classification of skin cancer with deep neural networks. *Nature.* 2017; 115-118.
7. Liu Y, Gadepalli K, Norouzi M, et al. Detecting cancer metastases on gigapixel pathology images. 2017; CoRR, abs/1703.02442.
8. Ronneberger O, Fischer P, Brox T. U-Net: Convolutional networks for biomedical image segmentation. *MICCAI 2015. LNCS 9351.* 2015:234-241.
9. Rajpurkar P, Irvin J, Zhu K, Yang B, Mehta H, Duan T, Ding D, Bagul A, Langlotz CP, Shpanskaya K, Lungren MP, Ng AY. CheXNet: Radiologist-level pneumonia detection on chest X-rays with deep learning. 2017; CoRR, abs/1711.05225.
10. Choi E, Bahadori MT, Schuetz A, Stewart WF, Sun J. Doctor AI: Predicting clinical events via recurrent neural networks. *JMLR Workshop Conf Proc.* 2016; 56:301-318.

(Received May 10, 2019; Revised June 26, 2019; Accepted June 28, 2019)

# The community-based integrated care system in Japan: Health care and nursing care challenges posed by super-aged society

Peipei Song<sup>1</sup>, Wei Tang<sup>2,\*</sup>

<sup>1</sup> The Institute for Global Health Policy Research, Bureau of International Health Cooperation, National Center for Global Health and Medicine, Tokyo, Japan;

<sup>2</sup> International Health Care Center, National Center for Global Health and Medicine, Tokyo, Japan.

## Summary

Japan is experiencing unprecedented aging of its population. People age 65 years or older accounted for 28.1% of the total population in 2018, and that proportion is expected to reach 33.3% in 2036 and 38.4% in 2065. In 2017, the average life expectancy in Japan was 81.09 years for men and 87.26 years for women. By 2065, it is expected to reach 84.95 years for men and 91.35 years for women. Population aging affects health and long-term care systems. The government proposed the establishment of "a community-based integrated care system" by 2025 with the purpose of comprehensively ensuring the provision of health care, nursing care, preventive care, housing, and livelihood support. This will require health care and nursing care professionals who are capable of fully understanding the physical and mental characteristics of elderly people and the fostering of organic collaboration with others professionals in the community-based integrated care system. A department of gerontology or geriatric medicine is desired to be established in each medical school to teach students medicine and efficient medical care, to conduct research, and to develop personnel to facilitate this paradigm shift. In 2018, there were 263 colleges of nursing with an admissions capacity of 23,667. In Japan, Certified Nurse Specialists can specialize in 13 areas as of December 2016. The number of Certified Nurse Specialists increased to 2,279 as of December 2018. One hundred and forty-four of those specialists specialized in Gerontological Nursing while 53 specialized in Home Care Nursing. The number of nurses specializing in Gerontological Nursing and Home Care Nursing is desired to be increased in order to implement and improve community-based comprehensive care.

**Keywords:** Health care, nursing care, super-aged society, community-based integrated care system, education

## 1. Population aging in Japan

An elderly population refers to the proportion of persons age 65 years or older out of the total population. The World Health Organization (WHO) and the United Nations define an "aging society" as one in which more than 7% of the population is 65 years or older, an "aged society" as a society in which more than 14% of the population is 65 years or older, and a "super-aged

society" as a society in which more than 21% of the population is 65 years or older (1,2).

Japan is experiencing population aging that is unprecedented. The elderly population (65 years or older) in Japan only accounted for about 5% of the total population in 1950, but that proportion exceeded 7% in 1970 and 14% in 1994. The rate of aging has continued to increase, reaching 21.5% in 2007 (3) and 28.1% in 2018 (4). The elderly population of Japan is forecast to continue to grow in the future and is expected to account for 33.3% of the population in 2036 and 38.4% in 2065 (Figure 1). In other words, 1 in 2.6 persons in the Japanese population will be elderly in 2065 (4).

At the same time, progress in medical technology has decreased mortality rates, prolonging the mean life

\*Address correspondence to:

Dr. Wei Tang, International Health Care Center, National Center for Global Health and Medicine, 1-21-1 Toyama Shinjuku-ku, Tokyo 162-8655, Japan.

E-mail: politang-ky@umin.ac.jp

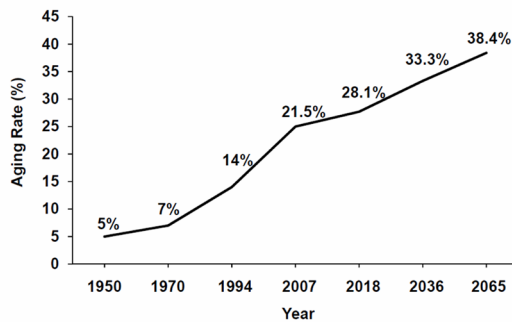


**Figure 1. Changes in population aging in Japan and estimates for the future. From:** Cabinet Office: White Paper on Population Aging (3,4).

span. The average life expectancy in Japan is 81.09 years for men and 87.26 years for women in 2017. By 2065, it is expected to reach 84.95 years for men and 91.35 years for women (4).

## 2. Medical care modality faced by super-aged society

Population aging affects health and long-term care systems. Long-term care for older adults has been a priority for the past two decades. In 2000, Japan implemented a universal social long-term care insurance system, under the slogan, "from care by family to care by society" (5,6). This historic policy provides a variety of home, community-based, and institutional services to which every Japanese person age 65 years or older is entitled based strictly on physical and mental status.

A point worth noting is that as the country's demographics change, the disease structure changes, and therefore the demand for medical care changes. Medical care for the elderly represents a field involving many care needs, including complications, comorbidities, and conditions unique to the elderly. Given the considerable aging of the general population in Japan, future demands for medical care will accelerate the transition to health care and nursing care services for degenerative diseases, such as dementia and geriatric syndrome (7). In addition to acute-stage medical care, the provision of health care and nursing care needs to be considered for the convalescent and chronic stages of conditions such as osteoporosis, atherosclerotic cardiovascular diseases (and cerebrovascular disorders in particular), and infections (and pneumonia in particular).

Moreover, medical care for the elderly that merely deals with disorders of organs is unsatisfactory. A broad perspective that considers the associated function of all organs, activities of daily living (ADL) and other indicators of physical function, mental care, and environmental modifications is required, so medical care is where holistic care is most needed.

With these facts in mind, the Japanese Government proposed the establishment of a "Community-based Integrated Care System" by 2025, when baby boomers

will become age 75 or older (8). The purpose of this system is to comprehensively ensure the provision of health care, nursing care, preventive care, housing, and livelihood support.

## 3. Promoting the education of health care and nursing care professionals for elderly people

The number of personnel engaged in providing community-based comprehensive care needs to be increased to implement the "Community-based Integrated Care System." Health care and nursing care professionals who are capable of fully understanding the physical and mental characteristics of the elderly are urgently needed, and to foster the organic collaboration with others professionals in the community-based integrated care system. The most important issues are educating health care and nursing care professionals engaged in medical care for the elderly as well as all students who aim to become healthcare providers and raising awareness of this situation. Thus, the education of health care and nursing care professionals for the elderly must be improved.

A department of gerontology or geriatric medicine is desired to be established in each medical school to teach students medicine and efficient medical care, to conduct research, and to develop personnel to facilitate this paradigm shift (7). Dedicated instructors in medical care for the elderly need to be assigned to every medical school, an educational system needs to be constructed, and collaboration with a wide variety of local entities, including medical facilities and welfare and nursing care facilities, needs to be promoted.

Many measures have also been implemented to provide education to nursing care professionals. According to data from the Ministry of Education, Culture, Sports, Science, and Technology of Japan, there were 263 colleges of nursing with an admissions capacity of 23,667 in 2018 (9). In Japan, Certified Nurse Specialists can specialize in 13 areas as of December 2016 (10). Gerontological Nursing was recognized as one such area in 2002. A nurse specializing in this area provides quality nursing care to improve the quality of life of elderly people with complex health problems such as dementia and dysphagia at facilities where the elderly are admitted, hospitalized, and cared for. Home Care Nursing is another area that was recognized in 2012. A nurse specializing in this area provides support to so that families can care for elderly patients at home. In addition, nurses specializing in this area will help to create a new system of home care and promote cooperation with existing services.

As of 2019, 107 universities provide an education for individuals seeking to become Certified Nurse Specialists; the curriculum on offer has expanded to 42 courses in Gerontological Nursing and 19 courses in Home Care Nursing (11). As of December 2018,

the number of Certified Nurse Specialists in the 13 specialties has increased to 2,279. Of those nurses, 144 are specialized in Gerontological Nursing and 53 are specialized in Home Care Nursing (12). The number of specialists in Gerontological Nursing and Home Care Nursing is desired to be increased to provide and improve community-based comprehensive care.

In conclusion, comprehensive care plays a particularly important role in the health care and nursing care faced by super-aged society. In order to implement the community-based integrated care system in Japan, health care and nursing care professionals who are capable of fully understanding the physical and mental characteristics of the elderly are urgently needed, and to foster the organic collaboration with others professionals. The number of nurses specializing in Gerontological Nursing and Home Care Nursing is desired to be increased in order to implement and improve community-based comprehensive care.

## References

1. Permanent Mission of Japan to the United Nations. Presentation by H.E. Mr. Yoshifumi Okamura, Ambassador and Deputy Representative of Japan to the United Nations At a side event to the High Level Political Forum "Mainstreaming Gender and Aging in the SDGs". <https://www.un.emb-japan.go.jp/jp/statements/okamura071316.html> (accessed May 6, 2019)
2. Tahara Y. Cardiopulmonary resuscitation in a super-aged society- Is there an age limit for cardiopulmonary resuscitation? *Circ J.* 2016; 80:1102-1103.
3. Cabinet Office. White Paper on Population Aging (2008 version). [https://www8.cao.go.jp/kourei/whitepaper/w-2008/zenbun/20pdf\\_index.html](https://www8.cao.go.jp/kourei/whitepaper/w-2008/zenbun/20pdf_index.html) (accessed May 8, 2019) (in Japanese)
4. Cabinet Office. White Paper on Population Aging (2019 version). [https://www8.cao.go.jp/kourei/whitepaper/w-2019/zenbun/01pdf\\_index.html](https://www8.cao.go.jp/kourei/whitepaper/w-2019/zenbun/01pdf_index.html) (accessed May 8, 2019) (in Japanese)
5. Ministry of Health, Labor, and Welfare of Japan. Long-term Care Insurance in Japan <https://www.mhlw.go.jp/english/topics/elderly/care/index.html> (accessed May 10, 2019)
6. Tamiya N, Noguchi H, Nishi A, et al. Population ageing and wellbeing: Lessons from Japan's long-term care insurance policy. *Lancet.* 2011; 378:1183-1192.
7. Arai H, Ouchi Y, Toba K, Endo T, Shimokado K, Tsubota K, Matsuo S, Mori H, Yumura W, Yokode M, Rakugi H, Ohshima S. Japan as the front-runner of super-aged societies: Perspectives from medicine and medical care in Japan. *Geriatr Gerontol Int.* 2015; 15:673-687.
8. Tsutsui T. Implementation process and challenges for the community-based integrated care system in Japan. *Int J Integr Care.* 2014; 14:e002.
9. Ministry of Education, Culture, Sports, Science, and Technology of Japan. Current status of and issues with nursing colleges. <http://www.janpu.or.jp/wp/wp-content/uploads/2018/06/monbukagakusyou20180618.pdf> (accessed May 11, 2019) (in Japanese)
10. Japanese Nursing Association. Certified Nurse Specialist. <https://nintei.nurse.or.jp/nursing/qualification/cns> (accessed May 13, 2019) (in Japanese)
11. Japanese Nursing Association. List of institutions providing an education to become a certified nurse specialist and courses. [https://nintei.nurse.or.jp/nursing/wp-content/uploads/2019/04/1\\_cns\\_kikan\\_kateitiran\\_2019.pdf](https://nintei.nurse.or.jp/nursing/wp-content/uploads/2019/04/1_cns_kikan_kateitiran_2019.pdf) (accessed May 13, 2019) (in Japanese)
12. Japanese Nursing Association. Number of certified nurse specialists registered in each prefecture. [https://nintei.nurse.or.jp/nursing/wp-content/uploads/2019/01/CNS\\_map-201812.pdf](https://nintei.nurse.or.jp/nursing/wp-content/uploads/2019/01/CNS_map-201812.pdf) (accessed May 13, 2019) (in Japanese)

(Received May 20, 2019; Accepted June 22, 2019)

## Overshadowed prospect of programmed cell death protein-1 (PD-1) inhibitor as monotherapy for patients with advanced hepatocellular carcinoma

Xu Yao, Lei Wang, Jianjun Gao\*

Department of Pharmacology, School of Pharmacy, Qingdao University, Qingdao, Shandong, China.

**Summary** Hepatocellular carcinoma (HCC) is a prevalent and refractory cancer in the world and very few drugs are available for the disease treatment currently. Programmed cell death protein-1 (PD-1) monoclonal antibodies including nivolumab and pembrolizumab has received accelerated approval for treatment of advanced HCC based on phase 1/2 clinical trials. However, the recently disclosed results of phase 3 clinical trials showed that both nivolumab and pembrolizumab as monotherapy failed to meet the primary objectives, which might overshadow the prospect of PD-1 inhibitors as monotherapy in treatment of advanced and unresectable HCC. The feasibility of PD-1 inhibitors in combination with other therapies or in other HCC settings requires further verification in the future.

**Keywords:** HCC, PD-1, immune checkpoint inhibitor, sorafenib, lenvatinib

Hepatocellular carcinoma (HCC) is a common and deadly cancer with limited treatment options. The vast majority of HCC occurs in Asian and sub-Saharan African countries and the incidence of HCC in the United States and other developing countries is increasing (1,2). Surgical removal of the tumor is associated with better cancer prognosis, but only 10-15% of patients are suitable for surgical resection due to the extent of disease or poor liver function (3,4). For more advanced disease, including spread of cancer beyond the liver or in persons who may not tolerate surgery, molecular targeted drugs including sorafenib, lenvatinib, regorafenib, and cabozantinib might be employed to decrease symptoms of disease and maximize duration of survival (5). Two programmed cell death protein-1 (PD-1) inhibitors, nivolumab and pembrolizumab, have received accelerated approval for HCC treatment based on the promising results of phase 1/2 clinical trials. However, the recently disclosed outcomes of phase 3 clinical trials of both drugs might overshadow the application of PD-1 inhibitors as monotherapy in advanced HCC patients (5-7).

Nivolumab is the first PD-1 monoclonal antibody approved for the second-line treatment of HCC. This approval was based on an open-label, non-comparative, phase 1/2 dose escalation and expansion trial (CheckMate 040). In this trial, the safety and efficacy of nivolumab was evaluated as a first-line treatment in patients who had not previously received sorafenib and as a second-line treatment in those with previous disease progression on sorafenib (8). In the study, nivolumab showed an objective response rate of 20% at a dose of 3 mg/kg in the expansion stage. Since the start of this study, nivolumab has been approved for the treatment of melanoma, non-small cell lung cancer, renal cell carcinoma, *etc.*, no new safety signals were observed in HCC patients (8). Supported by the results of CheckMate 040, a phase 3 randomized, multi-center study (CheckMate 459) was performed to evaluate nivolumab versus sorafenib as a first-line treatment in patients with advanced and unresectable HCC. On June 24, 2019, Bristol-Myers Squibb announced the topline results of this study. Although the trial showed a clear trend towards improvement in overall survival (OS) for patients treated with nivolumab compared to sorafenib, it did not achieve statistical significance for its primary endpoint of OS per the pre-specified analysis (HR = 0.85 [95% CI: 0.72-1.02];  $p = 0.0752$ ) (6). Results of this study demonstrated limited benefits of PD-1 antibody as a first-line drug for patients with advanced HCC.

\*Address correspondence to:

Dr. Jianjun Gao, Department of Pharmacology, School of Pharmacy, Qingdao University, Qingdao 266021, Shandong, China.

E-mail: gaojj@qdu.edu.cn

Pembrolizumab is another approved PD-1 monoclonal antibody for advanced HCC patients. In the non-randomized, open-label phase 2 trial (KEYNOTE-224), pembrolizumab displayed potential for patients whose disease progressed on previous sorafenib treatment (9). Overall, pembrolizumab was tolerable and showed an objective response of 17% and stable disease of 44% in 104 patients (9). The results accelerated the approval of pembrolizumab as a second-line treatment option for advanced HCC patients and promoted the initiation of phase 3, randomized trials for comprehensively evaluating the drug as a second-line treatment in advanced HCC patients. The trial of KEYNOTE-240 aimed to test the safety and efficacy of pembrolizumab versus best supportive care in participants with previously systemically treated advanced HCC. The complete results of this trial, published on May 26, 2019, showed that pembrolizumab improved OS (HR: 0.78;  $p = 0.0238$ ) and progression free survival (PFS) (HR: 0.78;  $p = 0.0209$ ) versus placebo, however, these differences did not meet significance per the prespecified statistical plan (7). Although the objective response rate (ORR) of pembrolizumab group is significantly higher than that of placebo group (16.9% versus 2.2%) (7), which is consistent with that of KEYNOTE-224, the OS and PFS data might compromise the confidence of pembrolizumab as a second-line monotherapy for advanced HCC given several second-line molecular targeted drugs are available in the market.

The treatment of HCC remains a huge challenge in the current stage. There have been no significant advances over sorafenib, which was approved in 2007, in more than a decade until the recent successes of lenvatinib, regorafenib, and cabozantinib as first- or second-line drugs. Immune checkpoint inhibitor brings new breakthrough for controlling cancers and has been introduced in HCC treatment with high expectations. Currently, various clinical trials are being carried out to evaluate the safety and efficacy of PD-1 or PD-L1 monoclonal antibodies alone or in combination of other drugs (e.g., lenvatinib and apatinib), adoptive T-cell therapy (e.g., CAR-GPC3 T cells), locoregional therapies (e.g., transhepatic arterial chemotherapy), or curative surgery for HCC treatment (10). The recently disclosed results of phase 3 clinical trials of nivolumab and pembrolizumab might be a setback for PD-1 monoclonal antibody as monotherapy in treatment of advanced HCC. The feasibility of PD-1/PD-L1

inhibitors in combination with other therapies or in other HCC settings requires further verification in the future.

## References

1. Kennedy K, Graham SM, Arora N, Shuhart MC, Kim HN. Hepatocellular carcinoma among US and non-US-born patients with chronic hepatitis B: Risk factors and age at diagnosis. *PLoS One*. 2018; 13:e0204031.
2. Gao J, Song P. Combination of triple biomarkers AFP, AFP-L3, and PIVAKII for early detection of hepatocellular carcinoma in China: Expectation. *Drug Discov Ther*. 2017; 11:168-169.
3. Song P, Cai Y, Tang H, Li C, Huang J. The clinical management of hepatocellular carcinoma worldwide: A concise review and comparison of current guidelines from 2001 to 2017. *Biosci Trends*. 2017; 11:389-398.
4. Liu W, Li X, Zheng W, Yao R, Zheng J. Preoperative evaluation of the degree of liver fibrosis based on matter-element analysis using serological indicators in patients with hepatocellular carcinoma. *Biosci Trends*. 2019; 13:70-76.
5. Li D, Sedano S, Allen R, Gong J, Cho M, Sharma S. Current treatment landscape for advanced hepatocellular carcinoma: Patient outcomes and the impact on quality of life. *Cancers (Basel)*. 2019; 11:E841.
6. Bristol-Myers Squibb Announces Results from CheckMate-459 Study Evaluating Opdivo (nivolumab) as a First-Line Treatment for Patients with Unresectable Hepatocellular Carcinoma. <https://news.bms.com/press-release/bmy/bristol-myers-squibb-announces-results-checkmate-459-study-evaluating-opdivo-nivolumab> (accessed June 25, 2019).
7. Finn R, Chan SL, Zhu AX, Knox J, Cheng AL, Siegel A, Bautista O, Watson PA, Kudo M. Pembrolizumab vs best supportive care for second-line advanced hepatocellular carcinoma: Randomized, phase 3 KEYNOTE-240 study. *Ann Oncol*. 2016; 27(suppl 6):713TiP.
8. El-Khoueiry AB, Sangro B, Yau T, *et al*. Nivolumab in patients with advanced hepatocellular carcinoma (CheckMate 040): An open-label, non-comparative, phase 1/2 dose escalation and expansion trial. *Lancet*. 2017; 389:2492-2502.
9. Zhu AX, Finn RS, Edeline J, *et al*. Pembrolizumab in patients with advanced hepatocellular carcinoma previously treated with sorafenib (KEYNOTE-224): Anon-randomised, open-label phase 2 trial. *Lancet Oncol*. 2018; 19:940-952.
10. ClinicalTrials.gov. <https://www.clinicaltrials.gov/ct2/results?cond=Hepatocellular+Carcinoma&term=PD-1&cntry=&state=&city=&dist=>. (Accessed June 26, 2019).

(Received June 26, 2019; Accepted June 28, 2019)

## New thoughts in exploring the pathogenesis, diagnosis, and treatment of threatened abortion

Jing Zhou<sup>1,2,3</sup>, Zengshu Huang<sup>1,2,3</sup>, Xinyao Pan<sup>1,2,3</sup>, Wing Ting Leung<sup>1,2,3</sup>, Chuyu Li<sup>1,2,3</sup>, Lijia Chen<sup>1,2,3</sup>, Yanzhi Zhang<sup>1,2,3</sup>, Lan Wang<sup>1,2,3</sup>, Yizhen Sima<sup>1,2,3</sup>, Na Zhang<sup>1,2,3</sup>, Xuemin Qiu<sup>1,2,3</sup>, Lisha Li<sup>1,2,3</sup>, Ling Wang<sup>1,2,3,\*</sup>

<sup>1</sup>Laboratory for Reproductive Immunology, Hospital & Institute of Obstetrics and Gynecology, Shanghai Medical College, Fudan University, Shanghai, China;

<sup>2</sup>The Academy of Integrative Medicine, Fudan University, Shanghai, China;

<sup>3</sup>Shanghai Key Laboratory of Female Reproductive Endocrine-related Diseases, Shanghai, China.

### Summary

Threatened abortion is a common complication of pregnancy. Since the underlying mechanisms behind this condition are complicated, predicting and treating threatened abortion is a challenge for clinicians. Interestingly, a recent article in *Bioscience Trends* (*Biosci Trends* 2019; DOI: 10.5582/bst.2019.01111) revealed a higher, not lower, level of  $\beta$ -human chorionic gonadotropin (hCG) and estrogen during the first 6 weeks of pregnancy, suggesting a novel association between  $\beta$ -hCG, estrogen, and threatened abortion. Unfortunately, this study was limited by its small sample size, unconvincing trial design, and inadequate exploration of the underlying mechanisms. This low-quality evidence indicates that a higher level of  $\beta$ -hCG and estrogen is associated with threatened abortion. However, that work provided some new insights for further studies of threatened abortion.

**Keywords:**  $\beta$ -human chorionic gonadotropin, estrogen, threatened abortion

Threatened abortion is defined as vaginal bleeding, a closed cervix, and the presence of the fetal heart beat (1). It is one of the most common complications of pregnancy, with an incidence of 20-25%, and can severely affect women's physical and emotional health (2,3). However, predicting threatened abortion is difficult because predictive methods are unreliable and because its underlying mechanisms are complicated. Hormone supplements including human chorionic gonadotropin (hCG), dydrogesterone, and estrogen are common treatments for threatened abortion, but their efficiency is a subject of debate (4). Thus, predicting and preventing threatened abortion is a challenge for clinicians, and its underlying mechanisms need to be explored.

An article entitled "Higher  $\beta$ -human chorionic gonadotropin and estrogen levels during the first 6 weeks of pregnancy are associated with threatened

abortion" was recently published in *Bioscience Trends* (*Biosci Trends* 2019; DOI: 10.5582/bst.2019.01111), and it interestingly revealed unexpected hCG and estrogen levels in patients with threatened abortion (5). The study described in that article analyzed the association between threatened abortion and the levels of pregnancy hormones in 220 patients (80 in the study group, 140 in the control group) in Obstetrics and Gynecology as part of a cross-sectional clinical trial. In statistical analysis, logarithm (Ln)-transformed variables were used instead of the original clinical values of  $\beta$ -hCG, estrogen, and progesterone in blood samples. Results indicated that  $\beta$ -hCG and estrogen levels in the first half of the first trimester are factors associated with threatened abortion, especially at gestational age  $\leq 6$  weeks. Although this study yielded novel findings, it was limited by its small sample size, less convincing trial design, and inadequate exploration of the underlying mechanisms behind threatened abortion.

Major flaws of that cross-sectional study are that it failed to observe the outcomes of the enrolled patients after the first trimester and it failed to describe the tendency of levels of pregnancy hormones to

\*Address correspondence to:

Dr. Ling Wang, Obstetrics & Gynecology Hospital of Fudan University, 419 Fangxie Road, Shanghai 200011, China.

E-mail: Dr.wangling@fudan.edu.cn

vary. Since pregnancy is an unstable and susceptible period and there are no reliable methods with which to diagnose threatened abortion, how that study defined threatened abortion is difficult to ascertain. For instance, patients with a threatened abortion may suffer a spontaneous abortion. Thus, higher  $\beta$ -hCG and estrogen levels in that study cannot be proved with certainty to be associated with threatened abortion. A case-control study with a larger sample size needs to be conducted in the future to explore the fluctuation in levels of pregnancy hormones in patients with threatened abortion. Live births, miscarriages, and still births should also be included in analysis. In addition, genetic testing of embryos should be performed to rule out unhealthy embryos as a cause.

The study analyzed the correlation between  $\beta$ -hCG, estrogen, and threatened abortion stratified by gestational age. When patients at a gestational age  $\leq 6$  weeks and at a gestational age  $> 6$  weeks were compared, a clear association between higher levels of pregnancy hormone and threatened abortion was evident in the former. Significant differences in hormonal level between a gestational age  $\leq 6$  and a gestational age  $> 6$  weeks is worthy of deep reflection and discussion. Based on the study's results, the first 6 weeks are believed to be an important period in pregnancy, and whether this period has physiological significance like that of the first trimester needs to be studied further.

The authors of the article offered possible interpretations of the higher  $\beta$ -hCG and estrogen levels, suggesting that abnormal spatio-temporal interaction in the maternal-fetal interface and stimulation of the maternal repair system by the imbalance in pregnancy hormone may explain this phenomenon. In a future study, luteinizing hormone (LH)/hCG receptors, trophoblastic cells, decidual cells, and immune cell subsets could be studied to explain the higher  $\beta$ -hCG and estrogen levels and to elucidate the mechanisms of threatened abortion. Generally, low levels of hCG, estrogen, and LH are considered to be a sign of adverse pregnancy. If high-quality evidence can prove that higher levels of higher pregnancy hormones are found in threatened abortion, this may be a new way to predict threatened abortion. Moreover, an hCG receptor antagonist and an hCG inhibitor to keep hormone levels stable may represent an appropriate tocolytic therapy, but its effectiveness needs to be demonstrated.

Although this clinical trial yielded a novel finding

of a correlation between levels of pregnancy hormones and threatened abortion not seen in a normal pregnancy, more high-quality evidence is needed to verify that finding in the future. On the bright side, this study offers new insights into the pathogenesis, diagnosis, and treatment of threatened abortion and it can encourage future studies to explore the underlying mechanism of that condition.

#### Acknowledgements

This work was supported by the 2018 Program to Guide Medicine ("Yixueyindao") of the Shanghai Municipal Science and Technology Commission (grant no. 18401902200 to Ling Wang), the Shanghai Committee of The China Democratic League (grant no. 02054 to Ling Wang), the National Natural Science Foundation of China (grant nos. 30801502 and 31571196 to Ling Wang), the 2015 Program to Guide Medicine ("Yixueyindao") of the Shanghai Municipal Science and Technology Commission (grant no. 15401932200 to Ling Wang), the 2008 JSPS Postdoctoral Fellowship for Foreign Researchers (grant no. P08471 to Ling Wang), the Shanghai Pujiang Program (grant no. 11PJ1401900 to Ling Wang), and the Shanghai Program for Support of Leading Disciplines-Integrative Medicine (grant no.20150407).

#### References

1. Kanmaz AG, Inan AH, Beyan E, Budak A. The effects of threatened abortions on pregnancy outcomes. *Ginekol Pol* 2019; 90:195-200.
2. Pillai RN, Konje JC, Tincello DG, Potdar N. Role of serum biomarkers in the prediction of outcome in women with threatened miscarriage: A systematic review and diagnostic accuracy meta-analysis. *Hum Reprod Update* 2016; 22:228-239.
3. Greene MF. Progesterone for threatened abortion. *N Engl J Med*. 2019; 380:1867-1868.
4. Wahabi HA, Fayed AA, Esmaeil SA, Bahkali KH. Progestogen for treating threatened miscarriage. *Cochrane Database Syst Rev*. 2018; 8:CD005943.
5. Xu L, Wei Q, Wu Q, Zhong Y, Li Y, Xu J, Zhu Y. Higher  $\beta$ -human chorionic gonadotropin and estrogen levels during the first 6 weeks of pregnancy are associated with threatened abortion. *Biosci Trends* 2019; DOI: 10.5582/bst.2019.01111.

(Received June 9, 2019; Revised June 28, 2019; Accepted June 30, 2019)

### Guide for Authors

#### 1. Scope of Articles

BioScience Trends is an international peer-reviewed journal. BioScience Trends devotes to publishing the latest and most exciting advances in scientific research. Articles cover fields of life science such as biochemistry, molecular biology, clinical research, public health, medical care system, and social science in order to encourage cooperation and exchange among scientists and clinical researchers.

#### 2. Submission Types

**Original Articles** should be well-documented, novel, and significant to the field as a whole. An Original Article should be arranged into the following sections: Title page, Abstract, Introduction, Materials and Methods, Results, Discussion, Acknowledgments, and References. Original articles should not exceed 5,000 words in length (excluding references) and should be limited to a maximum of 50 references. Articles may contain a maximum of 10 figures and/or tables.

**Brief Reports** definitively documenting either experimental results or informative clinical observations will be considered for publication in this category. Brief Reports are not intended for publication of incomplete or preliminary findings. Brief Reports should not exceed 3,000 words in length (excluding references) and should be limited to a maximum of 4 figures and/or tables and 30 references. A Brief Report contains the same sections as an Original Article, but the Results and Discussion sections should be combined.

**Reviews** should present a full and up-to-date account of recent developments within an area of research. Normally, reviews should not exceed 8,000 words in length (excluding references) and should be limited to a maximum of 100 references. Mini reviews are also accepted.

**Policy Forum** articles discuss research and policy issues in areas related to life science such as public health, the medical care system, and social science and may address governmental issues at district, national, and international levels of discourse. Policy Forum articles should not exceed 2,000 words in length (excluding references).

**Case Reports** should be detailed reports of the symptoms, signs, diagnosis, treatment, and follow-up of an individual patient. Case reports may contain a demographic profile of the patient but usually describe an unusual or novel occurrence. Unreported or unusual

side effects or adverse interactions involving medications will also be considered. Case Reports should not exceed 3,000 words in length (excluding references).

**News** articles should report the latest events in health sciences and medical research from around the world. News should not exceed 500 words in length.

**Letters** should present considered opinions in response to articles published in BioScience Trends in the last 6 months or issues of general interest. Letters should not exceed 800 words in length and may contain a maximum of 10 references.

#### 3. Editorial Policies

**Ethics:** BioScience Trends requires that authors of reports of investigations in humans or animals indicate that those studies were formally approved by a relevant ethics committee or review board.

**Conflict of Interest:** All authors are required to disclose any actual or potential conflict of interest including financial interests or relationships with other people or organizations that might raise questions of bias in the work reported. If no conflict of interest exists for each author, please state "There is no conflict of interest to disclose".

**Submission Declaration:** When a manuscript is considered for submission to BioScience Trends, the authors should confirm that 1) no part of this manuscript is currently under consideration for publication elsewhere; 2) this manuscript does not contain the same information in whole or in part as manuscripts that have been published, accepted, or are under review elsewhere, except in the form of an abstract, a letter to the editor, or part of a published lecture or academic thesis; 3) authorization for publication has been obtained from the authors' employer or institution; and 4) all contributing authors have agreed to submit this manuscript.

**Cover Letter:** The manuscript must be accompanied by a cover letter signed by the corresponding author on behalf of all authors. The letter should indicate the basic findings of the work and their significance. The letter should also include a statement affirming that all authors concur with the submission and that the material submitted for publication has not been published previously or is not under consideration for publication elsewhere. The cover letter should be submitted in PDF format. For example of Cover Letter, please visit <http://www.biosciencetrends.com/downcentre.php> (Download Centre).

**Copyright:** A signed JOURNAL PUBLISHING AGREEMENT (JPA) form must be provided by post, fax, or as a scanned file before acceptance of the article. Only forms with a hand-written signature are accepted. This copyright will ensure the widest possible dissemination of information. A form facilitating transfer of copyright can be downloaded by clicking the

appropriate link and can be returned to the e-mail address or fax number noted on the form (Please visit [Download Centre](#)). Please note that your manuscript will not proceed to the next step in publication until the JPA Form is received. In addition, if excerpts from other copyrighted works are included, the author(s) must obtain written permission from the copyright owners and credit the source(s) in the article.

**Suggested Reviewers:** A list of up to 3 reviewers who are qualified to assess the scientific merit of the study is welcomed. Reviewer information including names, affiliations, addresses, and e-mail should be provided at the same time the manuscript is submitted online. Please do not suggest reviewers with known conflicts of interest, including participants or anyone with a stake in the proposed research; anyone from the same institution; former students, advisors, or research collaborators (within the last three years); or close personal contacts. Please note that the Editor-in-Chief may accept one or more of the proposed reviewers or may request a review by other qualified persons.

**Language Editing:** Manuscripts prepared by authors whose native language is not English should have their work proofread by a native English speaker before submission. If not, this might delay the publication of your manuscript in BioScience Trends.

The Editing Support Organization can provide English proofreading, Japanese-English translation, and Chinese-English translation services to authors who want to publish in BioScience Trends and need assistance before submitting a manuscript. Authors can visit this organization directly at <http://www.iacmhr.com/iac-eso/support.php?lang=en>. IAC-ESO was established to facilitate manuscript preparation by researchers whose native language is not English and to help edit works intended for international academic journals.

#### 4. Manuscript Preparation

Manuscripts should be written in clear, grammatically correct English and submitted as a Microsoft Word file in a single-column format. Manuscripts must be paginated and typed in 12-point Times New Roman font with 24-point line spacing. Please do not embed figures in the text. Abbreviations should be used as little as possible and should be explained at first mention unless the term is a well-known abbreviation (e.g. DNA). Single words should not be abbreviated.

**Title Page:** The title page must include 1) the title of the paper (Please note the title should be short, informative, and contain the major key words); 2) full name(s) and affiliation(s) of the author(s), 3) abbreviated names of the author(s), 4) full name, mailing address, telephone/fax numbers, and e-mail address of the corresponding author; and 5) conflicts of interest (if you have an actual or potential conflict of interest to disclose, it must be included as a footnote on the title page of the manuscript; if no conflict of

interest exists for each author, please state "There is no conflict of interest to disclose"). Please visit [Download Centre](#) and refer to the title page of the manuscript sample.

**Abstract:** The abstract should briefly state the purpose of the study, methods, main findings, and conclusions. For article types including Original Article, Brief Report, Review, Policy Forum, and Case Report, a one-paragraph abstract consisting of no more than 250 words must be included in the manuscript. For News and Letters, a brief summary of main content in 150 words or fewer should be included in the manuscript. Abbreviations must be kept to a minimum and non-standard abbreviations explained in brackets at first mention. References should be avoided in the abstract. Key words or phrases that do not occur in the title should be included in the Abstract page.

**Introduction:** The introduction should be a concise statement of the basis for the study and its scientific context.

**Materials and Methods:** The description should be brief but with sufficient detail to enable others to reproduce the experiments. Procedures that have been published previously should not be described in detail but appropriate references should simply be cited. Only new and significant modifications of previously published procedures require complete description. Names of products and manufacturers with their locations (city and state/country) should be given and sources of animals and cell lines should always be indicated. All clinical investigations must have been conducted in accordance with Declaration of Helsinki principles. All human and animal studies must have been approved by the appropriate institutional review board(s) and a specific declaration of approval must be made within this section.

**Results:** The description of the experimental results should be succinct but in sufficient detail to allow the experiments to be analyzed and interpreted by an independent reader. If necessary, subheadings may be used for an orderly presentation. All figures and tables must be referred to in the text.

**Discussion:** The data should be interpreted concisely without repeating material already presented in the Results section. Speculation is permissible, but it must be well-founded, and discussion of the wider implications of the findings is encouraged. Conclusions derived from the study should be included in this section.

**Acknowledgments:** All funding sources should be credited in the Acknowledgments section. In addition, people who contributed to the work but who do not meet the criteria for authors should be listed along with their contributions.

**References:** References should be numbered in the order in which they appear in the text. Citing of unpublished results, personal communications, conference abstracts, and theses in the reference list is not recommended but these sources may be mentioned in the text. In the reference list,

cite the names of all authors when there are fifteen or fewer authors; if there are sixteen or more authors, list the first three followed by *et al.* Names of journals should be abbreviated in the style used in PubMed. Authors are responsible for the accuracy of the references. Examples are given below:

*Example 1* (Sample journal reference): Inagaki Y, Tang W, Zhang L, Du GH, Xu WF, Kokudo N. Novel aminopeptidase N (APN/CD13) inhibitor 24F can suppress invasion of hepatocellular carcinoma cells as well as angiogenesis. *Biosci Trends*. 2010; 4:56-60.

*Example 2* (Sample journal reference with more than 15 authors): Darby S, Hill D, Auvinen A, *et al.* Radon in homes and risk of lung cancer: Collaborative analysis of individual data from 13 European case-control studies. *BMJ*. 2005; 330:223.

*Example 3* (Sample book reference): Shalev AY. Post-traumatic stress disorder: diagnosis, history and life course. In: Post-traumatic Stress Disorder, Diagnosis, Management and Treatment (Nutt DJ, Davidson JR, Zohar J, eds.). Martin Dunitz, London, UK, 2000; pp. 1-15.

*Example 4* (Sample web page reference): Ministry of Health, Labour and Welfare of Japan. Dietary reference intakes for Japanese. <http://www.mhlw.go.jp/houdou/2004/11/h1122-2a.html> (accessed June 14, 2010).

**Tables:** All tables should be prepared in Microsoft Word or Excel and should be arranged at the end of the manuscript after the References section. Please note that tables should not be image format. All tables should have a concise title and should be numbered consecutively with Arabic numerals. If necessary, additional information should be given below the table.

**Figure Legend:** The figure legend should be typed on a separate page of the main manuscript and should include a short title and explanation. The legend should be concise but comprehensive and should be understood without referring to the text. Symbols used in figures must be explained.

**Figure Preparation:** All figures should be clear and cited in numerical order in the text. Figures must fit a one- or two-column format on the journal page: 8.3 cm (3.3 in.) wide for a single column, 17.3 cm (6.8 in.) wide for a double column; maximum height: 24.0 cm (9.5 in.). Please make sure that the symbols and numbers appeared in the figures should be clear. Please make sure that artwork files are in an acceptable format (TIFF or JPEG) at minimum resolution (600 dpi for illustrations, graphs, and annotated artwork, and 300 dpi for micrographs and photographs). Please provide all figures as separate files. Please note that low-resolution images are one of the leading causes of article resubmission and schedule delays. All color figures will be reproduced in full color in the online edition of the journal at no cost to authors.

**Units and Symbols:** Units and symbols

conforming to the International System of Units (SI) should be used for physicochemical quantities. Solidus notation (*e.g.* mg/kg, mg/mL, mol/mm<sup>2</sup>/min) should be used. Please refer to the SI Guide [www.bipm.org/en/si/](http://www.bipm.org/en/si/) for standard units.

**Supplemental data:** Supplemental data might be useful for supporting and enhancing your scientific research and BioScience Trends accepts the submission of these materials which will be only published online alongside the electronic version of your article. Supplemental files (figures, tables, and other text materials) should be prepared according to the above guidelines, numbered in Arabic numerals (*e.g.*, Figure S1, Figure S2, and Table S1, Table S2) and referred to in the text. All figures and tables should have titles and legends. All figure legends, tables and supplemental text materials should be placed at the end of the paper. Please note all of these supplemental data should be provided at the time of initial submission and note that the editors reserve the right to limit the size and length of Supplemental Data.

## 5. Submission Checklist

The Submission Checklist will be useful during the final checking of a manuscript prior to sending it to BioScience Trends for review. Please visit [Download Centre](#) and download the Submission Checklist file.

## 6. Online Submission

Manuscripts should be submitted to BioScience Trends online at <http://www.biosciencetrends.com>. The manuscript file should be smaller than 5 MB in size. If for any reason you are unable to submit a file online, please contact the Editorial Office by e-mail at [office@biosciencetrends.com](mailto:office@biosciencetrends.com).

## 7. Accepted Manuscripts

**Proofs:** Galley proofs in PDF format will be sent to the corresponding author via e-mail. Corrections must be returned to the editor ([proof-editing@biosciencetrends.com](mailto:proof-editing@biosciencetrends.com)) within 3 working days.

**Offprints:** Authors will be provided with electronic offprints of their article. Paper offprints can be ordered at prices quoted on the order form that accompanies the proofs.

**Page Charge:** Page charges will be levied on all manuscripts accepted for publication in BioScience Trends (\$140 per page for black white pages; \$340 per page for color pages). Under exceptional circumstances, the author(s) may apply to the editorial office for a waiver of the publication charges at the time of submission.

(Revised February 2013)

## Editorial and Head Office:

Pearl City Koishikawa 603  
2-4-5 Kasuga, Bunkyo-ku  
Tokyo 112-0003 Japan  
Tel: +81-3-5840-8764  
Fax: +81-3-5840-8765  
E-mail: [office@biosciencetrends.com](mailto:office@biosciencetrends.com)

---

### JOURNAL PUBLISHING AGREEMENT (JPA)

---

**Manuscript No.:**

**Title:**

**Corresponding Author:**

---

The International Advancement Center for Medicine & Health Research Co., Ltd. (IACMHR Co., Ltd.) is pleased to accept the above article for publication in BioScience Trends. The International Research and Cooperation Association for Bio & Socio-Sciences Advancement (IRCA-BSSA) reserves all rights to the published article. Your written acceptance of this JOURNAL PUBLISHING AGREEMENT is required before the article can be published. Please read this form carefully and sign it if you agree to its terms. The signed JOURNAL PUBLISHING AGREEMENT should be sent to the BioScience Trends office (Pearl City Koishikawa 603, 2-4-5 Kasuga, Bunkyo-ku, Tokyo 112-0003, Japan; E-mail: [office@biosciencetrends.com](mailto:office@biosciencetrends.com); Tel: +81-3-5840-8764; Fax: +81-3-5840-8765).

#### 1. Authorship Criteria

As the corresponding author, I certify on behalf of all of the authors that:

- 1) The article is an original work and does not involve fraud, fabrication, or plagiarism.
- 2) The article has not been published previously and is not currently under consideration for publication elsewhere. If accepted by BioScience Trends, the article will not be submitted for publication to any other journal.
- 3) The article contains no libelous or other unlawful statements and does not contain any materials that infringes upon individual privacy or proprietary rights or any statutory copyright.
- 4) I have obtained written permission from copyright owners for any excerpts from copyrighted works that are included and have credited the sources in my article.
- 5) All authors have made significant contributions to the study including the conception and design of this work, the analysis of the data, and the writing of the manuscript.
- 6) All authors have reviewed this manuscript and take responsibility for its content and approve its publication.
- 7) I have informed all of the authors of the terms of this publishing agreement and I am signing on their behalf as their agent.

#### 2. Copyright Transfer Agreement

I hereby assign and transfer to IACMHR Co., Ltd. all exclusive rights of copyright ownership to the above work in the journal BioScience Trends, including but not limited to the right 1) to publish, republish, derivate, distribute, transmit, sell, and otherwise use the work and other related material worldwide, in whole or in part, in all languages, in electronic, printed, or any other forms of media now known or hereafter developed and the right 2) to authorize or license third parties to do any of the above.

I understand that these exclusive rights will become the property of IACMHR Co., Ltd., from the date the article is accepted for publication in the journal BioScience Trends. I also understand that IACMHR Co., Ltd. as a copyright owner has sole authority to license and permit reproductions of the article.

I understand that except for copyright, other proprietary rights related to the Work (e.g. patent or other rights to any process or procedure) shall be retained by the authors. To reproduce any text, figures, tables, or illustrations from this Work in future works of their own, the authors must obtain written permission from IACMHR Co., Ltd.; such permission cannot be unreasonably withheld by IACMHR Co., Ltd.

#### 3. Conflict of Interest Disclosure

I confirm that all funding sources supporting the work and all institutions or people who contributed to the work but who do not meet the criteria for authors are acknowledged. I also confirm that all commercial affiliations, stock ownership, equity interests, or patent-licensing arrangements that could be considered to pose a financial conflict of interest in connection with the article have been disclosed.

---

**Corresponding Author's Name (Signature):**

**Date:**



